Summer 8-2012

Calcium Modulates MGLUR1 Folding in ER in the Trafficking Process and Regulates the Drug Activity Upon the Receptor Expressing on the Cell Membrane

Yusheng Jiang
Georgia state university

CALCIUM MODULATES MGLUR1 FOLDING IN ER IN THE TRAFFICKING PROCESS AND REGULATES THE DRUG ACTIVITY UPON THE RECEPTOR EXPRESSING ON THE CELL MEMBRANE

by

YUSHENG JIANG

Under the Direction of Dr. JENNY J. YANG

ABSTRACT

Metabotropic glutamate receptor 1α (mGluR1α) exerts important effects on numerous neurological processes. Although mGluR1α is known to respond to extracellular Ca^{2+} ($[Ca^{2+}]_o$) and the crystal structures of the extracellular domains (ECDs) of several mGluRs have been determined, the calcium-binding site(s) and structural determinants of Ca^{2+}-modulated signaling in the Glu receptor family remain elusive. Here, we identify a novel Ca^{2+}-binding site (Site 1) in the ECD-mGluR1α using a recently developed computational algorithm. This predicted site (D318, E325, D322 and the bound L-Glu) is situated in the hinge region in the ECD-mGluR1α adjacent to the reported Glu-binding site. Mutagenesis studies indicated that binding of L-Glu and Ca^{2+} to their distinct but partially overlapping binding sites synergistically modulated mGluR1α activation of

intracellular Ca^{2+} ($[Ca^{2+}]_i$) signaling. Mutating the Glu-binding site completely abolished Glu signaling while leaving its Ca^{2+}-sensing capability largely intact. Mutating the predicted Ca^{2+}-binding residues abolished or significantly reduced the sensitivity of mGluR1α not only to $[Ca^{2+}]$o and $[Gd^{3+}]_o$ but also, in some cases, to Glu. In addition, the Ca^{2+} effects on drugs targeting mGluR1α were investigated. Ca^{2+} enhances L-Quis response of the receptor by increasing L-Quis binding to ECD-mGluR1α and promotes the potency of Ro 67-4853, a positive allosteric modulator of mGluR1α. Increasing Ca^{2+} concentration, the inhibitory effects of a competitive antagonist ((s)-MCPG) and a non-competitive negative allosteric modulator (CPCCOEt), were eliminated. Furthermore, we also identified another potential Ca^{2+} binding pocket (Site 2) consists of S165, D208, Y236 and D318, which completely overlapped with L-Glu. Thapsigargin (TG) induced ER Ca^{2+} depletion reduced surface expression of mGluR1α, and D208I and Y236I also decreased the receptor trafficking to plasma membrane suggesting the role of Ca^{2+} binding in protein folding and trafficking in the ER. Further, to measure ER Ca^{2+}, a series of genetically encoded biosensors were designed by placing a Ca^{2+} binding pocket at the chromophore sensitive region of red florescent protein mCherry. The designed sensors are able to bind Ca^{2+} and monitor Ca^{2+} concentration change both in vitro and in cells. The findings in this dissertation open up new avenues for developing allosteric modulators of mGluR function that target related human diseases.

INDEX WORDS**:** Metabotropic glutamate receptor 1, GPCR, Calcium, Drug, Trafficking, Folding, MCherry, Calcium sensor

CALCIUM MODULATES MGLUR1 FOLDING IN ER IN THE TRAFFICKING PROCESS AND REGULATES THE DRUG ACTIVITY UPON THE RECEPTOR EXPRESSING ON THE CELL MEMBRANE

by

YUSHENG JIANG

A Dissertation Submitted in Partial Fulfillment of the Requirements for the Degree of

Doctor of Philosophy

in the College of Arts and Sciences

Georgia State University

2012

CALCIUM MODULATES MGLUR1 FOLDING IN ER IN THE TRAFFICKING PROCESS AND REGULATES THE DRUG ACTIVITY UPON THE RECEPTOR EXPRESSING ON THE CELL MEMBRANE

by

YUSHENG JIANG

Committee Chair: Jenny J. Yang

Committee: Edward M. Brown

Aimin Liu

Donald Hamelberg

Electronic Version Approved:

Office of Graduate Studies

College of Arts and Sciences

Georgia State University

August 2012

ACKNOWLEDGEMENTS

The work in this dissertation was originated and directed by Prof. Jenny Yang. My entire family and I deeply appreciate her support for my research and my daily life. Her encouragement, understanding and forgiveness inspire me not only on my scientific mind, but also my personality. I will cherish and remember my time spent in Dr. Jenny Yang's lab. I also would like to thank Dr. Edward Brown, Dr. Aimin Liu, Dr. Donald Hamelberg, and Dr. Randy Hall for their guidance in my research. Without their patient mentoring, all of this work couldn't be done. I also would like to thank Drs. Yun Huang and Yubin Zhou for their kindness and help setting up my life in the United States and for their patient teaching of science and techniques. Thank you to Dr. Jin Zou for teaching me protein engineering and related biophysical assays, Dr. Mulpuri Nagaraju for helping MD simulation and correlation calculation, Dr. Hing-Cheung for performing NMR experiments, Dr. Kasper Hansen for suggestions on experimental design, Deep Shukla for combination indices calculation, Chen Zhang for supporting data, Rebecca Meyer for teaching me radioactive binding assay and Kevin Paavola for helping on experiments when I was working in Dr. Randy Hall's lab. I also would like to thank Natalie White and Paul Gieschen for their careful proofreading and English polishing. Without their great help, this dissertation could not have been done on time. I also would like to thank my parents Yunfei Jiang and Lijing Zhao for their support and love, my sister Yinmei Jiang for her financial support. I would like to thank my family especially my deeply loved wife Yufang Wang for her understanding and support, my two cute sons Evan Jiang and Ebenezer Jiang. In addition, I would like to thank the other members in Dr. Jenny

Yang's lab. Each of them provided great help to me, and we have spent many wonderful and happy times together as I have not experienced previously in my life. Finally, I would like to thank Brain and Behaviors fellowship and NIH funding for financial support on my research. Thanks to all the faculty and staff in Chemistry and Biology departments for their support.

TABLE OF CONTENTS

ACKNOWLEDGEMENTS ..... **iv**

LIST OF FIGURES ..... **xiv**

1 INTRODUCTION **1**

1.1 Common features of GPCRs **2**

1.1.1 Structural features of family C GPCRs ***5***

1.1.2 Folding and trafficking of family C GPCRs ***7***

1.1.3 Ligand binding of family C GPCRs ***7***

1.1.4 Coupled signaling pathways of family C GPCRs ***9***

1.1.5 Drug development targeting family C GPCRs ***11***

1.2 Distribution, functions and drug development of mGluRs **11**

1.2.1 Distribution and function of mGluRs ***11***

1.2.2 Structural studies of mGluRs ***13***

1.2.3 mGluRs related diseases ***14***

1.2.4 Trafficking of mGluRs ***17***

1.2.5 Drug effects of mGluRs ***18***

1.3 Ca^{2+} sensitivity of mGluRs **21**

1.4 The function of Ca^{2+} in the neuronal system when coupling with mGluRs **24**

1.5 The impact of the Ca^{2+} binding site and co-activation model on drug development 25

1.6 Challenges to the study of metal effects on mGluR1α 26

1.7 Hypothesis in this dissertation 27

1.8 Approaches and strategies 27

1.8.1 Prediction of Ca^{2+} binding site using a computational algorithm..... 27

1.8.2 Grafting approach 28

1.8.3 Individual cell image 28

1.8.4 Radioactive binding assay 29

1.8.5 Developing an ER Ca^{2+} sensor using mCherry as a scaffold protein.... 29

1.9 Objectives of this study 29

1.9.1 Predicting and studying Ca^{2+} binding sites of mGluR1α..... 29

1.9.2 Studying the co-activation of mGluR1α by Ca^{2+} and L-Glu 30

1.9.3 Investigating the effects of Ca^{2+} upon drugs modulating mGluR1α..... 30

1.9.4 Investigating the function of Ca^{2+} in the process of mGluR1α trafficking 30

1.9.5 Developing an ER Ca^{2+} sensor using mCherry as the scaffold protein 31

1.10 Summary of variants generated in this dissertation 31

2 MATERIALS AND EXPERIMENTS..... 34

2.1 Materials and supplies 34

2.2 Materials and Methods..... 35

2.2.1 Structural modeling, autodocking, and Ca^{2+}-binding sites prediction..35

2.2.2 Protein expression and purification 36

2.2.3 Determine biophysical properties of purified proteins using circular dichroism, fluorimetry and NMR.....37

2.2.4 Tb^{3+} Titration and Ca^{2+} Competition.....39

2.2.5 Constructs, site mutagenesis, and expression of mGluR1α variants...39

2.2.6 Quantitatively Determined Membrane Expression of the mGluR1α Mutants Using Flow Cytometry.....40

2.2.7 Measurement of $[Ca^{2+}]_i$ Responses of mGluR1α and Its Mutants using Ca^{2+} indicator—Fura-2 AM 41

2.2.8 Determining the effect of $[Ca^{2+}]_o$ on (^3H)-L-Quis binding to mGluR1α and its mutants.....45

2.2.9 Measurement of IP one accumulation using an IP ONE kit.....46

2.2.10 Data Analysis and Curve Fitting 47

2.2.11 Analysis of the electrostatic potential of mCherry.....47

2.2.12 Screening mutations without losing fluorescence of mCherry 47

2.2.13 Design of Ca^{2+}-binding pockets on chomophore sensitive locations of mCherry 48

2.2.14 Expression and Purification of mCherry and its mutants 48

2.2.15 pH profiles of mutants K198D of mCherry.....49

2.2.16 Ca^{2+} titration of MC-D1 49

2.2.17 Ca^{2+} sensing properties of mCherry sensor candidates 49

3 ELUCIDATION OF A NOVEL EXTRACELLULAR CALCIUM-BINDING SITE ON METABOTROPIC GLUTAMATE RECEPTOR 1α (MGLUR1α) THAT CONTROLS RECEPTOR ACTIVATION..... 50

3.1 Introduction 50

3.2 Results 53

3.2.1 Prediction of a Novel Ca^{2+}-binding Site Adjacent to the Glu-binding Site in the ECD of mGluR1α..... 53

3.2.2 Conformational effect of grafted CD2 mutant (CD2.D1)..... 55

3.2.3 Membrane expression of wild type mGluR1α and its mutants..... 55

3.2.2 Obtaining Site-specific Ca^{2+}/Ln^{3+}-binding Affinities by a Grafting Approach 60

3.2.3 Membrane Expression of mGluR1α and Its Mutants 61

3.2.4 Extracellular Ca^{2+} Triggers mGluR1α-mediated Intracellular Responses 64

3.2.5 Effects of $[Ca^{2+}]_o$ on a Glu-induced $[Ca^{2+}]_i$ Release by Wild Type mGluR1α 71

3.2.6 Effects of Mutating Proposed Ca^{2+}-binding Residues on $[Ca^{2+}]_o$ - or Glu-evoked $[Ca^{2+}]_i$ Responses 72

3.2.7 Effects of Mutating Predicted Ca^{2+}-binding Residues on Glu-potentiated $[Ca^{2+}]_i$ Responses..... 74

3.2.8 Effect of Mutating the Glu-binding Site on $[Ca^{2+}]_i$ Responses to Glu and Ca^{2+} 76

3.2.9 Effects of Mutations in the Predicted Ca^{2+}-binding Site on Gd^{3+}-induced $[Ca^{2+}]_i$ Responses.....77

3.2.10 Glutamate and $[Ca^{2+}]_o$ synergistically modulate mGluR1α coupled signaling.....77

3.3 Discussion 81

4 EFFECTS OF EXTRACELLULAR CA^{2+} ON THE MODULATION OF METABOTROPIC GLUTAMATE RECEPTOR 1 ALPHA (MGLUR1A) BY L-QUIS, (S)-MCPG, CPCCOET AND RO 67-4853 89

4.1 Introduction 89

4.2 Results 95

4.2.1 An L-Quis binding pocket predicted by Autodock-Vina.....95

4.2.2 Glutamate or (s)-MCPG induced hinge motion by binding to ECD-mGluR1α. 96

4.2.3 Mutational effects on the correlated motion in ECD-mGluR1α.....96

4.2.4 Ca^{2+} enhances [^{3}H]-L-Quis binding to mGluR1α through binding to Ca^{2+} binding site 1 of the receptor.....98

4.2.5 (s)-MCPG inhibits the sensitivity of mGluR1α to extracellular glutamate and Ca^{2+}. 104

4.2.6 Ca^{2+} enhances the potency of Ro 67-4853 to mGluR1α.....109

4.2.7 CPCCOEt noncompetitively inhibits L-glutamate induced responses, but only slightly affects Ca^{2+}-mediated responses of mGluR1α. 110

4.3 Discussion 119

5 THE FUNCTION OF CALCIUM ON MGLUR1 FOLDING IN THE ER..... 124

5.1 Introduction 124

5.2 Results 125

5.2.1 Determine surface expression of WT-mGluR1α and its mutants 125

5.2.2 Effects of mutations of Ca^{2+}-binding site 2 to extracellular Ca^{2+} 126

5.3 Discussion 130

6 DEVELOPING an ER CALCIUM SENSOR USING MCHERRY 133

6.1 Introduction 133

6.2 Results 135

6.2.1 Mutation effects on mCherry 135

6.2.2 Designing a Ca^{2+}-binding pocket on mCherry 138

6.2.3 Determining the Ca^{2+} sensing properties of MC-D1 and MC-D2 in vitro 138

6.2.4 Determining the Ca^{2+} sensing properties of MC-D1 and MC-D2 in vivo 139

6.3 Discussion 143

7 SIGNIFICANCE OF THIS WORK..... 147

7.1 The impact of determination of Ca^{2+}-binding sites..... 147

7.2 The importance of discovery on Ca^{2+} effects on the developed drugs. 148

7.3 The role of Ca^{2+} in the process of protein folding and trafficking.. 149

7.4 The significance of development of genetically encoded biosensor 149

REFERENCES 151

APPENDIX 163

LIST OF TABLES

Table 1-1 Summary of variants created in terms of mGluR1α..... 31

Table 1-2 Summary of generated other variants..... 33

Table 3-1 Spectra fit of CD data of CD2 and grafting protein, CD2.D1..... 58

Table 3-2 Tb^{3+} binding affinities of the engineered protein CD2.D1 and its double mutants (*n*=3) 63

Table 3-3 $[Ca^{2+}]_i$ responses of WT mGluR1α and its mutants to $[Ca^{2+}]_o$ and Glu (*n*=3)..... 69

Table 3-4 $[Ca^{2+}]_i$ response of mutants in L-Glu binding site (n=3) 75

Table 3-5 Combination indices of glutamate and Ca^{2+} on mGluR1α..... 78

Table 4-1 Hinge motion analysis using Dymdon ……..…100

Table 4-2 $[Ca^{2+}]_o$ enhances L-Quis induced activation of mGluR1α 103

Table 4-3 Addition of 0.5 mM (s)-MCPG decreases the responses of mGluR1α to Ca^{2+} and L-Glu 105

Table 4-4 Ca^{2+} effects on Ro 67-4853 modulating mGluR1α..... 113

Table 4-5 CPCCOEt inhibits the L-Glu sensitivity of mGluR1α 117

Table 6-1 Mutation effects on the fluorescence of mCherry..... 136

LIST OF FIGURES

Figure 1-1 Families of G-protein coupled receptor 3

Figure 1-2 Common structural features of family C GPCRs 6

Figure 1-3 Modulators and signaling pathway of mGluR1α..... 10

Figure 1-4 Folding and trafficking of GPCRs. 16

Figure 1-5 The Glutamate cycle in the synaptic cleft. 19

Figure 1-6 Model structure of mGluR1α 20

Figure 3-1 Predicted Ca^{2+}-binding pocket in ECD of mGluR1α. 56

Figure 3-2 Secondary structure and folding of engineered proteins. 57

Figure 3-3 Membrane Expression of wt-mGluR1α, D318I-mGluR1α, D322I-mGluR1α, D324I-mGluR1α, E325I-mGluR1α, and E328I-mGluR1α using a gene reporter at HEK293 cells. 59

Figure 3-4 Metal binding properties of the grafted Ca^{2+}-binding site..... 62

Figure 3-5 Surface expression of WT mGluR1α and its mutants. 65

Figure 3-6 Intracellular Ca^{2+} responses of WT mGluR1α and its mutants... 66

Figure 3-7 Intracellular Ca^{2+} responses of WT mGluR1α and its mutants (D322I-mGluR1α, D324I-mGluR1α, E325I-mGluR1α, and E328I-mGluR1α) to $[Ca^{2+}]_o$ in the presence of Glu. 67

Figure 3-8 Intracellular Ca^{2+} responses to extracellular Glu in HEK293 cells transfected with WT mGluR1α or its mutants. 68

Figure 3-9 Extracellular Ca^{2+} enhanced mGluR1α to sense extracellular Glu. Responses of WT mGluR1α to extracellular Glu were assessed in buffers containing additional $[Ca^{2+}]_o$ (1.8, 5, and 10 mm). significantly decreased. 73

Figure 3-10 Receptors with mutations in the Glu-binding pocket can sense Ca^{2+} but not Glu in a physiological buffer. 79

Figure 3-11 Mutations D318I and E325I in the predicted Ca^{2+}-binding site abolish $[Ca^{2+}]_i$ responses of the receptor to $[Gd^{3+}]_o$. 80

Figure 3-12 A dual activation model for mGluR1α involving both extracellular Ca^{2+} and Glu via the overlapping and interacting binding pockets for the two ligands at the hinge region of the ECD. 84

Figure 4-1 Structural models of mGluR1α bound with orthosteric ligands, L-Quis and (s)-MCPG. 99

Figure 4-2 The effects of mutations of Ca^{2+} binding site 1 on correlated motion of ECD-mGluR1α..... 101

Figure 4-3 [^{3}H]-L-Quis binding to mGluR1α and its variants. 102

Figure 4-4 Extracellular Ca^{2+} enhances L-Quis activation of mGluR1α variants..... 106

Figure 4-5 (s)-MCPG competitively inhibits the response of wild type mGluR1α to extracellular L-glutamate. 107

Figure 4-6 (s)-MCPG competitively inhibits the potentiation of mGluR1α potentiated by $[Ca^{2+}]_o$ in L-Glu free buffer. 108

Figure 4-7 Extracellular Ca^{2+} enhances the potency of Ro 67-4853 on mGluR1α. HEK293 cells growing on coverslip were transiently expressed wild type mGluR1α. 112

Figure 4-8 Extracellular Ca^{2+} increases oscillatory events induced by Ro 67-4853…… ……115

Figure 4-9 CPCCOEt non-competitively reduces L-Glu sensitivity of mGluR1α…… .....….116

Figure 4-10 Effects of CPCCOEt upon the responses of wild type mGluR1α to Ca^{2+}…….118

Figure 5-1 Surface expression of mutants in Ca^{2+}-binding site 2 determined by FACS. 127

Figure 5-2 Mutations on the predicted Ca^{2+}-binding site 2 reduced intracellular Ca^{2+} mobilization triggered by extracellular Ca^{2+}. 128

Figure 5-3 Treatment of 300 nM thapsigagin reduces the surface expression of wild type mGluR1α. 129

Figure 6-1 The Chromophore environment of mCherry 134

Figure 6-2 Mutation effects on mCherry. 137

Figure 6-3 pH profile of MC-D2. 141

Figure 6-4 Ca^{2+} response of MC-D2..... 142

LIST OF ABBREVIATIONS

7TM Seven time transmembrane domain

AC Adenyl cyclase

ANS 8-anilino-1-naphthalenesulfonic acid

AI After induction

AIDA (RS)-1-Aminoindan-1,5-dicarboxylic acid

BI Before induction

CaM Calmodulin

CaSR Calcium-sensing receptor

CD Circular dichroism

CD2 Cluster of differentiation 2

CDPPB 3-Cyano-*N*-(1,3-diphenyl-1*H*-pyrazol-5-yl)benzamide

CPCCOEt 7-(Hydroxyimino)cyclopropa[*b*]chromen-1a-carboxylate ethyl ester

CR Cysteine rich domain

DAG Diacylglycerol

DMEM Dulbecco's modified Eagle's medium

ECD Extracelluar domain

EDTA Ethylenediaminetetraacetic acid

EGTA Ethylene glycol tetraacetic acid

ER Endoplasmic reticulum

FRET Fluorescence resonance energy transfer

GDP Guanosine diphosphate

GFP Green fluorescent protein

GPCR G protein-coupled receptor

GST Glutathione-S-transferase

GTP Guanosine triphosphate

HEK293 Human embryonic kidney cell line

iGluR ionotropic glutamate receptor

InsP3R Inosito-1,4,5-trispohosphate receptor

IPTG Isopropyl-β-D-thiogalactopyranoside

Kd Dissociation constant

LIVBP Leucine/isoleucine/valine-binding protein

LRET Luminesence resonance energy transfer

LTD Long term depression

LTP Long term potentiation

mGluR Metabotropic glutamate receptor

NAM Negative allosteric modulator

NMR Nuclear magnetic resonance

OD Optical density

PAM Positive allosteric modulator

PBS Phosphate-buffered saline

PCR Polymerase chain reaction

PIP2 Phosphatidylinositol 4,5-bisphosphate

PKA Protein kinase A

PKC Protein kinase C

PLC Phospholipase C

RyR Ryanonide receptors

SDS Sodium lauryl sulfate

SDS-PAGE Sodium dodecyl sulfate polyacrylamide gel electrophoresis

SERCA Sarco/endoplasmic reticulum Ca^{2+}-ATPase

(s)-MCPG (s)-α-Methyl-4-carboxyphenylglycine

SOCE Store-open Ca^{2+} entry

STIM1 Stromal interaction molecule 1

UV Ultraviolet

1 INTRODUCTION

Ca^{2+} is a versatile ion functioning as a first or second messenger in many signaling and metabolic pathways (1-4). It maintains blood Ca^{2+} homeostasis by regulating the extracellular Ca^{2+} sensing receptor coupled PTH secretion and calcitonin (5,6). It also mediates intracellular Ca^{2+} homeostasis through modulating the Ryanodine receptor and gap junction with the assistance of calmodulin (CaM) (7-10), and controlling channel gating by interacting with Ca^{2+} sensors, i.e. STIM1 on the ER membrane (11). In addition, Ca^{2+} is also known to facilitate cell adhesion by interacting with cadherins (12-14). In the blood system, Ca^{2+} is taken up from gut fluid with the assistance of vitamin D, and then secreted into urine in the kidney or deposited into the bones. Low gut Ca^{2+} absorption or high urine Ca^{2+} breaks the blood Ca^{2+} balance, which in turn changes the PTH or calcitonin level, thereby regulating bone resorption or Ca^{2+} absorption and Ca^{2+} secretion in the kidney (2,5,15,16). In cells, the Ca^{2+} homeostasis is primarily maintained by Ca^{2+} pumps and channels. Redundant Ca^{2+} in cytosol is either pumped out of the cells through Ca^{2+}-ATPase on the cell membrane or mobilized into the ER/SR lumens by SERCA pumps (Ca^{2+}-ATPase on ER/SR membranes) (17). The skeletal muscle ryanodine receptor, stated as RyR1, resides on the SR membrane, mediating Ca^{2+} release from the SR lumen, thereby leading to muscle contraction. Low cytosolic Ca^{2+} activates RyR1 while high Ca^{2+} concentration inhibits the channel activity (18). CaM was proved to be involved in switching the channel gating while in the presence of high or low concentrations of cytosolic Ca^{2+}. Mutants of CaM with reduced Ca^{2+} binding remains active to open RyR1, but fails to close the channel in the presence of high Ca^{2+}

concentration. This suggests Ca^{2+} is the key factor for regulating the RyR1 channel property through binding to CaM or directly binding to RyR1 (19). Similarly, the gating of the gap junction is coupled with CaM and dependent on Ca^{2+}. CaM binding sites were discovered at C-termini of Cx32, Cx35 and C36 (20,21). Increasing cytosolic Ca^{2+} concentration abolishes cell-cell communication by shutting down gap junctions, which can be converted by CaM inhibitor (22,23). In other words, the resource of intracellular Ca^{2+} depends on Ca^{2+} store-release; or extracellular influx through the TRP channel, voltage-gated Ca^{2+} channel; or store-open Ca^{2+} entry (SOCE). STIM1, expressing in ER, has an EF-hand in ER lumen side and can sense the ER Ca^{2+} depletion (24). STIM1 then aggregates to the ER membrane, thereby activating the Orai channel and inhibiting Cav1.2 channels (25).

Cadherins are single transmembrane proteins with three to five random, repeated, extracellular domains. The Ca^{2+} binding sites were revealed in the repeated motifs, which were suggested to be vital in cell-cell adhesion (13). Removal of extracellular Ca^{2+} abolishes the adhesive properties of cells while making cadherins to be easily digested by proteases (26).

1.1 Common features of GPCRs

G protein coupled receptors (GPCRs) are a huge family of cell surface receptors correlated to G proteins, with characteristic seven transmembrane domains. So far, 359 genes of GPCRs have been discovered according to the information from the IUPHAR database (http://www.iuphar.org/) and all the members are known to couple with heterotrimeric G proteins formed by Gα, Gβ and Gγ subunits. Basically, there are four classes of Gα ($G\alpha_s$, $G\alpha_i$/$G\alpha_o$, $G\alpha_q$/$G\alpha_{11}$ and $G\alpha_{12}$/$G\alpha_{13}$) and the type of Gα decides the

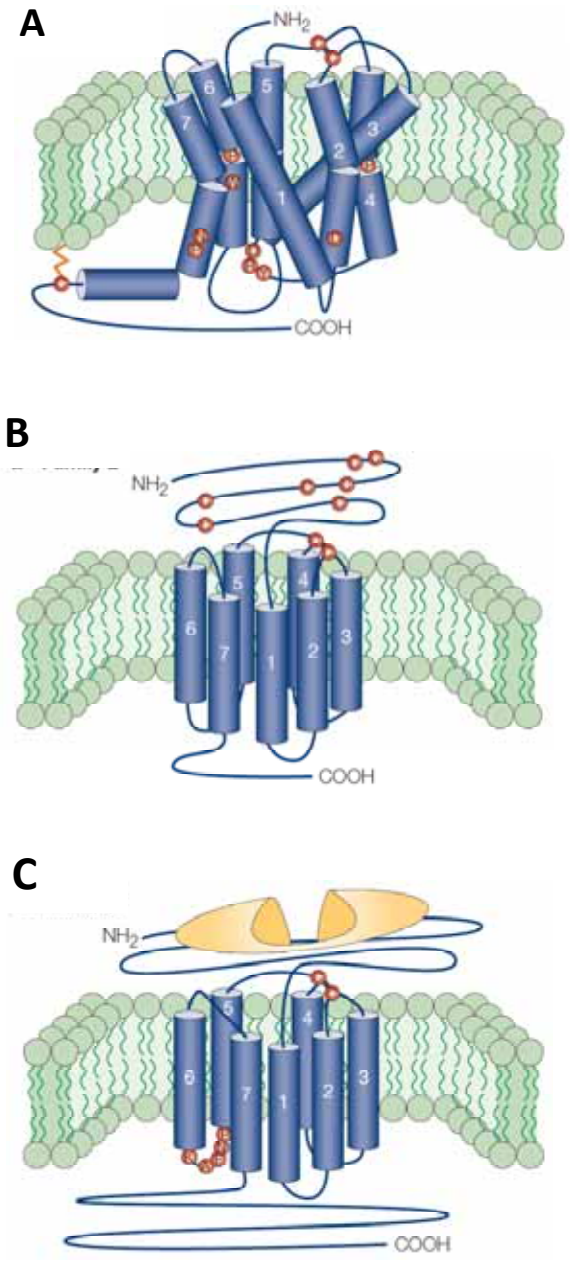

Figure 1-1 Families of G-protein coupled receptor (27). (A) Model structure of family A GPCRs. The N-terminal is very short, and the conserved Proline in the transmembrane domain bent the helical structures within the membrane. (B) Scheme structure of family B GPCRs. It has a relative long N-terminal which includes several pairs of disulfate bonds. (C) Model structure of family C GPCRs. Family C GPCRs has a long N-terminal functioning as ligand binding domain, a cysteine rich domain containing several pairs of anti-parallel beta-strands interacting through disulphate bonds, a transmembrane domain and a very long C-tail.

subsequent signaling pathway. In principle, binding of ligands releases GDP from Gα protein, which in turn associates with GTP. Upon binding with GTP, Gβ/γ complex dissociates from Gα protein, and subsequently, the downstream signaling pathway is activated. After GTP is hydrolyzed into GDP, G proteins cluster back into a heterotrimer (28). Based on their structural and genetic features, GPCRs fall into three major categories: family A, family B, and family C as shown in Fig. 1-1. Family A has a very short N-terminal and owns several highly conserved residues in the transmembrane helices. Some helices were bent due to the presence of Proline. Lots of members in family A have no endogenous ligands discovered, so they were named as orphan receptors. Rhodopsin expressing in rod photoreceptor cells belongs to family A GPCR, and it is a light sensitive receptor (29). Its inactive state consists of an apo-form opsin and a covalently bound 11-*cis*-retinal in the binding pocket. Determining the crystal structure of rhodopsin is the first time uncovering the seven-time transmembrane domain (7TM) in GPCRs (30). The structure has been widely applied to homological modeling especially in GPCRs. Family B has a relatively long amino terminal with several disulfate bridges which are conserved in almost all the members in the family. The ligands of family B are mainly hormones, including secretin, glucagon and parathyroid hormone. Family C is characterized with a large extracellular ligand binding domain (ECD), following a cystine rich domain which contains four pairs of disulfate bridges, a seven transmembrane domain, and a long C-tail (Fig. 1-2). They play vital roles in sensing vision, taste, and smell; and they couple to the signaling pathway initiated by numerous hormones, neurotransmitters, ions, photons, lipids and designed drugs (31,32). Family C contains the calcium sensing receptor (CaSR), the mGluRs, GABAb receptor, GPRC6, taste recep-

tors and some orphan receptors. All the members in family C have a Venus fly-trap like endogenous ligand binding domain, and some synthesized compounds were also revealed to bind to extracellular loops on transmembrane domains (33). ECD structures from four members of mGluRs have been delineated with the presence or absence of ligands, but little is known on the transmembrane domain.

1.1.1 Structural features of family C GPCRs

As shown in Fig. 1-2, the structure of family C GPCRs consist of a large extracellular domain, following with a cysteine rich domain, a seven transmembrane domain and a long C-tail. Most of the orthosteric and allosteric modulators bind to the extracellular domain while the transmembrane domain is also a target for a few allosteric modulators. Through forming a disulfate bond by two cysteines on the top of the protomers, the receptors function as a dimer. A cysteine rich domain contains three pairs of short antiparallel β strands. This domain is suggested to be the connection between the extracellular domain and the transmembrane domain. The three dimensional structure of a transmembrane domain is conserved in all the members in GPCRs, and even contains orthosteric modulator binding pockets in family A and B. So far, only allosteric modulators were discovered targeting the transmembrane domain. C tail along with intracellular loops interacts with signaling proteins inside of the cells, thereby coupling the activation signal to the downstream signaling pathways.

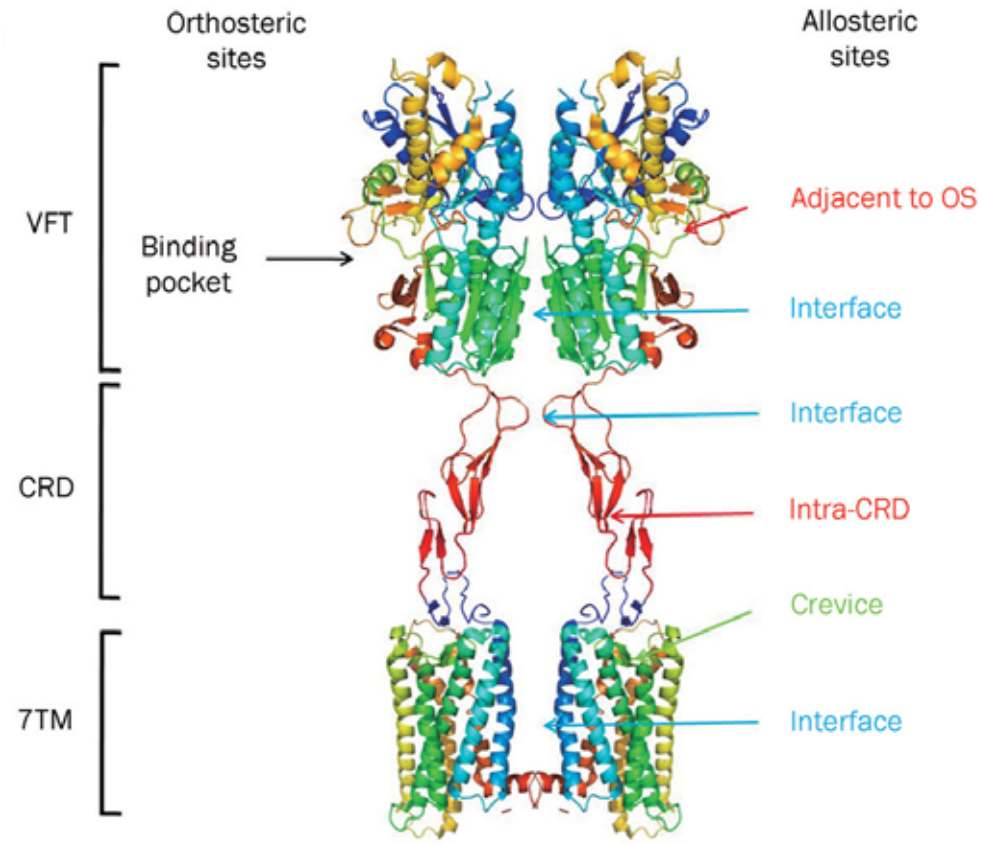

Figure 1-2 Common structural features of family C GPCRs (34). Family C GPCRs functions as dimmer. It consists of a large ligand binding domain, also known as extracellular domain (ECD) or Venus flytrap structure (VFT), a cysteine rich domain (CRD), a seven transmembrane domain (7TM) and a relative long C-tail (CT). Extracellular domain looks like a Venus flytrap structure, forming a dimmer through a disulfate bond generated by C140 in each protomer. The protomer has two lobes forming a cram-shell like structure, and the orthosteric ligand binding site resides at hinge region formed by two lobes. Following the ECD, there is a cysteine rich domain with three pairs of anti-parallel β-strands. Transmembrane domain is seven helical structures connected by three extracellular loops and three intracellular loops. These loops are important for binding of G-proteins and other coupled proteins. They are also good targets for some allosteric modulators. C-tail is pretty long comparing to the members in other family of GPCR. It mainly provides targets for binding of some signaling and scaffold proteins.

1.1.2 Folding and trafficking of family C GPCRs

Family C GPCRs, same as the whole family of GPCRs, are folded in ER facilitated by chaperones. Misfolded proteins are tagged with ubiquitin and transported to lysosome for degradation. The nascent proteins properly folded with the assistance of chaperones and quality control systems, exiting ER as homo- or hetero-dimers in exocytic vesicles and translocating to Golgi complex for further modification (Figure 1-4). During the transportation, the extracellular domain is buried inside of the vesicles. Once the extracellular domain arrives at the cell membrane, the whole structure flips over and anchors to the membrane. For example, correctly targeting of HSJ1b (HSP40) to the ER membrane enhances formation of rhodopsin inclusion (35), which suggests overexpression of chaperone, HSJ1b, and increases rhodopsin folding in the ER.

1.1.3 Ligand binding of family C GPCRs

As mentioned, family C GPCRs have a large extracellular ligand binding domain which likes a cram-shell forming by two lobes (Fig. 1-1C and Fig. 1-2). Binding pockets were classified as orthosteric and allosteric (36).The orthosteric binding pocket resides in the hinge region which allows the agonists or antagonists wedging in the pocket by interacting with the residues in both lobes. Except the orthosteric binding site, lots of allosteric binding pockets were discovered in the past decade (23,31,33,37-41) and even two drugs are available in market (22,42). Especially, only allosteric drugs binding sites were found on transmembrane domain in family C GPCRs. CaSR was cloned in 1983 by ED Brown, and it plays a very important role to keep Ca^{2+} in homeostasis and is able to sense Ca^{2+}, other poly-cations, and most of the amino acids (31). The challenge in that era was to illustrate where the Ca^{2+} bound in order to determine how to tune the

Ca^{2+} binding of the receptor through interference with the binding pockets, thereby relieving the syndrome induced by abnormal CaSR. In addition, a profile of amino acids was found to bind to extracellular domain of CaSR as well. As reported in Conigrave's article, lots of amino acids could allosterically activate CaSR, and CaSR prefers the amino acids with aromatic side chain (43). By aligning with the glutamate binding site in mGluR1, Silve C et al. found the corresponding residues in CaSR were highly conserved in both CaSR and all subtypes of mGluRs (44). This led them to test Ca^{2+} sensitivity while the conserved residues were knocked away using site-directed mutagenesis. The results came out that E297K, Q193A, F270A and S296A reduced Ca^{2+} sensitivity, which indicated these residues were important for Ca^{2+} sensing. Later on, Huang Y et al. used a Metal-finder (revised version of Dezymer, plus surface charge analysis) to determine five more Ca^{2+} binding sites on CaSR. The predicted sites were confirmed by using grafting and subdomain approaches in vitro and cell population assay in vivo (45,46).

The metal binding of CaSR triggered the search for metal sensitivity of mGluRs, which soon extended to other members in family C GPCR. Due to the high sequence identity, it was very likely mGluRs would be able to sense metals. Kubo Y's group pushed forward to demonstrate that group I mGluRs, including mGluR1 and mGluR5, could sense Ca^{2+}, Mg^{2+}, Ba^{2+}, Gd^{3+} and other metals, while group II mGluRs, including mGluR2 and mGluR3, also could respond to Ca^{2+} although mGluR2 needed a relatively higher Ca^{2+} concentration than physiological level (32). Mg^{2+} and Gd^{3+} were revealed in later crystallization work by Jingami's group in mGluR1 (47). In addition to mGluR1, Mg^{2+} was found to bind to mGluR5 in crystals (PDB bank, no publication). Moreover,

GABABR and GRPR6A were also found to sense extracellular Ca^{2+}. Interestingly, GABAB receptor functions as a heterodimer by interacting with mGluR1 through C-termini of these two receptors. Based on the accumulating evidence, we can conclude that most of the members in GPCR family can sense extracellular Ca^{2+}.

1.1.4 Coupled signaling pathways of family C GPCRs

One criterion to categorize mGluRs is the signaling pathway of the receptors coupled. Group I mGluRs, including mGluR1 and mGluR5, couple to $G\alpha_{q/11}$ protein which forms complex with GTP and hydrolyzes GTP into GDP. The following PLC then is activated and hydrolyzed PIP2 into DAG and IP3. IP3 binds to IP3 receptor on ER membrane, triggering Ca^{2+} mobilization from ER lumen to cytosol. Increasing cytosolic Ca^{2+} will further open ion channel on the cell membrane. DAG also can activate $PKC_{\beta.}$ In the meantime, group I mGluRs also can activate adenyl cyclase by coupling to $G\alpha_s$ (Fig. 1-3). Differently, Group II and III couple to a G protein ($G\alpha_{i/o}$) with opposite function. Activation of this group of receptor, the potency of adenyl cyclase is decreased. Group II mGluRs are suggested to control the L-Glu level in synaptic cleft. High concentration of L-Glu in synaptic cleft applies to group II mGluRs inhibits L-Glu release from pre-synapses. Excitatory CaSR also associates with $G\alpha_{q/11}$ and releases ER Ca^{2+} as group I mGluRs. But CaSR also the other two classes of G proteins, $G\alpha_{i/o}$ and $G\alpha_{12/13.}$ This makes the signaling of CaSR more versatile and complicated. The mechanism of CaSR selectively activates certain signaling pathway is still unclear. Additionally, GRPC6A is also related to Gαq/11, while taste receptors forms heterodimers (T1R1/T1R3,

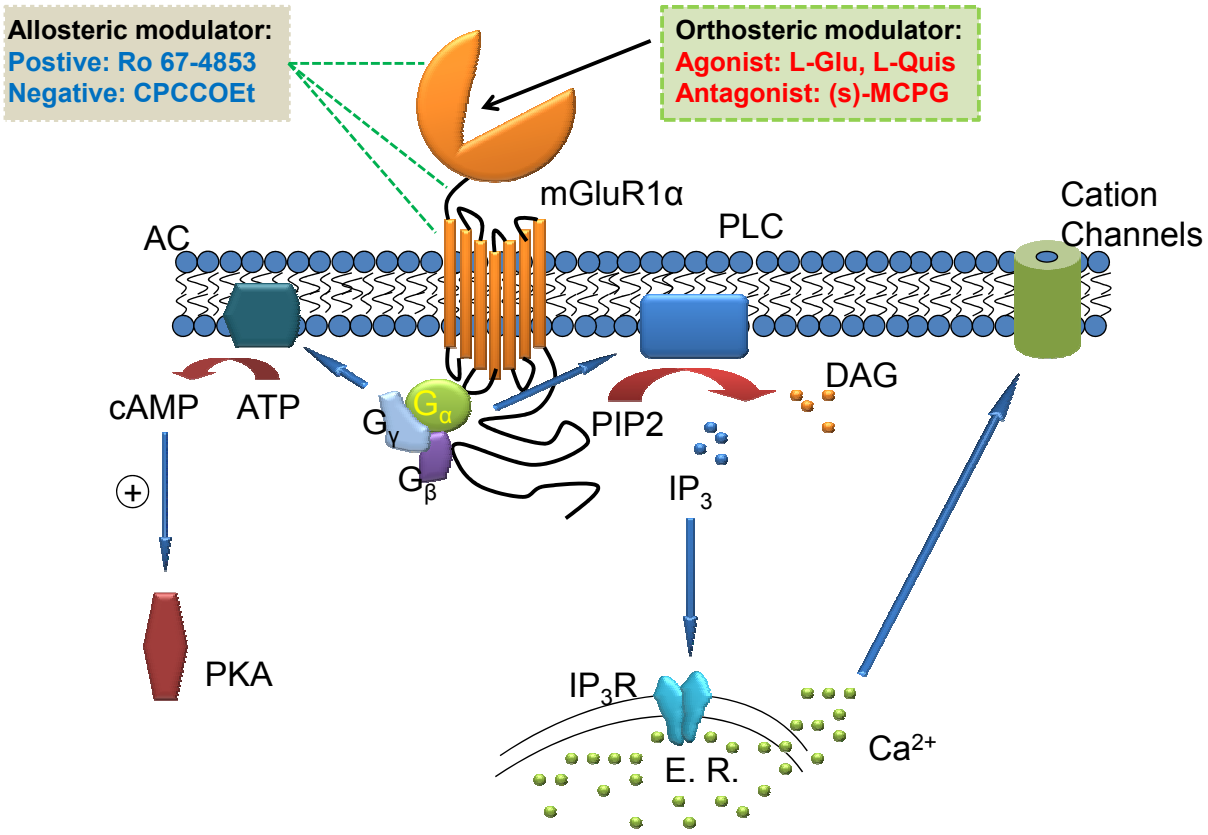

Figure 1-3 Modulators and signaling pathway of mGluR1α. MGluR1α can be activated by orthosteric modulators independently or be triggered by positive allosteric modulators in absence of agonists, for example L-Glu or Ca^{2+}. Activation of mGluR1α recruits G-proteins, thereby activating PLC which subsequently protelyzing PIP2 into DAG and IP_3. IP_3 then opens IP3R on ER membrane to release Ca^{2+} into cytosol, thus opening Ca^{2+} channel on cell membrane. At the same time, mGluR1α also can couple to cAMP pathway by activating AC which catalyzes ATP to circlize into cAMP, thereby activating PKA.

T1R2/T1R3) coupling to Gα-gustducin also results in PI-PLC activation (48).

1.1.5 Drug development targeting family C GPCRs

In the past decades, drug discoveries focused on GPCR were very successful, and even today, GPCRs are still very hot drug targets. As investigated by Flower DR, more than 50% of modern drugs target these receptors. In the 100 top-selling drugs, around 26% are suggested to target GPCRs, while another 13% are indirectly targeting these receptors (49).

1.2 Distribution, functions and drug development of mGluRs

1.2.1 Distribution and function of mGluRs.

MGluRs were discovered in mid-1980s. In 1987, Kano and Kato et al. demonstrated that activation of mGluRs expressed on Purkinje cells was the causes of long term depression (LTD) (50). The functions of mGluRs were then illustrated for the first time. Four years later, two independent labs cloned the gene of one of the members of mGluRs, which were named mGluR1 (51,52). In the following four years, overall eight members were discovered. According to their coupled signaling pathway, drug selectivity and sequence homology, mGluRs were categorized into three sub-groups. MGluRs mainly express in central neuronal system. Group I distributes around the iGluR core to form an annulus on the surface of post-synapses. Group II prefers to express on the active zone on pre-synapses. Group III has no preference but mGluR6 majorly expressed on glial cells. MGluR6 is related to retinal, and mutation in mGluR6 leads to night blindness. iGluRs are ligand gated ion channels. After receiving the ligand (L-Glu) released from pre-synapses, the channels were opened by ligand binding, thereby resulting in

Na^+ ions influx. Depolarization of post-synapses further removes the physiological inhibitor Mg^{2+}, which blocks AMPAR in resting state, and Ca^{2+} in synaptic cleft also enters into post-synapses. These events were shown as fast phase of action potential. However, the functions of mGluRs are different. Group I mGluRs can respond L-Glu, so that the coupled signaling pathway is triggered and which in turn also can open Ca^{2+} channel due to the Ca^{2+} depletion of ER lumen. But the current is relatively slow than the one generated by iGluRs, which corresponds to the slow phase in action potential. Because of this, group I mGluRs were related to neuronal plasticity, therefore, lots of physiological and pathophysiological possesses were related to group I mGluRs. As mentioned, Group II and III coupled to Gi protein, and Group II mostly expressed on pre-synapses. Activation of Group II mGluRs can inhibit L-Glu release from pre-synapses. Somehow, the high concentration of L-Glu in synaptic cleft could be feedback to pre-synapses by Group II or Group III mGluRs, thereby reducing L-Glu level and preventing over-exciting of the neurons. As described in Fig. 1-5, the rest of L-Glu can be pumped back to Glial cells or pre-synapses through L-Glu transporters, and finally the L-Glu recycled back to pre-synpses or Glial cells was re-packed into vesciles. Upon receiving action potential, the L-Glu will be released to synaptic cleft again by exocytosis. So, developing drugs targeting specific subtype of mGluRs is very important. Drugs targeting the orthosteric sites always activate or inhibit the whole family of mGluRs. To some extent, certain unexpected side effects could happen. In the past decade, lots of efforts were turned to discover allosteric modulators, but allosteric drug targeting site always not highly conserved in different species. This brought difficulty to perform pre-clinical trial.

1.2.2 Structural studies of mGluRs

Metabotropic glutamate receptors belong to family C GPCR, which has common features with a large extracellular domain (ECD) functioning as an endogenous agonist binding region, cystein rich (CR) domain, seven time transmembrane domain, (7-TM) and C-terminal. The receptor functions as a dimer linked by a disulfate bridge through C140 onto the ECD (53). An extracellular domain consists of two lobes which form a venus flytrap-like structure, which has a 3-dimensional structure very similar to bacterial leucine/isoleucine/valine-binding protein (LIVBP). Thus, the first homologous model was generated by O'Hara's group using LIVBP as a template. In this model structure, several key residues (T188, D208, Y236 and D318) for agonist binding, which were highly conserved in different species, were determined (54). In 2000, Kunishima N et al. reported several ECD structures, including two apo forms and one holo form with L-Glu and potential Mg^{2+}, using X-ray crystallography (47). Two years later, two additional forms bound with L-Glu, Gd^{3+}, and (s)-MCPG were reported. In L-Glu bound structures, the L-Glu binding pocket was sketched out confirming the model study on this receptor (55). These structures revealed 3 different kinds of conformations upon the bound ligands which were estimated as the activation mechanism of mGluR1α. Upon L-Glu binding, the receptor was stated to be a closed-open form, as LB1 and LB2 in the same protomer were closed even though two LB2 domains were kept open due to the charge repulsion in the interface (E238 and D242). In the presence of Gd^{3+}, the negative charge could be neutralized and two LB2 domains moved toward each other, forming a close-close form. Whether the LB2 domains were closed or open, the conformational change could still lead to a rearrangement of the transmembrane domain with the assis-

tance of a cysteine rich domain. The free form or antagonist bound form was known as a resting form, also called an open-open form. Similar to a free form, the receptor bound with s-MCPG or LY341495 shows as a relax state (Fig. 1-6). Although the constitutive activation was reported in mGluR1 due to the function of Homer1b binding to the C terminal, the activation of the receptor was ascribed to the predominance of a close form in dynamic equilibrium. This hypothesis was further improved by Tateyama et al. using the FRET technique. In brief, two intracellular loop 2 (i2) were brought closer upon the agonists stimulation (L-Glu and Ca^{2+}), while the antagonists increased the space between the loops (56).

1.2.3 mGluRs related diseases

Mebotropic glutamate receptor 1 (mGluR1) is widely expressed on the surface of post synapses in the central neuronal system. It senses glutamate following recruitment of hetero-trimeric G proteins, and the accumulation of DAG and IP3 which further modulates protein kinases involved cascade response and intracellular Ca^{2+} mobilization, respectively. This consequently leads to nonselective inward cation current. Shortly after the receptor was cloned, its versatility was revealed to respond to not only glutamate but also Ca^{2+} and other polyvalent ions. The activity of mGluR1α has been proved to be related to some important physiological and pathological processes, such as breast cancer, melanoma, and neuronal degenerative diseases. Down regulation of mGluR1α was detected in neurons of substantia nigra in Parkinson monkey models, suggesting mGluR1α plays an important role in the process of Parkinson disease. In addition, prepulse inhibition (PPI) was disrupted in mGluR1 knockout mice (57). PPI deficiency

usually appeared in patients with schizophrenia, this indicates mGluR1 is also involved in the process of schizophrenia. MGluR5 was suggested to be involved in Fragile X syndrome (58). Down regulating group I mGluRs could relieve Fragile X symptoms, while especially the antagonist of mGluR5, MPEP, can suppress the seizure phenotypes. MGluR4 were previously reported as a target to relieve pain. More recent, an original antagonist (PHCCC) of group I mGluRs was found to enhance the potency of an agonist of mGluR4 (L-AP4). Moreover, treating Parkinsonian rat model with PHCCC, the movement activity was reduced (59). This also suggests mGluR4 could be a therapeutic target for Parkinson's diseases. Furthermore, the agonist of mGluR2/3 (LY2140023) has shown to improve both positive and negative symptoms in patients with schizophrenia, and this drug has entered phase II clinical trial (60).

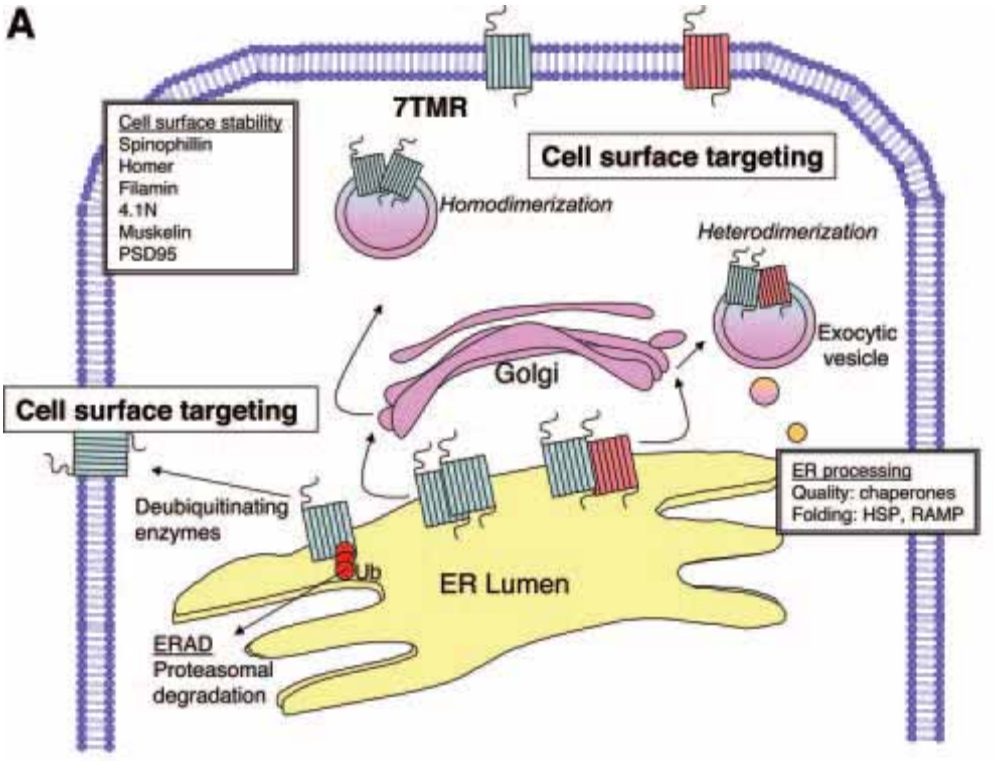

Figure 1-4 Folding and trafficking of GPCRs (61). Family C GPCRs could form homo- or heterodimer after synthesized in ER with the facilitation of chaperones and other quality control system. The well folded proteins were translocated to Golgi complex for further modification or directly anchored on the cell membrane through exocytic vesicles while abnormal proteins were ubiquitinated and delivered to lysosomes for degradation.

1.2.4 Trafficking of mGluRs

The activity of mGluRs is dependent of the receptor expression on cell surface. For instance, surface expression of mGluR7 plays an important role to control the neuronal plasticity (62). Decrease of surface mGluR5 by exposing to cocaine lead to loss of endocannabinoid retrograde LTD (63). MGluRs, like other members of GPCRs, are folded in ER lumen with the facilitation of chaperones and quality control system. The properly folded proteins were further modified in Golgi complex, and finally reached cell membrane. The misfolded receptors are usually uquibinated and protelyzed by proteases. In presence of agonists, the surface receptors will be desensitized and internalized with the assistance of lipid raft and caveolin. Mutants of mGluR1 lacking of caveolin binding motif were demonstrated to attenuate mGluR1 coupled ERK-MAPK signaling pathway (64). Several members of mGluRs have been proved to interact with calmodulin (CaM), including mGluR1, mGluR5 and mGluR7. A PKC phosphorylation site (S901) was found in mGluR5. Phosphorylation of this site eliminated CaM binding, thus reducing surface expression of mGluR5 (65). On the other hand, preventing S901 from phosphorylation enhances mGluR5 activity (65). However, the role of CaM binding in mGluR1 is not decided yet. MGluR7 also contains CaM binding site, which is highly conserved in mGluR4A and mGluR8 (66). Similarly, phosphorylation of mGluR7 also prevents CaM binding (67). The accumulating evidence suggests that CaM is the common factor of mGluRs serving as switch of internalization of the receptors.

1.2.5 Drug effects of mGluRs

Up to date, four classes of drugs have been developed targeting mGluRs. Drugs targeting the endogenous ligand binding pocket were called orthosteric modulators, including agonists and antagonists. Usually, orthosteric drugs compete with endogenous ligand for the binding pocket. As discussed before, L-Glu binds to the hinge region of extracellular domain of mGluRs, so the designed orthosteric drugs also target L-Glu binding pocket. Therefore, most of the drugs are modified from L-Glu, we also can call them L-Glu analogs. L-Quis is non-selective agonist of mGluRs, but has strongest potency upon mGluR1. L-Quis can activate mGluRs in absence of extracellular Ca^{2+}. (s)-MCPG is an antagonist applied to Group I mGluRs, which can inhibit L-Glu and Ca^{2+} induced Cl^{-}-Ca^{2+} current (32). Drugs targeting the locations other than orthosteric pocket are called allosteric modulators, containing positive (PAM) and negative modulators (NAM). The allosteric modulators can target to extracellular domain, transmembrane domain or sometimes C tail. Ro 67-4863 is a positive allosteric modulator which binds to transmembrane domain. Ro 67-4863 is unable to activate mGluR1 without Ca^{2+} (68,69). CPCCOEt, known as a negative allosteric modulator, inhibits mGluR1 activity also by binding to transmembrane domain (). However, it's not clear if Ca^{2+} can modulate all these drugs or not.

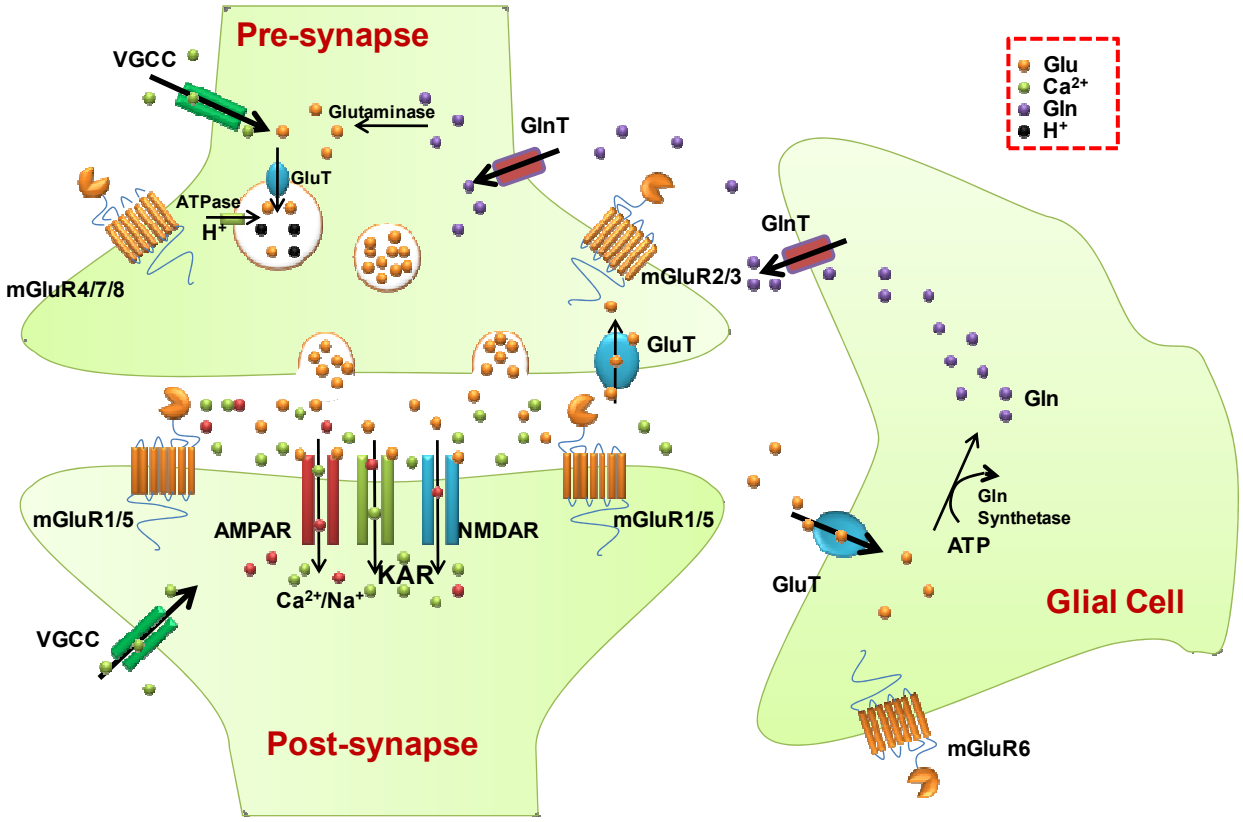

Figure 1-5 The Glutamate cycle in the synaptic cleft. L-Glu was released into synaptic by exocytosis when the presynapse received action potential. The release of L-Glutamate from pre-synapses results in the activation of mGluRs and iGluRs. The ligand-gated ion channels, iGluRs, are opened, leading to an influx of ions such as Ca^{2+} and Na^{+}. Subsequently, the voltage gated Ca^{2+} channel was also opened, thereby resulting in more Ca^{2+} influx. The remaining L-Glu is pumped back to presynapses or glial cells in which L-Glu was converted into L-Gln by L-Gln synthetase. The L-Gln is transported into presynapses, and L-Gln is then oxydased by glutaminase, forming L-Glu which will be packed into vesicles releasing back to synaptic cleft.

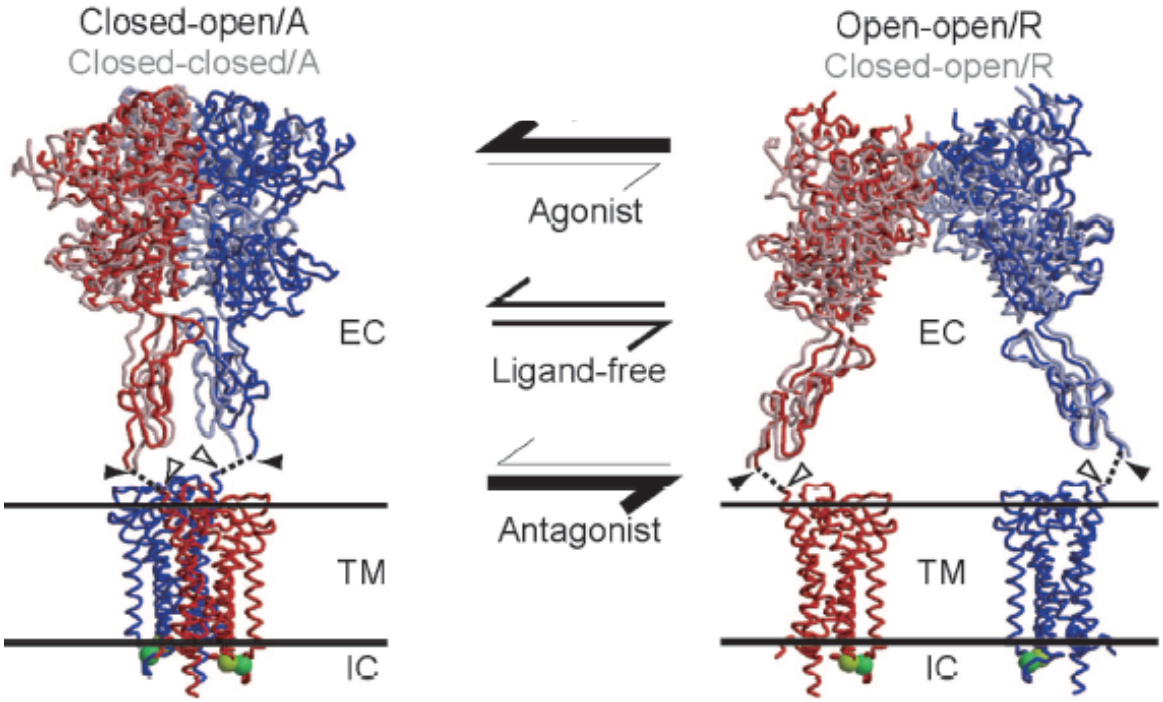

Figure 1-6 Model structure of mGluR1α (97).

The structure of mGluRs consists of a large ligand binding domain (ECD), cysteine rich domain (CR), seven-transmembrane domain (7TM) and C-tail (CT). The receptors were in equilibrium between free and liganding binding form in presence of agonists. Ligand-free or bound with antagonists, the receptors were stated as resting state. While bound with agonists in both protomers in the dimeric receptors, the receptors coupled signaling pathway will be activated due to the conformational change induced by ligand binding.

1.3 Ca^{2+} sensitivity of mGluRs

Ca^{2+} was known to activate mGluR1 independent of glutamate on the physiological level (32). 20 mM Ca^{2+} could induce inward current with the condition that mGluR1α was saturated with 200 μM glutamate, and vice versa. By increasing ex Ca^{2+} from 0.5 mM to 1.5 mM, a transient inward current was detected (32). This suggests Ca^{2+} does activate the process of mGluR1α expressing on oocytes in absent of glutamate. Fransesconi et al. claimed that mGluR1α expressed on HEK cells could sense extracellular Ca^{2+} in absence of glutamate, which was inhibited by Mg^{2+} (70). By removing the extracellular Ca^{2+}, intracellular Ca^{2+} oscillation induced by glutamate through mGluR1α was abolished, while on the HEK293 cells expressing mGluR5, the oscillatory frequency was obviously reduced (71). Another mGluR1 splicing variant, mGluR1d, shares the same ECD as mGluR1α, displaying the extracellular Ca^{2+} dependence for responding to L-Quis, L-Glu, ACPD and DHPG. In the absence of extracellular Ca^{2+}, the potential of mGluR1α to respond to L-Quis was decreased (72). Additionally, mGluR1b displayed the Ca^{2+} sensing property, suggesting the intracellular carboxyl-tail is not related to Ca^{2+} sensing in mGluR1 (70). Native mGluR1α in Pukinje's cells (PCs) shows responses when exposed to Ca^{2+}, but the PCs with mGluR1α knock-out entirely shut down the Ca^{2+} responses. MGluRs were profoundly expressed on synapses with its extracellular domain (ECD) extruding to the synaptic cleft, when the Ca^{2+} concentration in the synaptic cleft has been simulated to around 1.7 mM, the level needed to activate mGluR1α (Ed Brown). To address where the Ca^{2+} could bind to mGluR1, Kubo Y compared the sequences in mGluR subtypes, and found the residue Ser166 was conserved in mGluR1, 3 and 5. However, the residue in mGluR2 was replaced by Asp. The reduction

of Cl- induced inward current by a patch clamp on S166D suggested Ser166 was a key residue for the function of mGluR1 to sense Ca^{2+}, and the cell morphology was affected by this mutant (32). The Ser269 close to the corresponding residue in GABABR was studied, which similarly displayed a key role in Ca^{2+} potential (73). However, when mGluR2 was co-expressed with the chimeric G protein alpha subunit (GqGi3), the IP accumulation was detected when the cells expose to glutamate or Ca^{2+}, and this suggests that some other residues are sensitive to Ca^{2+} besides S166 (74). Silve C also postulated there could be one Ca^{2+} binding site in a hinge region similar to CaSR (44).

On the other hand, Nash et al. raised another consideration, concluding that Ca^{2+} had no effect on an L-quisqualte induced response upon mGluR1 (75). To this point, the reason could be that L-Quis has strong potential to activate the receptor due to its strong binding affinity, around 30 nM, so that Ca^{2+} only contributes a little to the response because of its low binding affinity (3 mM). Simultaneously, using fluorescent microscopy to measure such tiny changes of intracellular Ca^{2+} release is not reliable, and 1.3 mM (or 4 mM) of additional extracellular Ca^{2+} is too low to allow us to see the effects. In addition, the author didn't give evidence for the mGluR1α expression level, although the mGluR1α expression level is related to the response of the receptor. It's risky to compare the responses of two independent cells without seriously considering their expression level of the receptor. All in all, this paper is not solid enough to conclude mGluR1α cannot sense extracellular Ca^{2+}. To further determine the effects of Ca^{2+} upon the functions of the agonists and antagonists of mGluR1α, Selkirk JV et al. expressed ECD-mGluR1α and measured (3H)-L-Quis binding in the presence of 1.3 mM Ca^{2+}. The Ca^{2+} didn't display any effects on L-Quis binding although it showed a

little potential on glutamate binding (76). However, Jingami's group revealed Ca^{2+} showed positive effects on the binding potential of the agonists L-quis and L-glutamate, but negatively modulated the antagonists (s)-MCPG and LY367385 to the purified ECD-mGluR1α by using tryptophan fluorescence and a ligand binding assay (77). To address this controversy, it's important to show more direct evidence for Ca^{2+} binding on this receptor, such as where the Ca^{2+} binds and what is the relationship between Ca^{2+} and the bound ligands. Although S166D was shown as a Ca^{2+} sensitive mutation, introducing the charged residue to the hinge joint closing to the dimer interface in order to influence the Ca^{2+} sensitivity of the receptor is very risky, because the mutations (L116A, I120A and L174A) residing at the dimeric interface of lobe 2 also display the reduction of the Ca^{2+} sensing property (32,78).

With the assistance of computational algorithms developed by our lab, we first found a Ca^{2+} binding site constituted of D318, D322, E325, and the ligand glutamate. Ca^{2+} binding to this site was believed to function as a co-activator of glutamate since Ca^{2+} could enhance the responsiveness of mGluR1 to glutamate and its analogs. Ca^{2+} and glutamate share a common residue, D318. Mutations E325I and D318I almost eliminated the responses of mGluR1α to Ca^{2+}, while D322I significantly attenuated its Ca^{2+} potential. By observing the combination indices, Ca^{2+} and glutamate were found to synergistically activate mGluR1. The Ca^{2+} binding site and co-activation model were further confirmed by a (3H)-L-Quis binding assay. Ca^{2+} enhanced L-Quis binding to the cell pellet with transiently expressed mGluR1α, while D322I eliminated the Ca^{2+} effects. This suggests the Ca^{2+} binds to the Ca^{2+} binding site adjacent to the L-Quis binding pocket to

facilitate L-Quis binding. In spite of the controversy in the past, it's clear that mGluR1 does display as a Ca^{2+} sensing receptor based on the accumulated evidence to date.

1.4 The function of Ca^{2+} in the neuronal system when coupling with mGluRs

Ca^{2+} was known as a versatile ion working as both a first and second messengers. In a synaptic crevice in the central nervous system, the Ca^{2+} concentration was estimated to reach 1.7 mM by computational simulation, while the Ca^{2+} change from 0.5 mM or 1 mM to 1.5 mM could increase the inward Ca^{2+} coupled Cl- current on mGluR1α expressed Xenopus oocytes (32,79). The Ca^{2+} ions in the synaptic cleft were believed to modulate the neurotransmitter releasing from pre-synapses and the plasticity of post-synapses (80). The Ca^{2+} depletion in the synaptic cleft not only suppresses the exocytosis of the neurotransmitter from pre-synapses, but it also leads to a lowering of the post-synaptic efficacy as shown by quantal analysis and mEPSP analysis upon layer 2/3 of a rat visual cortex (80). Furthermore, the Ca^{2+} induced quantal size change of post-synapses was proved to be modulated by mGluR1, because mGluR1 specific allosteric antagonist—CPCCOEt—reduced the quantal size as well as the AP3 (group I mGluR specific antagonist) which was similar to the quantal size reduction caused by decreasing Ca^{2+} from 2.5 mM to 1 mM. On the other hand, the group I mGluR agonist (DHPG) displayed similar quantal size enhancement to the effects by increasing Ca^{2+} from 1 mM to 2.5 mM (80). MGluR1 was known to be widely expressed in the central nervous system, especially in neurons of the globus pallidus, substantia nigra, hippocampus, and lots of the thalamic nuclei which are the foci of chronic neuronal degenerative diseases like Parkinson's and Huntington's. Down-regulation of mGluR1 in globus pallidus and substantia nigra was found in a Parkinsonian monkey model, indicating the

function of mGluR1α in the process of Parkinson's disease is indispensable (81). The mGluR1 antagonist AIDA was suggested to reverse the muscle rigidity and catalepsy in a Parkinsonian model (2,11). Considering if the Ca^{2+} can function as an agonist of mGluR1α which could then neutralize the inhibitory effects of the antagonist, Ca^{2+} will be a very promising co-factor to relieve the severe side effects brought by the antagonists.

1.5 The impact of the Ca^{2+} binding site and co-activation model on drug development

As we noticed, the drug industry put tremendous effort into developing drugs which targeted mGluR1 for treatment of chronic, neuronal, degenerative diseases, but the drugs showed severe side effects. To date, there is no effective drug with light side effects available in the medicine market. As mentioned in Bräuner-Osborne's review, the highly conserved glutamate binding pocket hindered the development of subtype, specific, orthosteric modulators to some extent (82). Thus, the allosteric modulators attracted more and more attention with several, selective, allosteric candidates showing great promise, and thus are entering clinical trials. However, Ca^{2+} as a natural nutrient has its own advantage with low side effects. The molecular basis for Ca^{2+} modulating mGluR1α will open a new avenue for drug development. Firstly, the identified Ca^{2+} binding site can work as a complement for allosteric modulator discovery. Secondly, the effects of Ca^{2+} upon current agonists or antagonists binding to mGluR1α will bring forth new information useful for revising present drugs so that they are more effective or have lower toxicity. Thirdly, because the Ca^{2+} binding site residing at the hinge region which

partially overlapped the glutamate binding pocket is only conserved in group I mGluRs, interest in generating subtype selectively orthosteric modulators will be re-ignited.

1.6 Challenges to the study of metal effects on mGluR1α

Up to now, although seven structures of mGluR1 and mGluR5 were determined by x-ray crystallography, and mGluR1 and mGluR5 were suggested to be Ca^{2+} sensing receptors, no Ca^{2+} was visible in all of the crystals. This is because of the fast on and off-rate of Ca^{2+} due to its low binding affinity. Even if the Ca^{2+} binding sites are addressed, it's difficult to directly measure Ca^{2+} binding affinity, and it's difficult to study how Ca^{2+} plays a role in modulating mGluR1α. The Ca^{2+} binding affinity was estimated to be more than 3 mM. This hindered the ability to obtain binding affinity using direct binding experiments. In the meantime, multiple Ca^{2+} binding sites on the receptor could have cooperativity, thus disturbing the measurement of the function of a single Ca^{2+} binding pocket. Additionally, lots of orthosteric and allosteric drugs were developed to elevate or reduce mGluR1α activity, but the effects of the popular physiological Ca^{2+} ion upon them remain unknown. However, our lab uses a grafting approach coupled with Tb^{3+} LRET to study a continuous Ca^{2+} binding site. This allows us to delve into the intrinsic metal binding property of a single binding site. Tb^{3+}, as an analog of Ca^{2+}, allows us to capture its fluorescence once it binds to the protein along with a potential energy donor. Our lab also developed subdomain and ECD expression, and through the biophysical study on the purified subdomain and ECD could help us understand the Ca^{2+} binding capability of the whole protein. We also use site-mutagenesis and Ca^{2+} dye (fura-2 AM) to determine the effects of mutants on the predicted Ca^{2+} binding sites. Ca^{2+} image and radioactive

labeled L-quis binding assay allow us to measure the effects of Ca^{2+} upon the drugs modulating mGluR1α.

1.7 Hypothesis in this dissertation

Ca^{2+} and L-Glu synergistically activate mGluR1a, and Ca^{2+} can modulate drug effects of mGluR1a by enhancing the potency of agonists and positive allosteric modulators and attenuating the inhibitory effects of antagonists and negative allosteric modulators. In addition, Ca^{2+} also plays a role in receptor folding in ER.

1.8 Approaches and strategies

1.8.1 Prediction of Ca^{2+} binding site using a computational algorithm

The geometry of a Ca^{2+} binding site is known as bipyramidal pentagon. It is known that Ca^{2+} prefers the oxygen atoms from the carbonyl group of the main chain and the side chains of Asp, Glu, Asn, Gln, Ser, Thr and Tyr. Our lab developed computational methods to predict the location of the Ca^{2+} binding site based on the oxygen or carbon cluster extracted from reading X-rays, NMRs, or model structures. The three-dimensional coordinates of the crystal structures of the ECD of mGluR1α were obtained from the Protein Data Bank (PDB) [PDB entries: 1EWT, 1EWK (47), and 1ISR (55)]. Hydrogen atoms were added using the Sybyl 7.2 package (Tripos Inc., St. Louis, USA). The identification of putative Ca^{2+}-binding sites in the ECD of mGluR1α was performed using MUG, a graph theory-based algorithm (83) developed by our laboratory. The Ca-O distance in the software was set to 1.6 – 3.1 Å with a set average cut-off of 2.4 Å (84,85), and the O-O distance was set to 6.0 Å (83). Side chain atoms were rotated to accommodate Ca^{2+}-induced local conformational changes (Wang et al., submitted). Fur-

thermore, electrostatic surface potential maps were constructed using Delphi (86), and GRASP (87) was then used to render and modify the image.

1.8.2 Grafting approach

The continuous fragment containing the predicted Ca^{2+} binding site was grafted into a host protein, CD2. CD2 can tolerate pH change and insertion of foreign proteins. CD2 itself has no metal binding capability. The distance between Trp in CD2 and the inserted putative Ca^{2+} is around 12 Å, which allows the bound Tb^{3+} to accept the energy emitted from the excited Trp. Thus, the Tb^{3+} binding affinity on the engineered protein could be determined by measuring the emission intensity at 545 nm. By using Ca^{2+} competition assay, the Ca^{2+} binding affinity also could be measured. To find out which residues are involved in Ca^{2+} or metal binding, we mutated all the possible oxygen donors (from the side chain) into apolar residues. The residues with lower binding affinity were further tested by in vivo study.

1.8.3 Individual cell image

Intracellular Ca^{2+} mobilization could reflect the activity of mGluR1α, which could be monitored in real time. The ratiometric intensity of fura-2 (F340/F380) indicated Ca^{2+} concentration in the cytoplasm. HEK293 cells transiently expressed mGluR1α, and its mutants were seeded on the cover slip and mounted onto a chamber. The expression of mCherry tagged at the C-terminal of mGluR1α suggests the mGluR1α expression level. The Ca^{2+} increase in cytosol ascribes to the sensitivity of mGluR1α and its mutants to extracellular agonists or antagonists. Thus, the potential of drugs, Ca^{2+}, and mutant effects can be determined by Ca^{2+} imaging.

1.8.4 Radioactive binding assay

Owing to the low binding affinity of the Ca^{2+} of mGluR1α, a direct binding assay using ^{45}Ca was not feasible. To determine the effects of Ca^{2+} upon agonist binding; L-Quis, labeled with tritium, an L-Glu analog with strongest binding affinity, was applied. The radioactive signals, in the presence or absence of Ca^{2+}, were compared. Thus, the Ca^{2+} effects upon L-quis binding can be easily sketched out.

1.8.5 Developing an ER Ca^{2+} sensor using mCherry as a scaffold protein

Small organic dyes such as fura-2 AM and fluo-x were widely applied to monitor the intracellular Ca^{2+} release from ER (22). However, the small dyes usually diffuse to unexpected loci or were rejected by living cells, and therefore were pumped out over the long term. Thus, the sensitivity and resolution of Ca^{2+} change measured by small organic dyes is low. To specifically monitor the Ca^{2+} release in ER, we use mCherry as the scaffold protein in order to design a Ca^{2+} sensor which can be anchored in the ER lumen. A Ca^{2+} binding pocket will be constructed at a chromophore sensitive site using site-directed mutagenesis.

1.9 Objectives of this study

The objectives of this work are: to illustrate the roles of Ca^{2+} on mGluR1α, including the Ca^{2+} binding sites determination, to show the effects of Ca^{2+} on drug binding and modulation, and to show the effects of Ca^{2+} on mGluR1α trafficking.

1.9.1 Predicting and studying Ca^{2+} binding sites of mGluR1α

Using computational algorithms developed by our lab, four Ca^{2+} binding sites were predicted in the ECD of mGluR1α based on several crystal structures. Site 1 is a

continuous site adjacent to an L-Glu binding pocket and was investigated using a grafting approach and individual cell image assay using computational algorithms developed by our lab associated with site-mutagenesis. Site 2 and Site 3 was also studied using a grafting protein. As for Site 4, the residues contributing to Ca^{2+} binding are not continuous, so its Ca^{2+} sensing property is determined using an individual cell image.

1.9.2 Studying the co-activation of mGluR1α by Ca^{2+} and L-Glu

It's well known that L-Glu and Ca^{2+} can respectively activate mGluR1α, but little was understood how L-Glu and Ca^{2+} function when both are present. In our work, we measured the activation of L-Glu and Ca^{2+} in relation to mGluR1α. We also determined the L-Glu potential in the presence of different Ca^{2+} concentrations. In addition, the Ca^{2+} sensitivity of mGluR1α in the presence of L-Glu was observed. The co-activation model was developed by analyzing the relationship of L-Glu and Ca^{2+} in activating mGluR1α.

1.9.3 Investigating the effects of Ca^{2+} upon drugs modulating mGluR1α

The role of Ca^{2+} on three classes of drugs was investigated. L-Quis (orthosteric agonist), (s)-MCPG (orthosteric antagonist) and CPCCOEt (allosteric modulator) induced intracellular Ca^{2+} increases were measured in the presence or absence of extracellular Ca^{2+}.

1.9.4 Investigating the function of Ca^{2+} in the process of mGluR1α trafficking

We used thapsigargin to deplete ER Ca^{2+} and detected mGluR1α surface expression using flow cytometry. The role of Ca^{2+} in the stability of the receptor was studied by measuring the thermal stability of purified ECD-mGluR1α using circular dichroism (CD).

1.9.5 Developing an ER Ca^{2+} sensor using mCherry as the scaffold protein

Two Ca^{2+} binding sites were engineered to the chromophore sensitive sites. By tagging them with KDEL and ER targeting sequence of calreticulin (CRsig), the sensor could be specifically expressed in the ER lumen. The Ca^{2+} binding results in a fluorescence change so that ER Ca^{2+} could be monitored in real time.

1.10 Summary of variants generated in this dissertation

Table 1-1 Summary of variants created in terms of mGluR1α

Variants	Vector	Tag	Role
pcDNA-mGluR1-mCherry	pcDNA1.1	Flag	mGluR1 with mCherry reporter
Y74A	pcDNA1.1	Flag	Mutation of L-Glu binding site
D92I	pcDNA1.1	Flag	Mutation of Ca^{2+} binding site 2
S165A	pcDNA1.1	Flag	Mutation of L-Glu binding site
S166A	pcDNA1.1	Flag	Mutation of reported Ca^{2+} sensitive site
S166D	pcDNA1.1	Flag	Mutation of reported in Kubo's science paper
T188A	pcDNA1.1	Flag	Mutation of L-Glu binding site
S186A	pcDNA1.1	Flag	Mutation of L-Glu binding site
Y236F	pcDNA1.1	Flag	Mutation of L-Glu binding site
D318I	pcDNA1.1	Flag	Mutation on both Ca^{2+} binding site and L-Glu binding site
D322I	pcDNA1.1	Flag	Mutation of Ca^{2+} binding site 1

E324I	pcDNA1.1	Flag	Mutation adjacent to Ca^{2+} binding site 1
E325I	pcDNA1.1	Flag	Mutation of Ca^{2+} binding site 1
E328I	pcDNA1.1	Flag	Mutation adjacent to Ca^{2+} binding site 1
N335I	pcDNA1.1	Flag	Mutation adjacent to Ca^{2+} binding site 1
K409A	pcDNA1.1	Flag	Mutation of L-Glu binding site
CD2.D1	pGEX-2T		CD2 with grafted Ca^{2+} binding site 1
CD2.D1-1	pGEX-2T		CD2.D1 with E331I/E333I
CD2.D1-2	pGEX-2T		CD2.D1 with D324I/E325I
CD2.D1-3	pGEX-2T		CD2.D1 with D318I/D322I
CD2.D1-4	pGEX-2T		CD2.D1 with E328I/N335I

Table 1-2 Summary of generated other variants

Variants	Vector	Role
pGEM-172C2	pGEM-4Z	Recombined with EGFP grafting sensor using Spe I for CPFP screening
WT-ER	pcDNA3.1(+)	WT mCherry with ER signal peptide
WT-Ct	pcDNA3.1(+)	WT mCherry expressing in cytosol
MC-D1ER	pcDNA3.1(+)	MC-D1 with ER signal peptide
MC-D1Ct	pcDNA3.1(+)	MC-D1 expressing in cytosol
MC-D2ER	pcDNA3.1(+)	MC-D2 with ER signal peptide
MC-D2Ct	pcDNA3.1(+)	MC-D2 expressing in cytosol

2 MATERIALS AND EXPERIMENTS

2.1 Materials and supplies

L-Quis, (s)-MCPG and CPCCOEt were purchased from Tocris, UK. (3H)-L-quisqualae was bought from PerkinElmer. L-Glutamate was ordered from Sigma. Alexa 488 secondary antibody was purchased from Invitrogen. PcDNA1.1-mGluR1α tagged with Flag was provided by Dr. Randy Hall at Emory University. A site-directed mutagenesis kit and a miniprep plasmid extraction kit were bought from Strategene. A IP1 ELISA kit was purchased 0from Cisbio.

2.2 Materials and Methods

2.2.1 Structural modeling, autodocking, and Ca^{2+}-binding sites prediction

2.2.1.1 Dock L-Quis to ECD-mGluR1α using Autodock-vina and hinge motion analysis.

To elucidate L-Quis's binding on the extracellular domain of mGluR1α, L-Quis was docked into the crystal structure (1EWK). After removing the coordinates of the bound ligand, glutamate, the pdb file was loaded into Autodock tools to add polar hydrogen atoms and decide the docking center and grid box. The docking work was carried out by the newest version Autodock tool – Vina. The binding residues were analyzed by measuring the atoms within 6 Å of L-Quis. The hinge region of the glutamate and the (s)-MCPG binding were analyzed using Dymdon. The dihedral angles of the residues residing at the hinge joint were calculated using xxx.

2.2.1.2 *Computational Prediction of Ca^{2+}-binding Sites in mGluR1α and Molecular Modeling*

The three-dimensional coordinates of the crystal structures of the ECD of mGluR1α were obtained from the PDB (PDB entry codes: 1EWT, 1EWK (15), and 1ISR (14)). Hydrogen atoms were added using the Sybyl7.2 package (Tripos Inc., St. Louis, MO). The identification of putative Ca^{2+}-binding sites in the ECD of mGluR1α was performed using MUG, a graph theory-based algorithm (21) developed by our laboratory. The Ca–O distance in the software was set to 1.6–3.1 Å with a set average cutoff of 2.4 Å (26, 27), and the O–O distance was set to 6.0 Å (21). Side chain atoms were rotated to accommodate Ca^{2+}-induced local conformational changes (48). Furthermore, electrostatic surface potential maps were constructed using Delphi (28), and GRASP

(29) was then used to render and modify the image. The linear, putative Ca^{2+}-binding site was added into the scaffold protein CD2 between Ser-52 and Gly-53 with triple Gly linkers at both ends, and the combined grafting model was generated by Modeler 9v4 (30).

2.2.2 Protein expression and purification

2.2.2.1 Express and purify ECD-mGluR1 using E. coli (C43).

The cDNA of ECD-mGluR1 was subcloned into the pRsetB vector. The C43 cell strain was used to express ECD-mGluR1. Protein expression was induced by 200 μM ITPG as soon as the OD value reached approximately 1.2. After a four hour expression, the bacteria were collected and broken using a cell disrupter. The filtered supernatant was purified using Histag beads as described above.

2.2.2.2 The Expression and Purification of of Engineered Proteins—CD2.D1 and its variants with double mutations

The predicted linear Ca^{2+}-binding site, termed mGluR1-1, resides between Gly-316 and Gly-337 (GSDGWADRDEVIEGYEVEANGG). This sequence, grafted into CD2 between Ser-52 and Gly-53 in the plasmid pGEX-2T-CD2 (31), was named CD2.D1. The engineered protein was expressed as a GST fusion protein and purified using GS4B resin as described (32). Site-directed mutagenesis was performed using the multisite-directed mutagenesis kit (Stratagene, Cedar Creek, TX).

2.2.3 Determine biophysical properties of purified proteins using circular dichroism, fluorimetry and NMR

2.2.3.1 Determine Trp fluorescence of ECD-mGluR1 upon binding L-Glu, Ca^{2+} or (s)-MCPG.

The intrinsic Trp fluorescence change reflects the environmental change of Trp buried in the protein. The conformational change induced by ligand binding usually influences the local environment of certain Trp residues. The purified ECD-mGluR1α was resolved in a buffer with 20 mM HEPES, 50 mM NaCl (pH 7.4). The final protein concentration was 2 μM. The emission ranging from 300 to 400 nm was collected while Trp was excited at 280 nm.

2.2.3.2 Conformational analysis of engineered protein CD2.D1 and its variants using circular dichroism, Trp fluorescence, and NMR.

Far UV CD spectra were acquired from 190 to 260nm on a JASCO-810 circular dichroism spectropolarimeter. All spectra were the average of ten scans with a scan rate of 100 nm/min. All the measurements were carried out in a buffer consisting of 10 mM Tris-HCl. The secondary structural content of each sample was calculated using the program DICHROWEB (88).

Fluorescence spectra were acquired using a PTI lifetime fluorimeter at ambient temperature with a 1 cm path-length quartz cuvette. Intrinsic tryptophan emission spectra of protein samples were recorded from 300 to 400 nm with excitation set at 282 nm. The slit widths were set at 3.5 and 5 nm for excitation and emission, respectively. Protein samples (3.0 μM) were prepared in 20 mM PIPES-10 mM KCl at pH 6.8.

1D 1H NMR experiments were performed using a Varian Inova 500-MHz spectrometer. Spectra were acquired with a spectral width of about 13 ppm at 25 °C. NMR samples were prepared by dissolving 0.1 mM of protein in a Tris buffer at pH 7.4. NMR data were processed using FELIX 98 (Accelrys). The metal binding characteristics of CD2.D1 were examined using the same settings and conditions, titrating with 1 mM and 2 mM La^{3+}.

2.2.4 Tb^{3+} Titration and Ca^{2+} Competition

In Trp-sensitized Tb^{3+}-LRET experiments, emission spectra from 500 to 580 nm were recorded with excitation set at 282 nm; slit widths were set at 8 nm for excitation and 12 nm for emission. A glass filter with a cutoff of 320 nm was utilized to circumvent secondary Rayleigh scattering. Tb^{3+} titration and metal competition assays were performed as described previously (24). 500 mM K^{+}, 10 μM La^{3+}, 10 μM Gd^{3+}, 1 mM Mg^{2+}, and 1 mM Ca^{2+}, respectively, were used to selectively compete with Tb^{3+}. Each experiment was carried out independently in triplicate.

2.2.5 Constructs, site mutagenesis, and expression of mGluR1α variants.

The red fluorescent protein, mCherry, was genetically tagged to the C-terminal of mGluR1α by a flexible linker—GGNSGG.(89) The point mutations were carried out using a site-directed mutagenesis kit (Strategene). HEK293 cells were seeded and cultured on glass coverslips. MGluR1α and its mutants were transfected into cells utilizing lipofectamine 2000 (Invitrogen). The cells then were incubated for two additional days, so that mGluR1α and its mutants were expressed at sufficient levels. Cells were fixed on the coverslips with 4% formaldehyde, and nuclei were stained with DAPI. The expression of mGluR1α and its variants were detected by measuring red fluorescence using confocal microscopy.

2.2.6 Quantitatively Determined Membrane Expression of the mGluR1α Mutants Using Flow Cytometry

PcDNA-mGluR1α (donated by Dr. Randy Hall's laboratory) contained a FLAG tag at the N terminus of the receptor, and mCherry was genetically fused to the C terminus with a linker, GGNSGG. After 2 days of transient expression of mGluR1α and its mutants (D318I, D322I, E325I, and N335I) in HEK293 cells grown on polylysine-coated dishes, cells were incubated in 1x phosphate-buffered saline (PBS) supplemented with 1/1000 anti-FLAG and 1/100 fetal bovine serum (FBS) at 4 °C. The cells were then washed three times with 1x Tris-buffered saline (TBS) and fixed using 4% formaldehyde at room temperature for 15 min. After being washed three times with 1x TBS, the receptors on the cell surface were then labeled with Alexa Fluor® 488 goat anti-mouse IgG (Invitrogen) for 30 min at 37 °C. The cells were then collected in 1x PBS, and the intensities of green and red fluorescence were measured using LSRFortessa (BD Biosciences). The ratios of green and red fluorescence from mGluR1α and the mutated receptors were normalized to the amount of receptors expressing on the cell surface relative to the total receptors (total cellular expression of receptor). Data were collected from three dishes.

2.2.7 Measurement of $[Ca^{2+}]_i$ Responses of mGluR1α and Its Mutants using Ca^{2+} indicator—Fura-2 AM

2.2.7.1 Measurement of $[Ca^{2+}]_i$ Responses of mGluR1α and Its Mutants with or without $[Ca^{2+}]_o$ or Glu

Measurement of $[Ca^{2+}]_i$ was performed as described (24). In brief, wild type mGluR1α and its mutants (D318I, D322I, D324I, E325I, and E328I) were transiently transfected into HEK293 cells and cultured for 2 additional days. The cells on the coverslips were subsequently loaded using 4 μM Fura-2 AM in 2 ml of physiological saline buffer (10 mM HEPES, 140 mM NaCl, 5 mM KCl, 0.55 mM $MgCl_2$, and 1 mM $CaCl_2$, pH 7.4). The coverslips were mounted in a bathing chamber on the stage of a fluorescence microscope. Fura-2 emission signals from single cells excited at 340 or 380 nm were collected utilizing a Leica DM6000 fluorescence microscope in real time as the concentration of extracellular Ca^{2+} was increased in a stepwise manner. The ratio of emitted fluorescence at 510 nm resulting from excitation at 340 or 380 nm was further analyzed to obtain the intracellular Ca^{2+}response as a function of changes in $[Ca^{2+}]_o$. Then, the sensitivity of mGluR1α and its mutants (D322I, D324I, E325I, and E328I) to extracellular glutamate was measured by increasing the extracellular glutamate concentration in the presence of 1.8 mM Ca^{2+}. The glutamate concentrations at which the intracellular Ca^{2+} responses of mGluR1α and its mutants were first observed, and subsequently saturated, were determined. Moreover, to further characterize the influence of $[Ca^{2+}]_o$ to Glu-induced $[Ca^{2+}]_i$ release through wild type mGluR1α, an additional 5 or 10 mM Ca^{2+} was added to the perfusate. $[Ca^{2+}]_i$ was measured as described above during changes in $[Ca^{2+}]_o$ and/or Glu.

2.2.7.2 Measurement of Intracellular Ca^{2+} Release Mediated by mGluR1α and Its Mutants in the Presence of Extracellular Gd^{3+}

Changes in $[Ca^{2+}]_i$ in response to the addition of Gd^{3+} were determined as just described. Specifically, cells were incubated in an incubation buffer (140 mM NaCl, 4 mM KOH, 10 mM HEPES, 1.5 mM $CaCl_2$, 1 mM $MgCl_2$, 10 mM glucose, pH 7.4) for up to 1.5 h, and Gd^{3+} (made up in 140 mM NaCl, 4 mM KOH, 10 mM HEPES, and 0.3 mM $MgCl_2$, pH 7.4) was added at the concentrations described under "Results." The $[Ca^{2+}]_i$ responses of mGluR1α after the introduction of mutations in the Glu-binding site were measured similarly.

2.2.7.3 Determining the effect of $[Ca^{2+}]_o$ on activation of mGluR1α and its mutants by L-Quis.

Measurement of $[Ca^{2+}]_i$ was performed as described (46). In brief, wild type mGluR1α was transiently transfected into the cells and cultured for two additional days. The cells on the coverslips were subsequently loaded using 4 μM Fura-2 AM in 2 mL physiological saline buffer (10 mM HEPES, 140 mM NaCl, 5 mM KCl, 0.55 mM $MgCl_2$, 1 mM $CaCl_2$ and pH 7.4) for 30 mins. The coverslips then were mounted in a bathing chamber on the stage of a fluorescence microscope. Fura-2 emission signals from single cells excited at 340 or 380 nm were collected utilizing a Leica DM6000 fluorescence microscope in real time as the concentration of L-Quis was progressively increased in the presence or absence of extracellular Ca^{2+}. The ratio of emitted fluorescence resulting from excitation at 340 or 380 nm was further analyzed to obtain the intracellular Ca^{2+} response as a function of changes in L-Quis. Only the individual cells with mCherry expressed were selected for analysis.

2.2.7.4 Measurement of $[Ca^{2+}]_i$ responses of mGluR1α to $[Ca^{2+}]_o$ or Glu in presence of 0.5 mM s-MCPG.

The methods to measure intracellular Ca^{2+} mobilization were described above. In the presence of (s)-MCPG, the cells were incubated with 0.5 mM (s)-MCPG in a saline buffer for 30 more minutes after Fura-2 loading. Then, the sensitivity of mGluR1α to extracellular Ca^{2+} or glutamate was measured either by increasing the extracellular Ca^{2+} or the glutamate concentration in the presence of 1.8 mM Ca^{2+}, or by increasing extracellular Ca^{2+} in a saline buffer with or without 0.5 mM (s)-MCPG. The glutamate concentrations at which the intracellular Ca^{2+} responses of mGluR1α were measured when first observed and then when saturated.

2.2.7.5 Determining the effects of $[Ca^{2+}]_o$ on the potency of Ro 67-4853 to mGluR1α.

As described above, Fura-2AM was used for monitoring cytosolic Ca^{2+} in real time. Ro 67-4853 was unable to potentiate mGluR1α in absence of L-Glu (ref, jeff conn). To obtain intracellular Ca^{2+} readout, HEK293 cells expressing mGluR1α were pre-incubated with 0.5 mM Ca^{2+} and 5 nM Ro 67-4853 for more than 10 minutes. Cells loaded with Fura-2AM were mounted onto a chamber perfused with saline buffer. By increasing concentration of Ro 67-4853 in presence of 0.5 mM and 1.8 mM Ca^{2+}, re-spectively, cytosolic Ca^{2+} was record by ratiometric change of fura-2AM upon binding with Ca^{2+}. The effect of Ca^{2+} was analyzed by comparing the intracellular Ca^{2+} release by Ro 67-4853 in different concentration of Ca^{2+} in perfusion buffer.

2.2.7.6 Measurement of $[Ca^{2+}]_i$ responses of mGluR1α to $[Ca^{2+}]_o$ or Glu in presence of CPCCOEt.

The methods to measure intracellular Ca^{2+} release were mentioned above. After the coverslip was mounted to the microscope, the cells were perfused with a saline buffer containing 0, 5 or 40 μM CPCCOEt for more than 10 mins. Increasing concentrations of extracellular Ca^{2+} or Glu were added into the chamber in the presence of a varying concentration of CPCCOEt.

2.2.8 Determining the effect of $[Ca^{2+}]_o$ on (^{3}H)-L-Quis binding to mGluR1α and its mutants.

HEK293 cells transiently transfected with wild type mGluR1α and its mutants were maintained in a 5% CO_2 37^{o}C incubator for an additional 48 hours. Cells then were collected in ice cold hypotonic buffer (20 mM HEPES, 100 mM NaCl, 5 mM $MgCl^2$, 5 mM KCl, 0.5 mM EDTA, 1% protease inhibitor at pH 7.0-7.5). The cell pellet was further washed twice using hypotonic buffer to remove the glutamate in the cell debris. The crude membrane protein (100 μg) was mixed with 30 nM (^{3}H)-L-Quis in 100 μL of hypotonic buffer. The nonspecific binding was determined with addition of 200 μM glutamate. To study the effects of Ca^{2+} on L-Quis binding to mGluR1α, increasing concentrations of Ca^{2+} were applied. The reaction mixtures were incubated on ice for more than 1 hour, and the membrane bound with (^{3}H)-L-Quis was captured on the filter paper when flowing through a Brandel cell harvestor by vacuum. The filter paper was transferred to scintillation fluid and the radioactive signal was detected using a Beckman LS 6500 multi-purpose scintillation counter.

2.2.9 Measurement of IP one accumulation using an IP ONE kit.

To normalize the IP one readout, cells which were transfected with the receptors were re-seeded in a 24-well plate with the density of 80,000 cells per well. The transfection rate was measured using flow cytometry on parallel prepared dishes. The procedure followed the protocol provided by the IP one ELISA kit. In brief, the cells in the wells were treated with Ca^{2+}, Glu in the presence or absence of 0.5 mM (s)-MCPG. After one hour stimulation, the cells were lysed and the lysate was transferred onto a pre-coated ELISA plate. The plate was then treated with the reagents in the kit and washed for the plate reader. To minimize the effect of the proliferation rate on different mutations, the IP1 concentration was normalized by whole protein concentration of the cell lysate.

2.2.10 Data Analysis and Curve Fitting

At each agonist concentration, all of the transfected cells in the microscopic field from three independent experiments were selected for analysis, and at least 60% of the cells displaying normal responses were analyzed. The cells that did not respond to the agonists or displayed a sigmoidal curve with a stable plateau after treatment with high $[Ca^{2+}]_o$ were excluded. These latter cells exhibited a constant, high plateau of the intracellular Ca^{2+} concentration, perhaps because the plasma membrane was excessively permeable to Ca^{2+}. To normalize the concentration response curves for the responses to $[Ca^{2+}]_o$, the maximal response of wild type mGluR1α to extracellular Glu was set at 100% so that the maximal responses of mutant receptors to $[Ca^{2+}]_o$ or Glu were transformed into percentages relative to the response of WT mGluR1α to Glu. Data were fitted using the Hill equation as described previously (23).

2.2.11 Analysis of the electrostatic potential of mCherry

Our lab uses Delphi and GRASP to calculate the electrostatic potential of mCherry. A PDB file (2H5Q) of mCherry was downloaded from a protein data bank, and hydrogen was adding onto it by Sybyl7.2. Delphi respectively defines the salt concentration, interior and exterior dielectric constants as 0, 2, and 80, and the Poisson Boltzmann equation was imposed until convergence was reached. Then GRASP constructed the electron surface of the protein in the presence of hydrogen.

2.2.12 Screening mutations without losing fluorescence of mCherry

Some residues of mCherry are not essential to its protein folding and chromophore maturation. Mutations on these residues could change the fluorescent features

but not eliminate the fluorescence of the protein. The residues away from the chromophore interacting sites were selected to either add or remove charges in order to disturb the local electrostability. All the mutations were randomly picked.

2.2.13 Design of Ca^{2+}-binding pockets on chomophore sensitive locations of mCherry

As described in Shen Tang's article, Ca^{2+}-binding to the chomophore interactive residues have a high potential to produce fluorescence change. By analyzing the crystal structure (2H5Q), it can be seen that R95, S146, Y181, and E215 directly interact with the chromophore of mCherry, and E144 and L199 contact the chromophore through a water molecule. W143-S146 is a short loop with high solvent accessibility which can tolerate mutations. In our previous studies, we designed a series of variants with Ca^{2+}-binding properties on CD2. The rationale of designing a Ca^{2+}-binding site on CD2 was applied to mCherry. The mutations were performed using a Quickchange, multiple site-directed, mutagenesis kit (Stratagene).

2.2.14 Expression and Purification of mCherry and its mutants

Mutants were made by using a multi-site directed mutagenesis kit, which can make more than 5 mutants in one step in only one day. mCherry and its mutants in the pRsetB was transformed into BL21plys competent cells, and then a single round-shaped clone was chosen to incubate in LB medium with ampicillin. After shaking overnight in 37^{o}C, the medium was transferred into 4L of LB with ampicillin. When the OD600 reached around 1.2, ITPG was used to induce expression of mCherry proteins. The bacteria were collected and pressed using a French Press. The proteins were puri-

fied using a nickel column by FPLC. Purified proteins were dialyzed in a Tris buffer for more than 12 hours.

2.2.15 pH profiles of mutants K198D of mCherry

A new putative Ca^{2+}-binding pocket, which contains E144, K198D, D200, Y214E, and R216E, was designed by mimicking the pocket on a CD2 variant 7E15. Purified protein was solubilized in sodium citrate (pH=4.5), sodium acetate (pH=5), tris-HCl (pH= 6.5, 7.4, 8.5 and 9), and CAPSO (pH=10). The excitation maximum and emission maximum of protein in the above buffers were measured under λ_{ex}=587 nm and λ_{em}=608 nm.

2.2.16 Ca^{2+} titration of MC-D1

The protein was prepared in Tris-HCl with a pH= 7.11 and 8.44 which belong to the pH independent range. The emission spectrum and excitation spectrum were scanned with progressively increasing Ca^{2+} concentrations in the buffer. The Ca^{2+} was prepared in a 10 mM Tris-HCl buffer with a pH=7.4, eliminating any pH effect on the titration experiments.

2.2.17 Ca^{2+} sensing properties of mCherry sensor candidates

The excitation maximum and emission maximum were scanned by Felix fluorometry. The emission scan was excited at 587 nm, while the emission was set to 610 nm for the excitation spectrum scanning. The secondary structure of mCherry protein was assessed by its CD spectrum. The corresponding responses of MC-D1 and MC-D2 upon addition of Ca^{2+} were measured by assessing the excitation or emission peaks in the presence of Ca^{2+}.

3 ELUCIDATION OF A NOVEL EXTRACELLULAR CALCIUM-BINDING SITE ON METABOTROPIC GLUTAMATE RECEPTOR 1α (MGLUR1α) THAT CONTROLS RECEPTOR ACTIVATION

3.1 Introduction

Metabotropic glutamate receptors (mGluRs) have key functions in a variety of different neurological processes, including memory, learning, pain, synaptic plasticity, and the control of the activity of various circuits throughout the brain (50). The mGluRs belong to family C of the large superfamily of G protein-coupled receptors (GPCRs). Family C GPCRs (also referred to as family 3 GPCRs, the nomenclature that will be utilized here) also include the Ca^{2+}-sensing receptor (CaSR), GABAB receptors, taste receptors, and putative pheromone receptors (90). All members of the family 3 GPCRs share similar domain architecture, including venus flytrap-like extracellular domains (ECD), heptahelical transmembrane domains, and intracellular C-terminal C-tails. The mGluRs fall into three groups and eight subtypes. Group I comprises mGluR1 and mGluR5 (91). MGluR1 is expressed mainly around a core of ionotropic glutamate receptors in the postsynaptic densities of neurons and functions as a disulfide-linked homodimer (52). Upon activation by its agonists, the intracellular domains of the group I mGluRs associate with the G protein Gq/11 to activate phospholipase C, which subsequently converts phosphatidylinositol bisphosphate (PIP_2) to diacylglycerol and inositol trisphosphate (IP_3), thereby releasing Ca^{2+} from the endoplasmic reticulum, as well as activating protein kinase C (PKC) and other downstream effectors (92).

The issues of whether mGluRs respond to extracellular calcium ($[Ca^{2+}]_o$) and how calcium binding modulates the family 3 GPCRs have attracted extensive investigation. On the basis of sequence homology to CaSR, mGluRs were postulated to be capable of responding to $[Ca^{2+}]_o$. $[Ca^{2+}]_o$ has been proposed to either activate mGluR1 directly or to act as a positive mGluR1 modulator (32,93). Kubo et al. (32,94) reported that $[Ca^{2+}]_o$, as well as Glu, can trigger intracellular responses elicited by mGluR1, mGluR3, and mGluR5. $[Ca^{2+}]_o$ or Gd^{3+} further stimulate the activity of mGluR1α even after saturation of the Glu response and vice versa (32). In addition, mGluR1α responds to 5 mM $[Ca^{2+}]_o$ in Purkinje cells prepared from global mGluR1α knock-out mice in which the receptor has been specifically knocked into Purkinje cells, whereas the Purkinje cells from the mGluR1α global knock-out mice themselves cannot sense $[Ca^{2+}]_o$ (95,96). On the basis of these studies, $[Ca^{2+}]_o$ is postulated to mediate postsynaptic efficacy through its action on mGluR1 (80). Moreover, Glu triggers $[Ca^{2+}]_i$ oscillations in a manner that is modulated by $[Ca^{2+}]_o$ (71), as R, 5-3, 5-Dihydroxylphenylglycine, an agonist of group I mGluRs, generated inward currents that were enhanced by $[Ca^{2+}]$o (95). In contrast, Nash et al. (75) concluded that mGluR1α is not a calcium-sensing receptor because its response to the agonist L-Quis is not sensitive to $[Ca^{2+}]_o$. However, the effect of $[Ca^{2+}]$o on the EC_{50} for L-Quis was not examined. Any putative Ca^{2+}-binding sites capable of regulating mGluR signaling remain "invisible" in six crystal structures of the ECD of mGluR1α determined to date (47,55), as well as the ECDs and cysteine-rich domains of mGluR3 and mGluR7 (47,97). One Gd^{3+} ion binds to mGluR1 between the helices of lobe 2 (LB2) at the dimer interface of the ECD, far from the Glu-binding site (55,98). Removing the Gd^{3+}-binding residue, E238Q, eliminated sensitivity to Gd^{3+} but not sensi-

tivity to [Ca^{2+}]o and Glu (56,98). Two Gd^{3+} ions visible in the crystal structure were ignored by these authors, although one of them is located near the critical hinge region coordinated by Asp-322, Asp-324, and Asp-493 (55). This observation also suggests strongly that a Ca^{2+} ion could bind to this region of the protein. The invisibility of Ca^{2+}-binding sites in the x-ray structures of the mGluRs represents a major challenge shared among other Ca^{2+}-modulated proteins functioning at high Ca^{2+} concentrations, like those in the extracellular fluids, due to their low Ca^{2+}-binding affinities (Kd, ~0.1–1.5 mM) and irregular binding geometries (99). Our understanding of the role of Ca^{2+} as an extracellular signal acting via family 3 GPCRs beyond CaSR is severely hampered by the lack of adequate information about the location and properties of the Ca^{2+}-binding sites of this class of proteins.

We report herein the identification of a novel Ca^{2+}-binding site adjacent to the Glu-binding site in the hinge region of the ECD of mGluR1α (47,55), which was found by using our recently developed ~~the~~ MUG (multiple geometries) algorithm (83,100,101). MUG is a graphic geometry-based Ca^{2+}-binding site prediction software. It extracts oxygen clusters from Protein Data Bank (PDB) files and assumes a Ca^{2+} center for each cluster. The clusters then are verified by setting parameters for geometric filters that define the range of distance between oxygen atoms and Ca^{2+}. The clusters satisfying the parameter setting were considered candidates for Ca^{2+}-binding pockets. The putative Ca^{2+}-binding pockets of lower quality were further modified by allowing rotation of the side chains of predicted liganding residues. To investigate a single Ca^{2+}-binding site present within a short stretch of amino acids, normally less than 30 residues, we engineered the short loop into a scaffold protein, CD2. Intact CD2 does not bind Ca^{2+} and is tolerant of

site-directed mutagenesis without undergoing changes in its overall structure. Then the metal-binding capabilities of the key predicted Ca^{2+}-binding residues were further characterized using luminescence energy transfer (LRET) and site-directed mutagenesis (45,46). Finally, we investigated the intracellular Ca^{2+} responses resulting from the binding of $[Ca^{2+}]_o$, $[Gd^{3+}]_o$, or Glu individually or of both $[Ca^{2+}]$o and Glu together by expressing wild type and mGluR1α variants with predicted ligand residues mutated. Our studies suggest that Asp-318, Asp-322, and Glu-325 at the predicted site are involved in Ca^{2+}-binding and that mutation at Asp-318 and Glu-325 also abolishes responsiveness of the receptor to $[Gd^{3+}]_o$. The ligands for Glu binding, in contrast, although also including Asp-318, are otherwise distinct (47,55,78). Notably, the carboxylate group of the side chain of Glu also contributes to the binding site for Ca^{2+}. We propose a dual activation mechanism whereby the simultaneous binding of Glu and Ca^{2+}, at their separate but partially overlapping binding sites, potentiates one another's actions to yield maximal activation of mGluR1

3.2 Results

3.2.1 Prediction of a Novel Ca^{2+}-binding Site Adjacent to the Glu-binding Site in the ECD of mGluR1α

We recently developed the computational algorithm MUG, which predicts Ca^{2+}-binding sites using graph theory by identifying all possible liganding oxygen clusters and finding maximal cliques. The positions of Ca^{2+} and its liganding groups in 144 calcium-binding proteins can be predicted with 0.22–0.49 Å accuracy by geometric filters established on the basis of an extensive survey of known Ca^{2+}-binding sites in the Protein

Data Bank (99). To accommodate Ca^{2+}-induced conformational changes, the side chains of putative Ca^{2+}-binding ligand residues were subjected to rotation using a rotamer library (MUGSR) (102). Fig. 3-1 shows one predicted Ca^{2+}-binding site identified here in the crystal structure of the mGluR1$_a$ ECD (PDB entry code: 1EWK) using the MUG algorithm. Two other predicted sites not included in this report were also revealed by MUG, one of them (site 2) residing in the Mg^{2+}-binding pocket (Leu-86—Gly-102) inferred from the crystal structure and the other one located within a long loop (Asp-125—Lys-153) that was invisible in the crystal structure because of its high flexibility and was repaired using Modeler (103). The third predicted Ca^{2+}-binding site (site 3), encompassing Ser-129 to Gly-144, was present within this missing loop.

The predicted Ca^{2+}-binding site studied in detail here comprises the carboxyl side chains of Asp-318 and Glu-325, the main chain carbonyl Asp-322 in a flexible loop of mGluR1$_a$, and the carboxyl side chain of Glu-701 (a ligand for glutamate). This predicted Ca^{2+}-binding site is located at the hinge region in the ECD adjacent to the reported Glu-binding site (Arg-74, Ser-165, Thr-188, Asp-208, Tyr-236, Asp-318, and Lys-409) (15, 25), with Asp-318 predicted to be involved in both Glu and Ca^{2+}-binding. Thus, Ca^{2+} and Glu, when bound to the receptor, both bind to Asp-318. Asp-318 and Asp-322 can be identified in the Glu-free form (PDB entry code: 1EWT), whereas the direct binding of Ca^{2+} to the carboxyl side chain of the agonist Glu-701 is visualized only in the Glu-loaded form (PDB entry code: 1EWK). Thus, the agonist Glu provides an additional ligand for Ca^{2+} when the former is bound to the receptor, which is very different from intracellular Ca^{2+}-binding trigger proteins such as calmodulin that lack any additional chelating groups from molecules other than the residues within the Ca^{2+}-binding protein

itself, except for water. Fig. 3-1B shows that the predicted Ca^{2+}-binding pocket has a highly negatively charged surface as revealed by Delphi in the structures of three solved forms of the ECD within mGluR1α (Fig. 3-1B).

3.2.2 Conformational effect of grafted CD2 mutant (CD2.D1).

In our previous study, grafting of EF-hand loops from CaM (104,105) and a viral protease from the rubella virus (106), or continuous Ca^{2+}-binding sites from a calcium-sensing receptor into CD2 (46), did not significantly affect the secondary structure of the host protein. (46,104-106). To ensure that the structural integrity of the host protein was not disrupted, we used far UV CD, Trp fluorescence and 1D 1H NMR to monitor any structural changes in the host protein after grafting the predicted Ca^{2+}-binding sequence from mGluR1α. As shown in Fig. 3-2A, the engineered proteins and wild type CD2.D1 have a common negative peak at around 216 nm, which suggests that these engineered proteins did not modify the β sheet characteristic of intact CD2. Extra negative signals at around 201 nm for CD2.D1 could be contributed to by the inserted loop, which increases the amount of random coil in the grafted proteins (Fig. 3-2A, Table 3-1). 1D 1H NMR studies further confirmed this point by demonstrating the similar spectra of CD2 and CD2.D1 (Fig. 3-2C).

3.2.3 Membrane expression of wild type mGluR1α and its mutants.

We first examined the expression and membrane targeting of WT and mutant mGluR1α using confocal microscopy by attaching mCherry, a monomeric variant of red

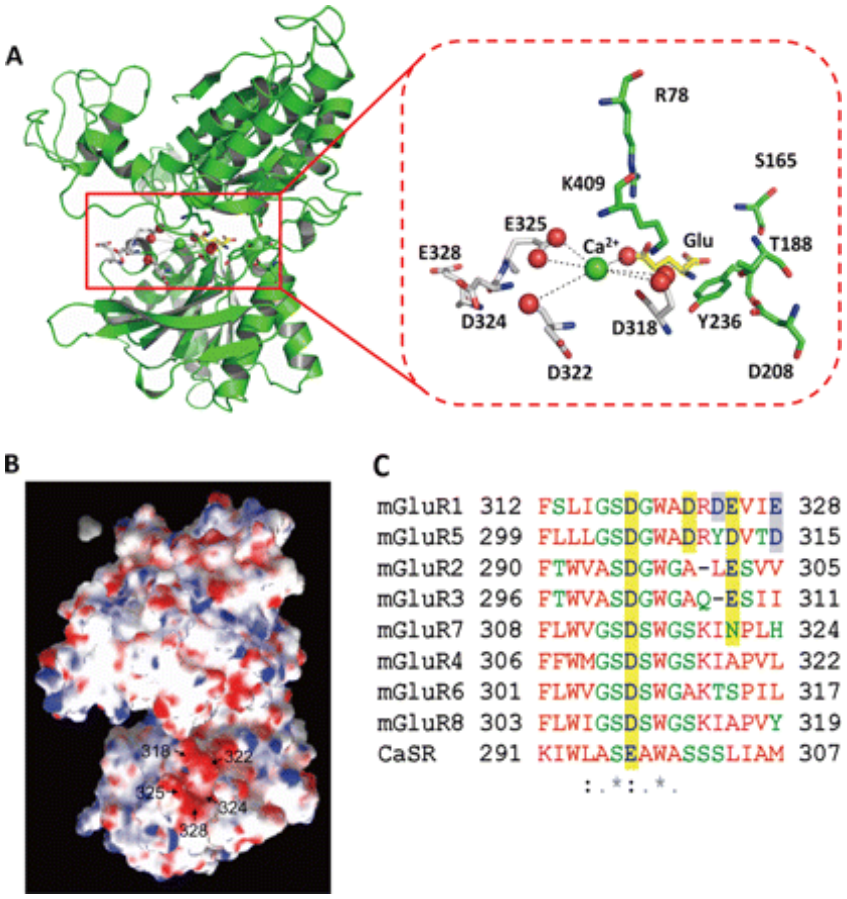

Figure 3-1 Predicted Ca^{2+}-binding pocket in ECD of mGluR1α. (*A)* Location of the predicted Ca^{2+}-binding site in the ECD (PDB entry code: 1EWK). The proposed key residues are indicated and highlighted in *red* (model generated by PyMOL). (*B*) Electrostatic potential map of ECD. The predicted Ca^{2+}-binding site is in the hinge region and shares residue Asp-318 with the Glu-binding site. (*C*) Alignment of the grafted fragment in mGluRs and CaSR. Asp-318 is conserved in all of the receptors; Glu-325 is conserved in group I and II mGluRs; Asp-322 is conserved in group I mGluRs.

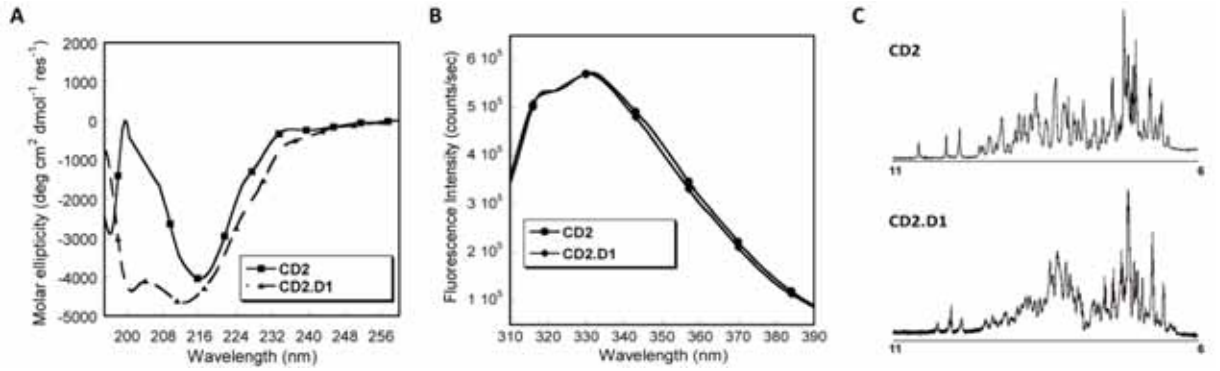

Figure 3-2 Secondary structure and folding of engineered proteins. (A) Far UV CD spectra of wild type CD2 and CD2.D1. All spectra were performed in 10 mM Tirs buffer, and were the average of ten scan at a rate of 100 nm/min. (B) Trp fluorescence spectra of wild type CD2 and CD2.D1. The sample contained 3 μM proteins in 20 mM PIPES and 10 mM KCL with pH at 6.8. The slit widths for excitation and emission were 3.5 and 5 nm, respectively. (C) 1H-1D NMR spectra of CD2 and CD2.D1. The samples were prepared with 0.1 mM protein in 10 mM Tris buffer with pH at 7.4.

Table 3-1 Spectra fit of CD data of CD2 and grafting protein, CD2.D1

	α-Helix	***β-Sheet***	***Turn***
CD2	0.057 ± 0.049	0.384 ± 0.014	0.553 ± 0.037
CD2.D1	0.079 ± 0.013	0.362 ± 0.023	0.553 ± 0.034

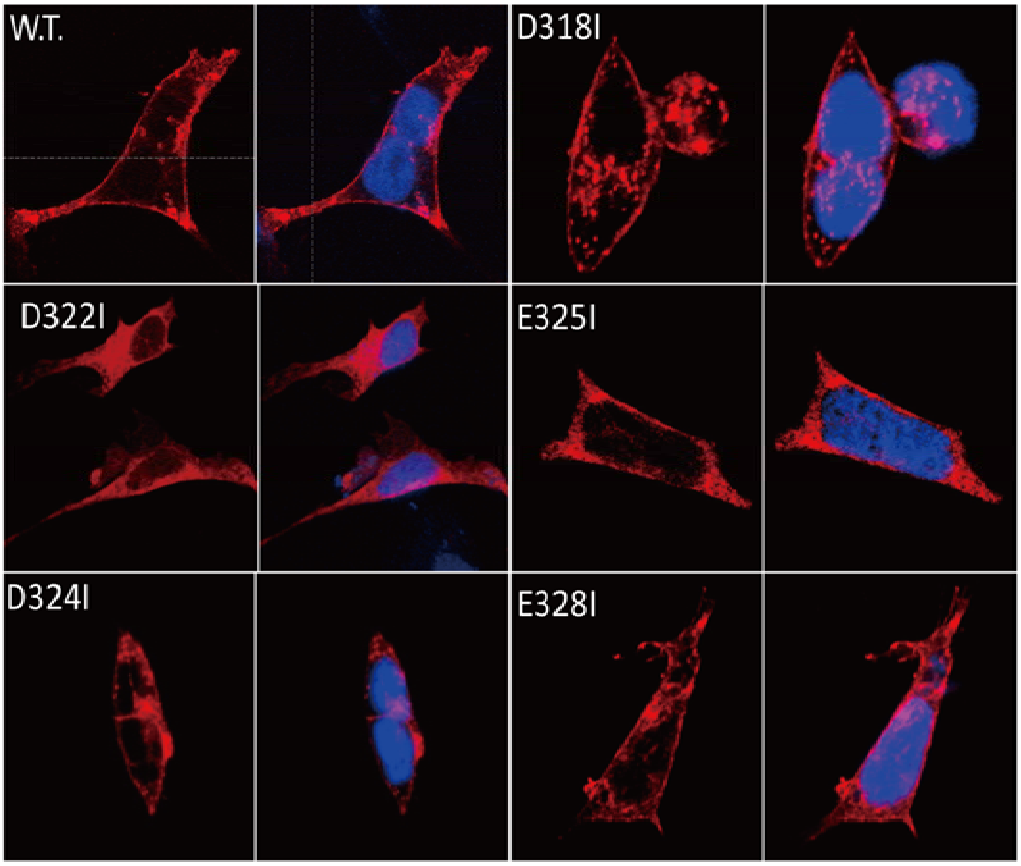

Figure 3-3 Membrane Expression of wt-mGluR1α, D318I-mGluR1α, D322I-mGluR1α, D324I-mGluR1α, E325I-mGluR1α, and E328I-mGluR1α using a gene reporter at HEK293 cells. MGluR1α were genetically tagged with red fluorescent protein, mCherry, at the C-terminal by linker GGNSGG. Wt-mGluR1α, D322I, D324I, E325I, E328I express well on the membrane of cells, and the nucleus is stained by DAPI (blue); D318I-mGluR1α also expresses on the membrane but is partially clustered in cytosol.

fluorescent protein, to the C-termini of these proteins (Fig. 3-3). Both WT mGluR1α and its mutated variants were successfully expressed with the respective receptor targeted to the HEK293 cell membrane. The mutant D318I-mGluR1α displayed some clusters of fluorescence in the cytosol, possibly due to retention of mutant receptors in the ER lumen. However, the receptor level on the membrane is close to that of WT-mGluR1α.

3.2.2 Obtaining Site-specific Ca^{2+}/Ln^{3+}-binding Affinities by a Grafting Approach

To probe the Ca^{2+}-binding capability of the predicted Ca^{2+}-binding site in mGluR1α, we utilized our grafting approach by inserting the protein sequence encompassing the putative mGluR1α Ca^{2+}-binding site into the host protein, CD2.D1 (denoted as CD2-mGluR1-1). The inserted sequence contains all predicted Ca^{2+}-binding residues except Glu-701. This approach had previously enabled us to obtain site-specific Ca^{2+}-binding affinities of the EF-hand motifs from calmodulin and linear Ca^{2+}-binding sequences, free from the limitations of working with membrane proteins (32, 33). The putative mGluR1α Ca^{2+}-binding site was flanked by flexible triple-Gly linkers and inserted between Ser-52 and Gly-53 of CD2.D1 (Fig. 3-4A) to ensure a native-like conformation and close proximity (<15~20 Å) to Trp-32 in order to enhance the Tb^{3+}-LRET signal. Indeed, grafting the putative Ca^{2+}-binding loop from mGluR1α did not significantly change the secondary and tertiary structures of CD2, as revealed by circular dichroism, Trp fluorescence, and NMR chemical shifts (supplemental Fig. 3-2). Fig. 3-4B shows that Tb^{3+} (which has the same coordination chemistry as Ca^{2+}) elicits an increase in fluorescence of CD2.D1 at 550 nm when excited at 280 nm due to Tb^{3+}- LRET. CD2.D1 had a Tb^{3+} binding affinity of 49 ± 9 μM (Fig. 3-4B and Table 3-2). Ca^{2+} displaced bound Tb^{3+} (Fig.

3-4B), thereby decreasing the Tb^{3+}-LRET signal. CD2.D1 has a Ca^{2+} dissociation constant of 1.80 ± 0.12 mM determined in this manner (Table 3-2).

Because mGluR1$_\alpha$ is modulated by various polyvalent cations, including Ca^{2+}, Gd^{3+}, Tb^{3+}, La^{3+}, Mn^{2+}, and Mg^{2+} (6), we tested the metal binding selectivity of CD2.D1 by applying K^+, Mg^{2+}, La^{3+}, or Gd^{3+} to compete with prebound Tb^{3+}. Fig. 3-4C shows that the luminescence intensity of Tb^{3+} decreased significantly upon adding trivalent La^{3+} or Gd^{3+}, indicating that Tb^{3+} bound to the pocket was replaced by these metal ions. Gd^{3+} had the strongest capacity to displace Tb^{3+}. Similarly, adding La^{3+} to CD2.D1 produced a split in the resonance of CD2.D1 at 10 ppm (Fig. 3-4D). Ca^{2+} competed more effectively than Mg^{2+}, whereas K^+ failed to compete with Tb^{3+}.

Next, we utilized mutagenesis studies to examine the contribution of proposed ligand-binding residues to metal-binding capability. Double substitutions of negatively charged residues by Ile to delete negative charges but preserve bulky side chains in the proposed binding pocket, as seen in the mutants D324I/E325I, D318I/D322I, and E328I/N335I, produced 2.3-, 6.1-, or 98-fold increases in the respective dissociation constant values (Fig. 3-4, B and E). However, removing the negative charges from the non-Ca^{2+}-binding residues, Glu-331 and Glu-333 (E331I/E333I) (Fig. 3-4, B and E) produced a less than 2-fold change in the Kd, with a modest alteration in Tb^{3+} binding to the predicted binding pocket.

3.2.3 Membrane Expression of mGluR1$_\alpha$ and Its Mutants

WT mGluR1$_\alpha$ and its mutant forms (D318I, D322I, and E325I) were expressed heterogeneously in HEK293 cells. The receptors expressed on the cell membrane were

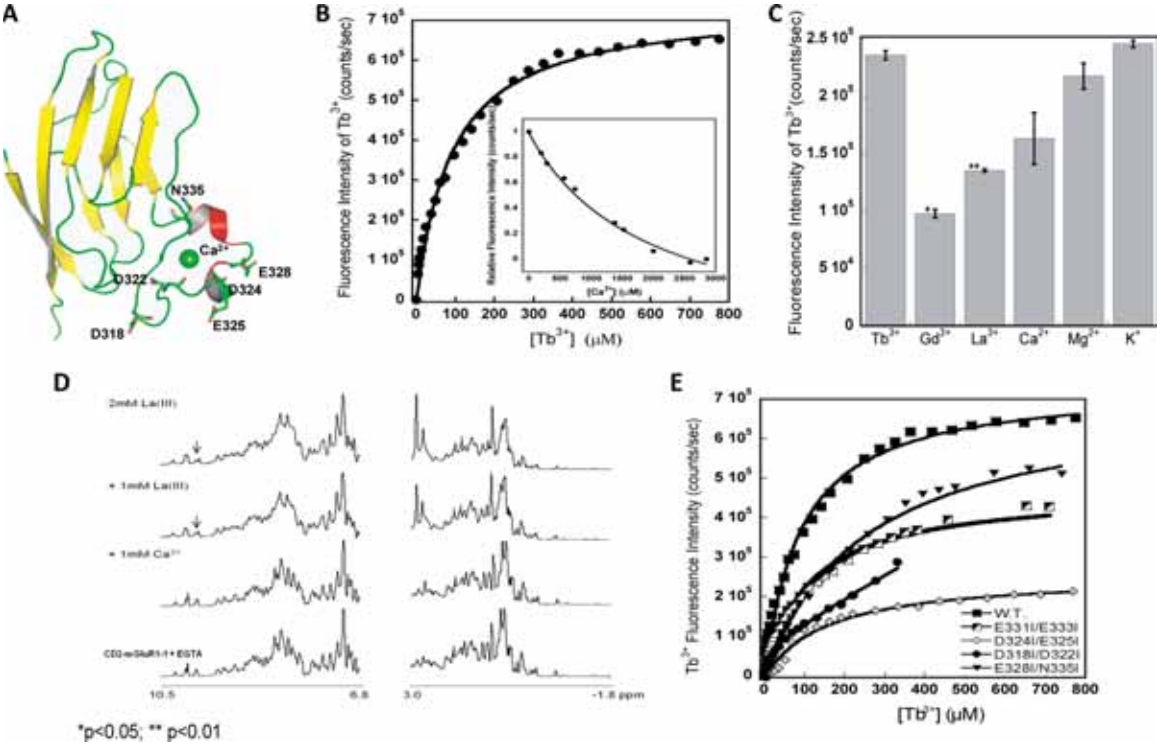

Figure 3-4 Metal binding properties of the grafted Ca^{2+}-binding site. *A*, three-dimensional illustration of the modeled structure of the engineered protein CD2.D1, based on the crystal structures of CD2 (PDB entry code: 1HNG (35)) and the mGluR1α ECD (PDB entry code: 1EWT (8)). *B*, Tb^{3+} titration and Ca^{2+} competition (shown as *inset*) of CD2.D1. The engineered protein bound Tb^{3+} and Ca^{2+} with dissociation constants of 49 ± 9 μm and 1.8 ± 0.1 mm, respectively. Substitution of putative metal-binding ligand residues with Ile decreases Tb^{3+} binding affinity. Tb^{3+} binding curves of a series of CD2-mGluR1 double mutants, E331I/E333I, D324I/E325I, D318I/D322I, and E328I/N335I. All measurements were carried out in a buffer containing 20 mm PIPES and 10 mm KCl, pH 6.8. *C*, Tb^{3+} binding curves of a series of CD2-mGluR1 double mutants: CD2.D1-1 (E331I/E333I), CD2.D1-2 (D324I/E325I), CD2.D1-3 (D318I/D322I), and CD2.D1-4 (E328I/N335I). All of the measurements were carried out in a buffer containing 20 mm PIPES and 10 mm KCl, pH 6.8. D318I/D322I obviously decreased Tb^{3+} binding affinity, whereas D324I/E325I displays two phases. The Tb^{3+} binding affinity of the engineered protein was clearly impaired by these two pairs of mutations (n = 3). *D*, La^{3+} binding to the engineered protein CD2.D1 monitored by $^{1}D^{1}H$ NMR. 1 or 2 mm La^{3+} results in the peak split at the aromatic group region. *E*, metal selectivity of CD2.D1. The addition of 500 mm K^{+}, 1 mm Ca^{2+}, 1 mm Mg^{2+}, 100 μm Gd^{3+}, or 100 μm La^{3+} to the pre-equilibrated Tb^{3+} (30 μm) and protein (3 μm) solution was carried out independently. The resultant changes in the Tb^{3+} luminescence signal were monitored at 545 nm (*, p < 0.05; **, p < 0.01).

Table 3-2 Tb^{3+} binding affinities of the engineered protein CD2.D1 and its double mutants (*n*=3)

Proteins	Mutations	Dissociation constant (K_d)
CD2.D1	WT	49 ± 9 μM (Ca^{2+}, 1.8 ± 0.1 mM)
CD2.D1-1	E331/E333I	85 ± 18 μM*
CD2.D1-2	D324/E325I	113 ± 5 μM
CD2.D1-3	D318/D322I	>4.8 mM*
CD2.D1-4	E328/N335I	299 ± 15 μM*

*, $p < 0.05$.

visualized by confocal microscopy (supplemental Fig. 3-3) and flow cytometry (Fig. 3-5). Supplemental Fig. 3-3 shows that the mutations did not affect the distribution of the receptors on the membrane. We calculated the ratio of intensities of green and red fluorescence measured using flow cytometry (LSRFortessa, BD Biosciences); the mutant receptors displayed expression levels on the cell membrane comparable with that of the wild type receptor, although E325I displayed a somewhat lower membrane expression level (Fig. 3-5; n = 3). Thus, the mutations involving the predicted Ca^{2+}-binding site had little effect on the surface expression of the respective mutant receptors.

3.2.4 Extracellular Ca^{2+} Triggers mGluR1α-mediated Intracellular Responses

We next examined the mGluR-mediated intracellular Ca^{2+} responses in HEK293 cells transfected with mGluR1α-mCherry. The fluorescent protein mCherry was fused to mGluR1α to correlate cellular responses with the expression of mGluR1α. We chose HEK293 cells as a model because this cell line lacks endogenous mGluR1α (34). mGluR1α-mCherry was well expressed and correctly targeted to the cell membrane (Figs. 3-5 and 3-6A and supplemental Fig. 3-3), and Fura-2 was efficiently loaded (Fig. 3-6B). Single cell, real time imaging was performed using fluorescence microscopy. To minimize receptor desensitization by agonists, the responses to each concentration of added Ca^{2+} or Glu were examined using separate coverslips.

In the absence of exogenous Glu, the addition of $[Ca^{2+}]_o$ at less than 1.8 mM did not induce any $[Ca^{2+}]_i$ response in HEK293 cells transfected with WT mGluR1α. Adding $\geq$3.0 mM Ca^{2+} to the medium elicited a transient $[Ca^{2+}]_i$ increase followed by a long lasting plateau (Fig. 3-6C); this response was maximal at $\geq$5.0 mM $[Ca^{2+}]_o$, with an EC50 of

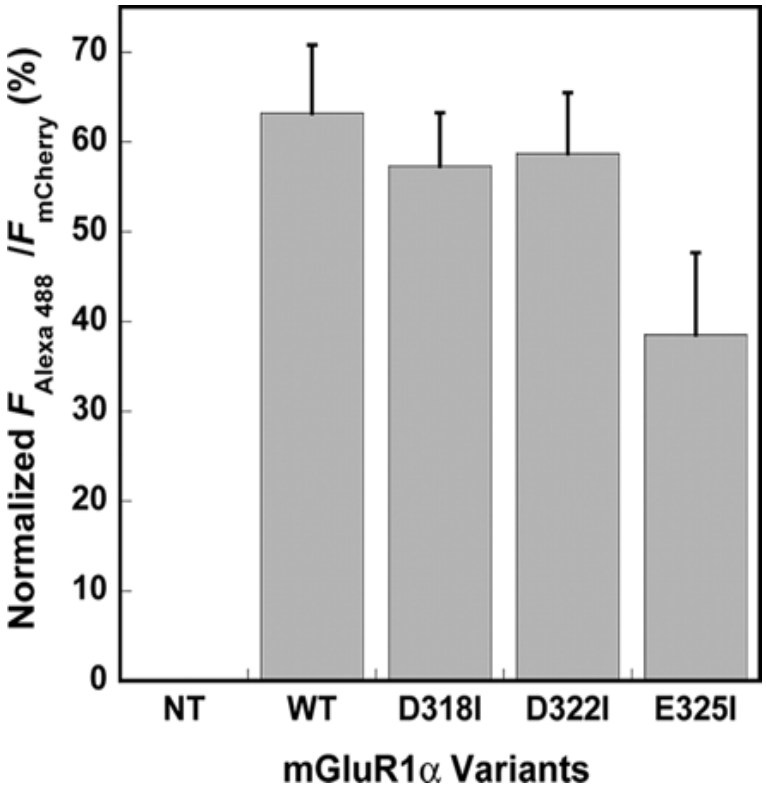

Figure 3-5 Surface expression of WT mGluR1α and its mutants. mGluR1α carries a FLAG tag at its N terminus and mCherry at its C terminus. mGluR1α and its mutants were transiently expressed in HEK293 cells seeded on 50-mm dishes coated with poly-lysine. After incubation with anti-FLAG, the receptors on the membrane could be visualized using a secondary antibody, Alexa 488-anti-mouse IgG (Invitrogen). Emissions at 520 and 610 nm were collected by flow cytometry (LSRFortessa, BD Biosciences); these represent receptors present on the cell membrane and overall, respectively. Ratios of fluorescence at 520–610 nm indicate the membrane expression levels of WT mGluR1α and its mutants. Emission at 520 nm (green signal) reflects the membrane expressed receptors, whereas the red signal at 610 nm from mCherry is a measure of total expression of the receptor. *NT* indicates non-transfected cells, which display no fluorescence. Although E325I displays a relatively lower surface expression, the other mutants have membrane expression levels comparable with that of WT mGluR1α (*n* = 3). The buffer used in this experiment is 1X PBS.

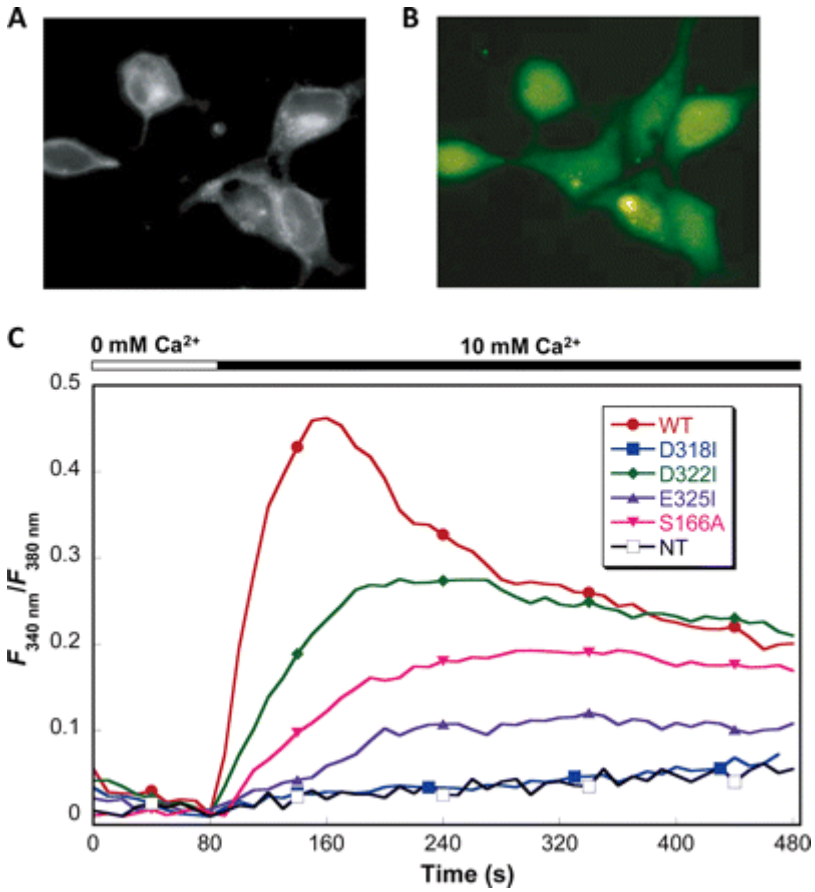

Figure 3-6 Intracellular Ca^{2+} responses of WT mGluR1α and its mutants. WT mGluR1α and D318I-mGluR1α were overexpressed in HEK293 cells. Fura-2 was then loaded into the cells, and the $[Ca^{2+}]_i$ level was measured by monitoring emission at 510 nm with excitation at 340 or 380 nm. *A*, *red* fluorescence of mCherry on the C terminus of mGluR1α indicates the presence of the receptor or its mutants. *B*, cells were loaded with Fura-2-AM to measure $[Ca^{2+}]_i$ level. *C*, $[Ca^{2+}]_i$ release triggered by $[Ca^{2+}]_o$ in WT mGluR1α and its mutants. D318I and E325I eliminate the $[Ca^{2+}]_i$ response, whereas D322I and S166A reduce it. All the buffers used in this experiment are 10 mM HEPES, 140 mM NaCl, 5 mM KCl, 0.55 mM $MgCl_2$ and various Ca^{2+} concentration (pH 7.4). *NT*, non-transfected cells.

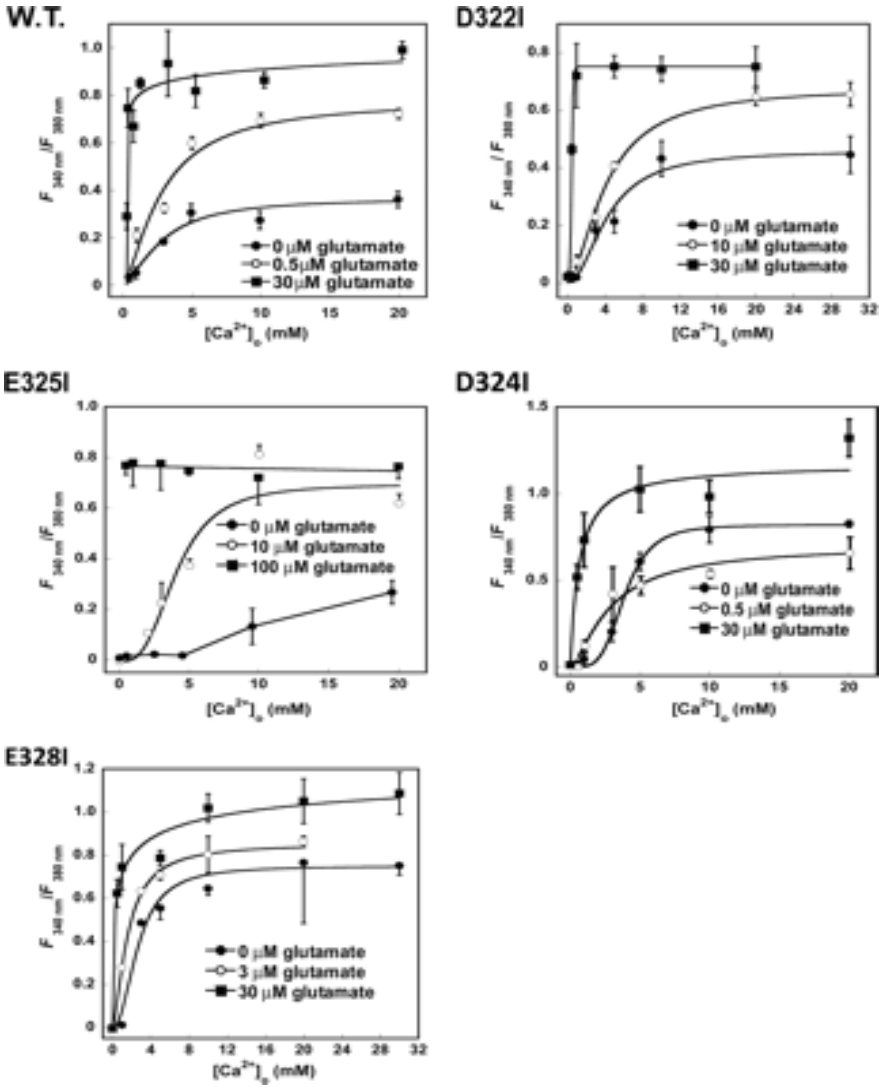

Figure 3-7 Intracellular Ca^{2+} responses of WT mGluR1α and its mutants (D322I-mGluR1α, D324I-mGluR1α, E325I-mGluR1α, and E328I-mGluR1α) to $[Ca^{2+}]_o$ in the presence of Glu. Shown are the additional Glu-enhanced responses of WT mGluR1α and all of its mutants to $[Ca^{2+}]_o$. The Glu concentrations that were added were determined by the responses of the wild type receptor or its mutants to Glu. That is, the Glu concentrations that evoked initial activation of or saturated the receptors were utilized for the $[Ca^{2+}]_o$-induced responses of the wild type receptor and its mutants. $[Ca^{2+}]_i$ levels were measured by the same methods described above. Notably, E325I loses sensitivity to $[Ca^{2+}]_o$ but can still sense $[Glu]_o$. However, its responsiveness to $[Ca^{2+}]_o$ in the presence of high concentration $[Glu]_o$ was not affected by increasing $[Ca^{2+}]_o$ (n = 3). The buffer used in this set of experiments is 10 mM HEPES, 140 mM NaCl, 5 mM KCl, 0.55 mM $MgCl_2$ and various L-Glu and Ca^{2+} concentration (pH 7.4).

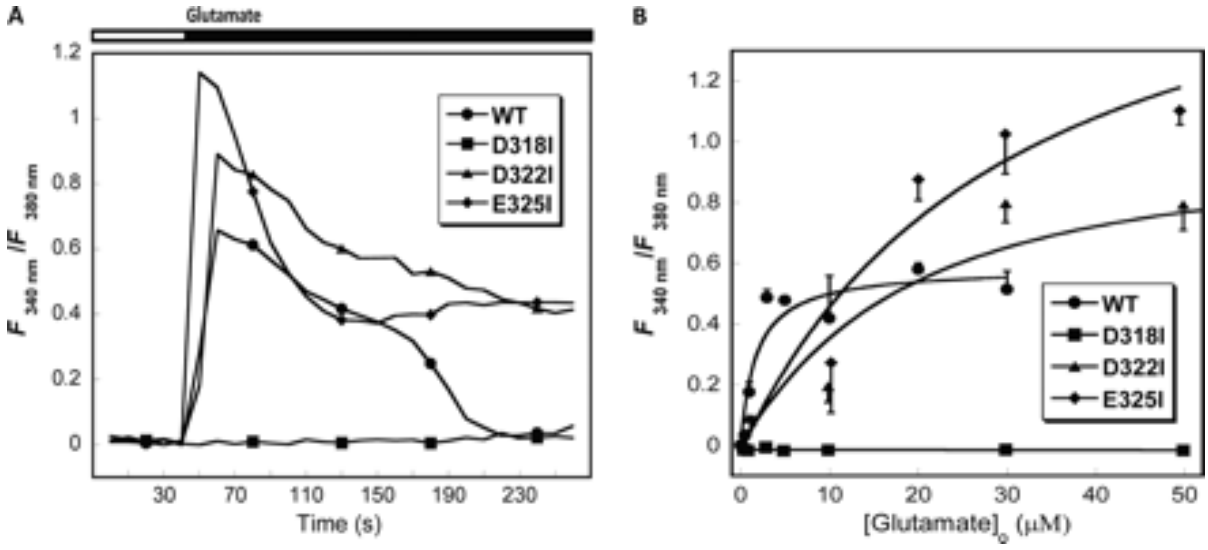

Figure 3-8 Intracellular Ca^{2+} responses to extracellular Glu in HEK293 cells transfected with WT mGluR1α or its mutants. Three negatively charged residues in the predicted Ca^{2+}-binding pocket (Asp-318, Asp-322, and Glu-325) were mutated into Ile. Along with WT mGluR1α, the mutants were transiently expressed in HEK293 cells. In the presence of 1.8 mm Ca^{2+}, extracellular Glu-induced intracellular Ca^{2+} release was measured by recording emission intensities at 510 nm excited at 340 and 380 nm, respectively. *A*, responses to Glu of mutations on Ca^{2+}-binding site. Except for mutant D318I, two other mutants, D322I, E325I, and WT mGluR1α display responsiveness to Glu. *B*, maximal response of WT mGluR1α and its mutants to Glu at a saturating concentration. The buffer used in this set of experiments is 10 mM HEPES, 140 mM NaCl, 5 mM KCl, 0.55 mM $MgCl_2$ and 1.8 mM Ca^{2+} concentration (pH 7.4). Each single data point was performed in an individual dish, and the cells expressing mGluR1α and showing responses to Glu were selected for analysis (*n* = 3).

Table 3-3 $[Ca^{2+}]_i$ responses of WT mGluR1α and its mutants to $[Ca^{2+}]_o$ and Glu (*n*=3)

Variants	$[Ca^{2+}]_o$				Glu	
	Glu concentration	EC_{50}	n_{Hill}	Maximal response[a]	EC_{50}[b]	Maximal response[a]
	μM	mM		%	μM	%
WT	0	3.0	1.7	75 ± 3	1.7	100 ± 3
	0.5	2.8	1.4	109 ± 7	0.9[c]	108 ± 1[c]
	30	0.1	0.5	128 ± 6	0.4[d]	130 ± 8[d]
D318I	0	None	None	No response	None	No response
D322I	0	4.3	2.0	63 ± 2	13.2	111 ± 2
	10	4.1	1.7	86 ± 5		
	30	0.5	7.2	105 ± 3		
E325I	0	None	None	No response	30.5	146 ± 2
	10	4.3	2.3	89 ± 12		
	100	ND[e]	ND[e]	117 ± 3		
D324I	0	3.9	4.1	104 ± 10	0.3	117 ± 7
	0.5	2.9	1.8	144 ± 4		
	30	0.6	1.0	162 ± 6		
E328I	0	2.5	2.7	102 ± 5	1.2	107 ± 12
	3	1.6	1.5	135 ± 13		
	30	2.2	0.3	147 ± 3		

[a] The maximal responses are normalized to the maximal response of wild type mGluR1α to Glu.
[b] Glu dose response was performed in 1.8 mM Ca^{2+}.
[c] Experiments performed in 5 mM Ca^{2+}.
[d] Experiments perfomed in 10 mM Ca^{2+}.
[e] ND: not determined

3.0 mM. Furthermore, adding 0.5 or 30 μM Glu significantly enhanced the maximal response of mGluR1$_\alpha$ to $[Ca^{2+}]_o$ by 1.3- and 1.7-fold, respectively (Fig. 3-7). The EC_{50} value for $[Ca^{2+}]_o$ decreased from 3.0 to 2.8 and 0.1 mM, respectively (Fig. 3-7 and Table 3-3). The response of wild type mGluR1$_\alpha$ to Glu was investigated in a physiological saline buffer with 1.8 mM Ca^{2+}. Wild type mGluR1$_\alpha$ only responded at ≥0.5 μM Glu, and this response was saturated at 30 μM Glu. Fig. 3-8A shows that at 1.8 mM Ca^{2+}, the addition of >30 μM Glu evoked large $[Ca^{2+}]_i$ responses. On the other hand, when $[Ca^{2+}]_o$ was reduced from 1.8 mM to close to zero (no Ca^{2+} added to the medium), 30 μM Glu still activated mGluR1$_\alpha$ (Fig. 3-7). There was, however, a reduced maximal response (29%) (Fig. 3-7), possibly because of the depletion of intracellular calcium stores. This result suggests that Glu triggers the activation of mGluR1$_\alpha$ and that this effect can be enhanced by $[Ca^{2+}]_o$.

To study the synergy of $[Ca^{2+}]_o$ and Glu binding to mGluR1$_\alpha$, the combination indices for quantitative evaluation of synergism were calculated using Calcusyn (35). With 0.5 or 30 μM Glu, the combination indices were <1 when $[Ca^{2+}]_o$ reached a physiological level (>0.5 mM) (supplemental Table 3-5), suggesting that Glu and Ca^{2+} synergistically modulate mGluR1$_\alpha$-mediated signaling.

3.2.5 Effects of $[Ca^{2+}]_o$ on a Glu-induced $[Ca^{2+}]_i$ Release by Wild Type mGluR1α

To determine the role of $[Ca^{2+}]$o on Glu-mediated activation of wild type mGluR1α, 5 and 10 mM $[Ca^{2+}]_o$ were added to the perfusion system in addition to the 1.8 mM already present in the perfusate. As shown in Fig. 3-9, compared with the response in 1.8 mM $[Ca^{2+}]_o$ o, both 5 and 10 mM $[Ca^{2+}]_o$ enhanced the responses of WT mGluR1α to Glu by reducing the EC_{50} values from 1.7 to 0.9 and 0.4 μM, respectively (Table 3-3), although the maximal responses remained comparable with those at 1.8 mM $[Ca^{2+}]_o$. This indicates that $[Ca^{2+}]_o$ potentiates the sensitivity of mGluR1α to Glu and that this effect increases at higher levels of $[Ca^{2+}]_o$.

3.2.6 Effects of Mutating Proposed Ca^{2+}-binding Residues on $[Ca^{2+}]_o$ - or Glu-evoked $[Ca^{2+}]_i$ Responses

To further understand the potential physiological role of this proposed Ca^{2+}-binding site, we compared the mGluR-mediated $[Ca^{2+}]_i$ responses in HEK293 cells transfected with the WT or mutated versions of mGluR1$_\alpha$. Fig. 3-6C shows that without Glu, substituting the predicted Ca^{2+}-binding residues Asp-318 and Glu-325 with Ile eliminates the transient $[Ca^{2+}]_i$ response toward $[Ca^{2+}]_o$. In addition, the mutation D322I also reduced the transient $[Ca^{2+}]_i$ response by 16–20% while increasing the EC50 from 3.0 mM $[Ca^{2+}]_o$ for the wild type receptor to 4.2 mM for D322I (Fig. 3-7 and Table 3-3), although all mutants were expressed at levels comparable with the WT receptor, as assessed by immunofluorescence and flow cytometry (Fig. 3-3 and Fig. 3-5). These results suggest that the predicted Ca^{2+}-binding residues, Asp-318, Glu-325, and Asp-322 (especially the first two), are important for the sensitivity of mGluR1$_\alpha$ to modulation by $[Ca^{2+}]$o. However, S166A maintains Ca^{2+} sensitivity with a lower maximal response (Fig. 3-6C), although Ser-166 was previously reported to be a potential Ca^{2+}-binding residue (6).

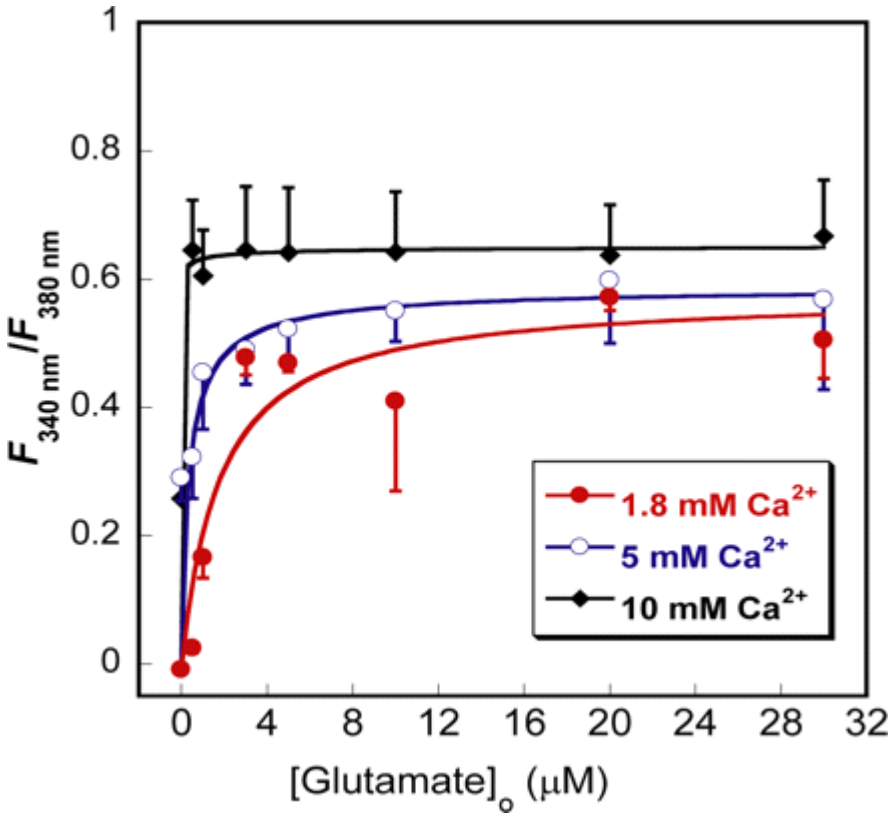

Figure 3-9 Extracellular Ca^{2+} enhanced mGluR1α to sense extracellular Glu. Responses of WT mGluR1α to extracellular Glu were assessed in buffers containing additional $[Ca^{2+}]_o$ (1.8, 5, and 10 mm). The maximal responses of the receptor to $[Glu]_o$ in 1.8, 5, and 10 mm $[Ca^{2+}]_o$ are comparable, but the EC_{50} values for the responses in the presence of 5 and 10 mm $[Ca^{2+}]_o$ are significantly decreased. Clearly, higher $[Ca^{2+}]_o$ reduces the EC_{50} of the receptor for $[Glu]_o$ (n = 3). The buffer used in this set of experiments is 10 mM HEPES, 140 mM NaCl, 5 mM KCl, 0.55 mM $MgCl_2$ and various L-Glu and Ca^{2+} concentration (pH 7.4).

3.2.7 Effects of Mutating Predicted Ca^{2+}-binding Residues on Glu-potentiated $[Ca^{2+}]_i$ Responses

The Ca^{2+}-binding site identified here is adjacent to the previously defined Glu-binding site (Arg-78, Ser-165, Thr-188, Asp-208, Tyr-236, Asp-318, and Lys-409) (15, 25) (Fig. 3-1B). Asp-318 is the lone residue used in both the Glu- and Ca^{2+}-binding sites. Figs. 3-6 and 3-8 show that the mutation D318I completely eliminates the $[Ca^{2+}]_i$ response of mGluR1$_{\alpha}$ to both $[Ca^{2+}]_o$ and Glu, even at concentrations of the latter as high as 30 μM. In contrast, the mutant E325I completely abolishes $[Ca^{2+}]_o$-mediated $[Ca^{2+}]_i$ responses without the agonist Glu (Figs. 3-6C and 3-7 and Table 3-3) but retains Glu-mediated $[Ca^{2+}]_i$ responses (Fig. 3-8A).

However, its EC_{50} value for Glu-mediated responses is increased by ~18-fold (Fig. 3-8B and Table 3-3). These results further confirm that Glu-325 contributes to Ca^{2+}-binding without directly liganding Glu (as shown by earlier studies of the binding site for Glu, which did not identify Glu-325 as a Glu ligand). However, the proximity of the Ca^{2+}- and Glu-binding sites may produce indirect, conformational effects of mutating residue 325 on Glu binding. Furthermore, D322I exhibited a reduction in EC_{50} for $[Ca^{2+}]_o$ by only 33%, consistent with it making a relatively minor contribution as a ligand for Ca^{2+}-binding. In contrast to the marked impact of D318I and E325I on the EC50 for $[Ca^{2+}]_o$, removal of other charged residues, such as D324I and E328I, did not alter either the EC_{50} (3 and 8% changes, respectively) or the magnitude of the response to $[Ca^{2+}]_o$ significantly in the absence of Glu (104 ± 10 and 102 ± 5, respectively, of the control level) (Fig. 3-7 and Table 3-3).

Table 3-4 $[Ca^{2+}]_i$ response of mutants in L-Glu binding site (n=3)

Mutants	EC_{50}	n_{Hill}	Maximal response[a]
	mM		%
S165A	8.1	3.1	86 ± 3
T188A	3.4	2.2	74 ± 2
D208I	4.6	2.3	95 ± 3
Y236F	3.3	10.9	33 ± 3

[a] Maximal responses are normalized to the maximal response of wild type mGluR1α to Glu.

3.2.8 Effect of Mutating the Glu-binding Site on $[Ca^{2+}]_i$ Responses to Glu and Ca^{2+}

To further explore the synergistic interaction between the predicted Ca^{2+}- and Glu-binding sites, four mutations at Glu ligand residues (S165A, T188A, D208I, and Y236F) were generated. Consistent with studies reported previously (25), T188A and D208I entirely eliminated Glu sensitivity, whereas S165A and Y236F could be activated only by high concentrations (100 μM) of Glu (3-10A). Interestingly, all receptors with mutated Glu-binding ligand residues (with the exception of Asp-318) retained a sensitivity to $[Ca^{2+}]_o$ (Fig. 3-10B and Table 3-4), although their EC_{50} values were increased compared with that of wild type mGluR1α (Table 3-4). This again may be due to local conformational effects of mutating the Glu-binding site on Ca^{2+}-binding. S165A and D208I increased the EC_{50} of the wild type receptor for $[Ca^{2+}]_o$ from 3.0 to 8.1 and 4.6 mM, respectively, although their maximal responses were comparable to that of the wild type receptor (Fig. 3-10B and Table 3-4). Conversely, T188A and D208I exhibited much reduced maximal responses (26 and 66%, respectively), whereas their EC_{50} values were comparable with that of the wild type receptor (Table 3-4). Taken together, the data shows that it is possible to generate mGluR1α variants responding to either Glu or Ca^{2+} alone. Thus mGluR1α can function as a true $[Ca^{2+}]_o$- sensing receptor, (no comma) as certain mutants, such as S165A and D208I, do not respond to Glu but maintain their Ca^{2+}-sensing capability with only a modest increase in the EC50 for $[Ca^{2+}]_o$.

3.2.9 Effects of Mutations in the Predicted Ca^{2+}-binding Site on Gd^{3+}-induced $[Ca^{2+}]_i$ Responses

Gd^{3+} is also revealed at the hinge region in the Fourier map, where it shares residues Asp-322 and Asp-324 from the loop that contributes to Ca^{2+}-binding (14). Because of the low resolution of this crystal structure (4 Å), the highly flexible loop that binds Gd^{3+} in the crystal structure, and the similarity of the binding geometries of Gd^{3+} and Ca^{2+}, these two cations probably share, at least in part, the same residues. To address this possibility, the responses to $[Gd^{3+}]_o$ of D318I and E325I were compared with that of the wild type receptor. Consistent with results reported by Abe et al. (17, 36), the dose-response profiles of wild type mGluR1α display a bell-shaped curve, this could be high concentration of Gd^{3+} blocked some types of Ca^{2+} channels on membrane. However, the introduction of the mutation D318I or E325I completely eliminated the receptor sensitivity to $[Gd^{3+}]_o$ (Fig. 3-11).

3.2.10 Glutamate and $[Ca^{2+}]_o$ synergistically modulate mGluR1α coupled signaling.

The synergistic effect of Glu and $[Ca^{2+}]_o$ was quantitatively described by combination indices. As shown in Table 3-5, in the presence of 5 or 30 μM Glu, the combination index values became significantly smaller than 1, suggesting that Glu and $[Ca^{2+}]_o$ regulate mGluR1α synergistically.

Table 3-5 Combination indices of glutamate and Ca^{2+} on mGluR1α

[Ca^{2+}], (mM)	Combination Indices	
	0.5 μM Glutamate	30 μM Glutamate
0.5	4.751	0.968
1	0.402	0.244
3	0.363	0.078
5	0.151	0.368
10	0.177	0.261
20	0.294	0.011

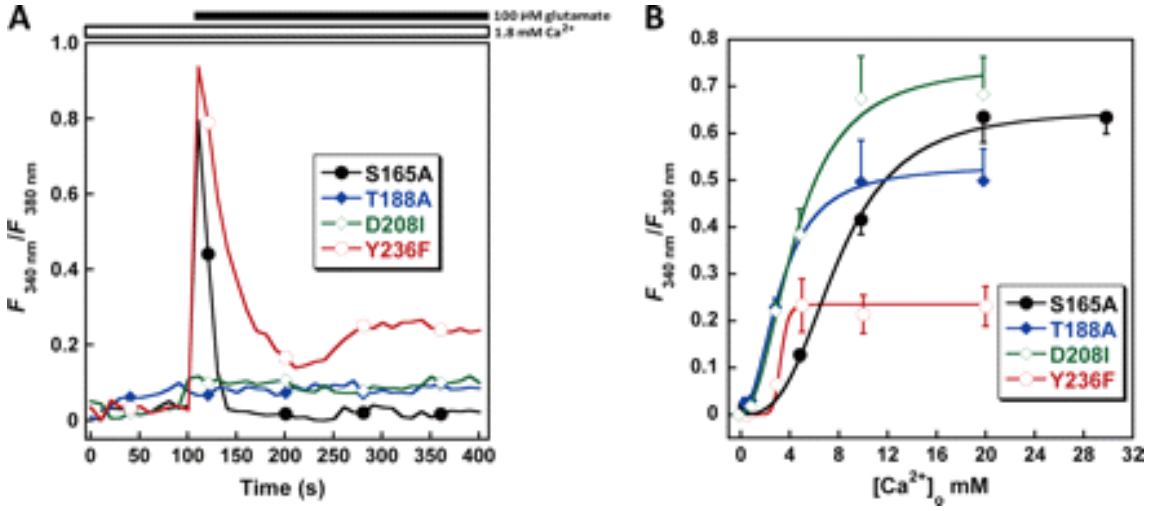

Figure 3-10 Receptors with mutations in the Glu-binding pocket can sense Ca^{2+} but not Glu in a physiological buffer. Four residues from the reported Glu-binding pocket were selected to mutate into non-polar residues. Intracellular Ca^{2+} levels indicated by Fura-2 were recorded using fluorescence microscopy, which detected the ratio of the emission at 510 nm with excitation at 340 and 380 nm. *A*, T188A and D208I abolish sensitivity to Glu, but S165A and Y236F still respond to 100 μm Glu. *B*, mutants S165A, T188A, D208I, and Y236F remain capable of responding to $[Ca^{2+}]_o$; the maximal responses of S165A, T188A, and D208I are comparable with that of WT mGluR1α, whereas Y236F decreases the sensitivity of the receptor to $[Ca^{2+}]_o$ (n = 3). The buffer used in this set of experiments is 10 mM HEPES, 140 mM NaCl, 5 mM KCl, 0.55 mM $MgCl_2$ and various Ca^{2+} concentration (pH 7.4).

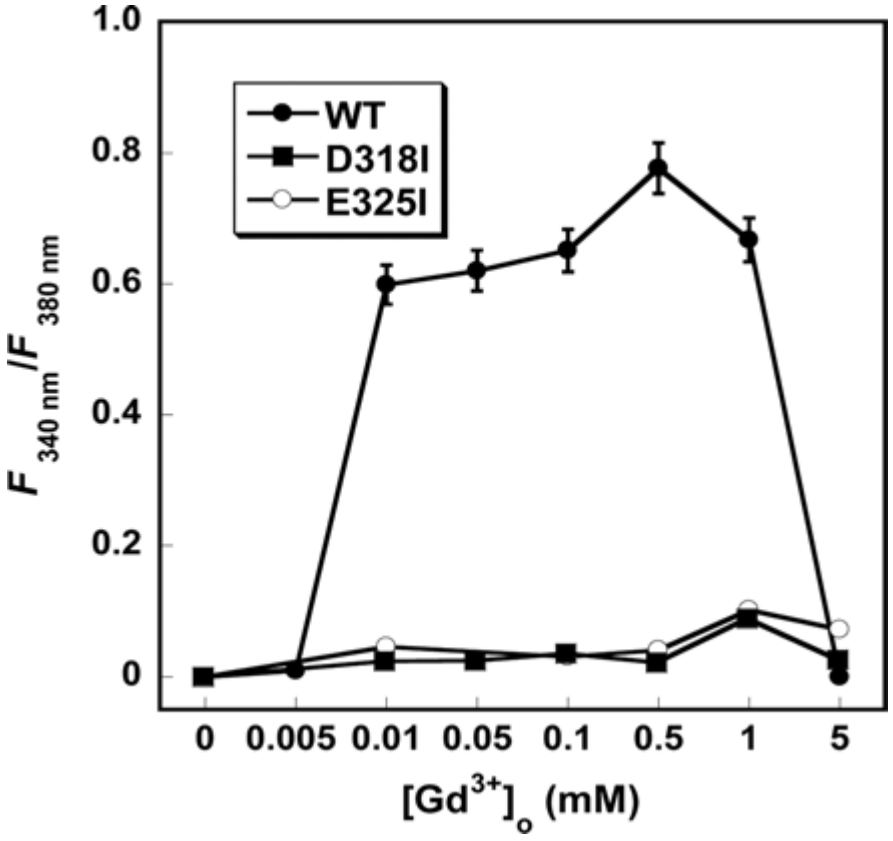

Figure 3-11 Mutations D318I and E325I in the predicted Ca^{2+}-binding site abolish $[Ca^{2+}]_i$ responses of the receptor to $[Gd^{3+}]_o$. HEK293 cells expressing D318I, E325I, and WT mGluR1α were preincubated in 140 mm NaCl, 4 mm KOH, 10 mm HEPES, 1.5 mm Ca^{2+}, 1 mm $MgCl_2$, and 10 mm glucose, pH 7.5, for up to 1.5 h before fluorescence microscopy was carried out. Gd^{3+} was added into the loading buffer (140 mm NaCl, 4 mm KOH, 10 mm HEPES, and 0.3 $MgCl_2$, pH 7.4) in the perfusion system. $[Ca^{2+}]_i$ levels indicated by Fura-2 are presented by the ratio of the fluorescence at 510 nm when excited at 340 and 380 nm as above. The $[Ca^{2+}]_i$ response of wild type mGluR1α displays a bell-shape curve, but D318I and E325I completely abolish $[Ca^{2+}]_i$ release to $[Gd^{3+}]_o$ (*n* = 3).

.

3.3 Discussion

We utilized the computational algorithm MUG (22) to predict a novel Ca^{2+}-binding site in mGluR1α adjacent to the Glu-binding site shown in Fig. 3-1. This predicted Ca^{2+}-binding site (comprising Asp-318, Glu-325, Asp-322, and the carboxylate side chain of Glu-701) does not completely overlap the Glu-binding site (15, 25). However, both sites include Asp-318, which our data suggests is involved in both Glu and Ca^{2+}-binding. The metal-binding capability of the predicted Ca^{2+}-binding residues in mGluR1α was verified by a grafting approach. Like wild type mGluR1α, the predicted Ca^{2+}-binding site grafted into a scaffold protein (CD2) exhibited metal selectivity for Ca^{2+} and its trivalent analogs, Gd^{3+}, Tb^{3+}, and La^{3+}, in contrast to the physiological monovalent cation, K^{+}, which exhibited no measurable affinity for the predicted site. The metal-binding capability of the predicted metal-binding ligand residues in mGluR1α was further verified by replacing negatively charged residues with Ile. The Ca^{2+}-binding affinity of mGluR1α determined by the grafting approach (~1.8 mM) is within the physiological concentration of $[Ca^{2+}]o$ in the nervous system (0.8–1.5 mM) (37), although this Ca^{2+}-binding constant may be changed slightly in vivo by the local microenvironment and/or the presence of Glu released by nearby cells.

We further demonstrated that mGluR1α could be activated by either Glu or $[Ca^{2+}]_o$. Indeed, Glu and $[Ca^{2+}]_o$ act synergistically to elicit the maximal $[Ca^{2+}]i$ responses observed here (Table 3-3). Mutating the Glu-binding site, such as T188A and D208I, in mGluR1α (Fig. 3-10A and Table 3-4), completely abolished the Glu-signaling capability of the receptor while leaving its Ca^{2+}-sensing capability largely intact with only modest

increases in EC50 for $[Ca^{2+}]_o$. These results suggest that mGluR1α can function as a true $[Ca^{2+}]_o$-sensing receptor, i.e. exhibiting robust activation by $[Ca^{2+}]_o$ in the absence of added Glu. Although we cannot rule out release of low concentrations of Glu by the HEK293 cells, it should be noted that some mutants of the receptor retained responsiveness to $[Ca^{2+}]_o$ despite complete loss of responsiveness to Glu. Moreover, even the addition of high exogenous concentrations of Glu failed to activate these mutants.

We have also shown that mutating predicted Ca^{2+}-binding residues abolishes, but it also significantly reduces $[Ca^{2+}]_o$ sensitivity and, in some cases, affects Glu-mediated responses. For example, E325I completely abolished $[Ca^{2+}]_o$-mediated $[Ca^{2+}]_i$ responses in the absence of Glu (Fig. 3-5C and Table 3-3). At the same time, this mutant retained sensitivity to Glu, albeit with an ~18-fold reduction in EC_{50} (without any decrease in maximal response) (Fig. 3-7 and Table 3-3). Thus, despite its not being a Glu-binding residue, the presence of an intact Ca^{2+}-binding ligand at Glu-325 considerably enhanced the affinity of mGluR1α for Glu. How could this take place? These results, in fact, are consistent with separate but overlapping Ca^{2+}- and Glu-binding sites (Figs. 3-1 and 3-12). As noted, positively charged Arg-323 is also very close to Ca^{2+} in the model, but it might not affect Ca^{2+}-binding because of the flexible backbone in the loop. Glu-325 is predicted to be a ligand for binding Ca^{2+} and not Glu. Glu-325 could be identified only in the x-ray structure of Glu-complexed mGluR1α (PDB entry code: 1EWK), indicating that 1) the binding of Glu could stabilize the side chain of Glu-325 in a conformation favorable for it to serve as a ligand for Ca^{2+}, and/or 2) the bound Glu could then further enhance $[Ca^{2+}]_o$ binding by contributing an additional Ca^{2+}-binding ligand. Conversely, binding of Ca^{2+} to mGluR1α could increase the affinity of the Glu-binding site for its li-

gand by providing Ca^{2+} as an additional Glu ligand (Glu-701). Overall, mutating residues involved only in binding $[Ca^{2+}]_o$ (with the exception of Asp-318) had less dramatic effects than mutations at the Glu-binding site. Most of these mutants can be fully activated on binding Glu, because the addition of high levels of Glu restores their EC_{50} and maximal responses to $[Ca^{2+}]_o$ to levels close to those of the wild type receptor. Additionally, a Gd^{3+} ion is also revealed in the crystal structure adjacent to the predicted Ca^{2+}-binding site, and it shares the same loop that contributes to Ca^{2+}-binding. Mutations in the Ca^{2+}-binding residues in the loop, D318I and E325I, entirely eliminated Gd^{3+}-induced $[Ca^{2+}]i$ release (Fig. 3-11). Although Glu-238, located at the interface of the two protomers, has been reported as a functional Gd^{3+} site, I120A, another mutation located at the interface of the receptor loses sensitivity to $[Ca^{2+}]_o$ (25). This indicates that the mutations at the interface of the two monomers cause markedly reduced activation of the receptor by either $[Gd^{3+}]_o$ or $[Ca^{2+}]_o$ and that the site at the hinge region is a true Gd^{3+}-binding site. This also highly suggests that our predicted Ca^{2+}-binding site can likewise bind Gd^{3+}.

In view of these findings, we propose a working model of dual activation of mGluR1α by the two physiological activators, $[Ca^{2+}]_o$ and Glu, via their overlapping and interacting binding pockets at the hinge region of the ECD (Fig. 3-12). Increased concentrations of either Glu or $[Ca^{2+}]_o$ partially activate mGluR1α. However, full activation of mGluR1α with maximal sensitivity and maximal amplitude of the response to Glu requires simultaneous binding of both Glu and Ca^{2+}, with Asp-318 playing a key role in the synergy between the two agonists. In this sense, mGluR1α can be viewed as a "coincidence detector," requiring the binding of both ligands for maximal intracellular signaling.

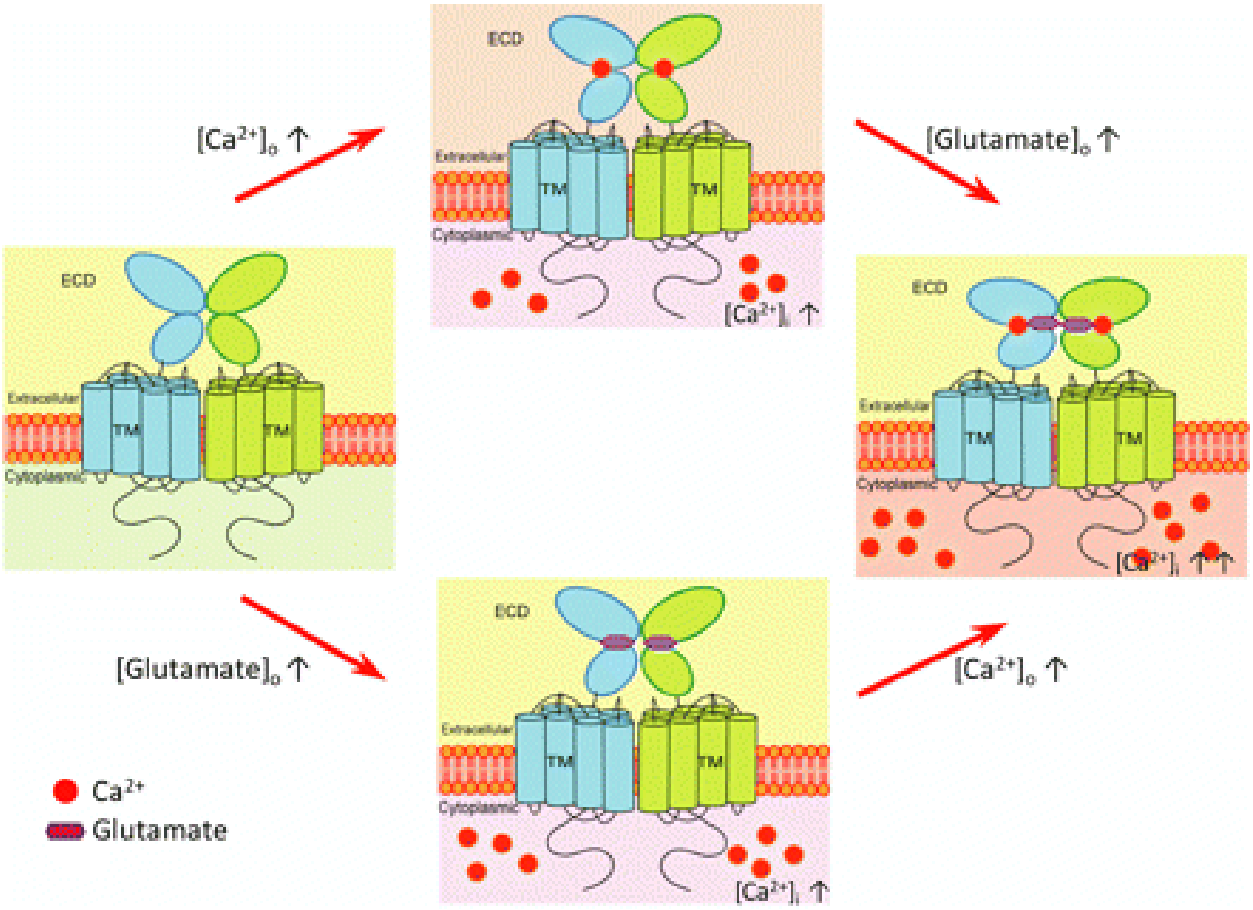

Figure 3-12 A dual activation model for mGluR1α involving both extracellular Ca^{2+} and Glu via the overlapping and interacting binding pockets for the two ligands at the hinge region of the ECD. Increasing either Glu or $[Ca^{2+}]_o$ partially activates mGluR1α. However, full activation of intracellular Ca^{2+} signaling by mGluR1α requires the simultaneous binding of both Glu and Ca^{2+}; Asp-318 plays a key role in the synergy between the two agonists. In this sense, mGluR1α can be viewed as a coincidence detector, requiring the binding of both ligands for maximal intracellular signaling.

Our proposed working model of mGluR1α is supported by previous studies from a number of groups working on both cultured cells and native brain tissue (6). Francesconi and Duvoisin (38) reported that mGluR1α in transfected cells is activated by $[Ca^{2+}]_o$ in the absence of Glu, indicating that mGluR1α is a Ca^{2+}-sensing receptor. Kubo et al. (6) showed that $[Ca^{2+}]_o$, as well as Glu, triggers intracellular responses in cultured cells and oocytes expressing mGluR1, mGluR3, and mGluR5. In terms of studies on endogenous mGluRs in native neurons, Tabata et al. (10) showed that $[Ca^{2+}]_o$ fails to induce $[Ca^{2+}]_i$ mobilization in the Purkinje cells from mGluR1 knock-out mice, whereas $[Ca^{2+}]$i is elevated by $[Ca^{2+}]_o$ in Purkinje cells from mGluR1α rescued mice. Furthermore, brain slice experiments from Hardingham et al. (11) demonstrated that $[Ca^{2+}]_o$ mediates postsynaptic efficacy via activation of group I mGluRs. Taken together, these studies represent strong evidence that $[Ca^{2+}]_o$ is a physiologically relevant modulator of mGluR1α activity in the central nervous system. Based on mutational analyses, the Ca^{2+}- and Glu-binding sites were postulated to be close to one another but not completely overlapping (6). For example, S166D decreases $[Ca^{2+}]_i$ responses (6) and lowers sensitivity to Glu (39). Our data show that S166A maintains sensitivity to $[Ca^{2+}]_o$, albeit with reduced responsiveness (Fig. 3-6C). This residue is located at the ECD hinge joint but away from our predicted site in the flexible hinge region (Fig. 3-1B). The observed decrease in mGluR1α sensitivity observed with S166D could be a result of tuning the Ca^{2+}-binding affinity and Ca^{2+}-induced conformational change by altering electrostatic interactions around the predicted Ca^{2+}-binding site (40).

As shown in Fig. 3-1C, the predicted Ca^{2+}-binding residue Asp-322 is conserved in group I mGluRs. Glu-325 is highly conserved in group I (mGluR1 and mGluR5) and group II (mGluR2 and mGluR3) mGluRs (Fig. 3-1C). Interestingly, mGluR5 in group I and mGluR3 in group II sense $[Ca^{2+}]_o$ at physiological levels, whereas mGluR2 is activated only when $[Ca^{2+}]_o$ is more than 10 mM (6). On the basis of our observation that E325I abolished Ca^{2+}-induced responses for mGluR1α but retained responsiveness to

Glu, we concluded that Glu-325 might be very important for Ca^{2+}-binding in the mGluR family generally. Analysis by the Contacts of Structural Units server indicates that Glu-325 interacts electrostatically with Arg-297 and Arg-323 in the Glu-bound structures of mGluR1α (41), suggesting that Glu-325 stabilizes the local structure through an electrostatic interaction. As revealed by the grafting approach (Fig. 3-4A), E325I significantly reduces the Ca^{2+}-binding ability in mGluR1α, possibly by disturbing the favorable local charge environment.

Fig. 3-1C shows that Asp-318 in mGluR1α, located at the hinge region, is conserved in all members of the three GPCRs, corresponding to Asp-295 of mGluR2, Asp-301 of mGluR3, Asp-309 of mGluR8, and Glu-297 of CaSR (23, 24, 42). Figs. 3-6 and 3-8 clearly demonstrate that Asp-318 contributes not only to Ca^{2+}- but also Glu-triggered $[Ca^{2+}]_i$ responses. This residue seems to play an essential role in the activation of mGluRs. Consistent with this finding, a D318A mutation was shown previously to reduce receptor expression on the membrane and abolish Glu-triggered $[Ca^{2+}]_i$ and inositol trisphosphate responses (25).

Our findings also appear to be applicable to other members of the three GPCRs, especially CaSR. The mutation E297I in CaSR, equivalent to D318I in mGluR1α, impairs receptor activation (23, 24, 42). Glu-297 is an important residue in our reported Ca^{2+}-binding site in the CaSR hinge region (23, 24); the mutant E297I significantly impairs sensitivity to $[Ca^{2+}]$o with an EC50 of 9.6 ± 0.2 mM $[Ca^{2+}]_o$. Mutations at or around this Ca^{2+}-binding site are also associated with clinical syndromes (autosomal dominant hypocalcemia and familial hypocalciuric hypercalcemia) because of either an increase

or a decrease in the sensitivity of the respective receptors to $[Ca^{2+}]_o$. Zhang et al. (43) and others (44, 45) have also reported that mutations around this site, Ser-147, Ser-170, Asp-190, Tyr-218, and E297K, impair the activation of human CaSR by $[Ca^{2+}]_o$. Recently Silve et al. (42) have shown that the missense mutations E297K and Y218S significantly reduce the maximal response of the CaSR. Although E297K was considered a key factor in impairing protein folding, thus leading to lower expression on the cell surface and impaired responsiveness to $[Ca^{2+}]_o$, our unpublished data show that E297I has a membrane expression level comparable with that of the wild type CaSR. Therefore, the low expression level of E297K could be, at least in part, the result of the substitution of an unfavorable positive charge, which modifies the local charge balance, leading to reduced folding efficiency. Furthermore, our assessment of the surface expression of D318I by flow cytometry showed that it was at the same level as a wild type; this echoes the impact of mutating the equivalent residue in CaSR (e.g. Glu-297). It has been postulated that residues Ser-170, Asp-190, Gln-193, Ser-296, and Glu-297 are critical for Ca^{2+}-binding to CaSR and functionality of the receptor (42), which is in excellent agreement with our prediction. In addition, CaSR functions primarily as a $[Ca^{2+}]_o$-sensing receptor but can also integrate information about protein metabolism (i.e. amino acids) with that of divalent cations (e.g. calcium) (46). CaSR displays sensitivity to amino acids, especially phenylalanine and other aromatic amino acids, likely via three serine residues (Ser-169—Ser-171) at a site corresponding to the Glu-binding pocket in mGluR1$_\alpha$. The double mutation T145A/S170T specifically abolishes CaSR responsiveness to amino acids while leaving $[Ca^{2+}]_o$ sensing intact (47). Our unpublished data

show that Ca^{2+} and phenylalanine also synergistically modulate the signaling functions of CaSR.

In summary, we have predicted and confirmed experimentally a calcium-binding site in the extracellular domain of mGluR1α. We have also shed new light on the co-activation of mGluR1α by Glu and $[Ca^{2+}]_o$. These findings provide novel perspectives on mGluR1α, which may be viewed as capable of integrating information from two very different types of ligands (an amino acid neurotransmitter and a divalent cation). The levels of $[Ca^{2+}]_o$ in the brain are highly dynamic (37), and the affinity constants that we have determined in our studies on calcium binding to mGluR1α are well within the dynamic, physiological range of $[Ca^{2+}]_o$ in the brain. For family 3 GPCRs other than CaSR, the physiological importance of $[Ca^{2+}]_o$ binding has been uncertain; but the findings reported here may be useful in resolving this mystery by allowing for the development of knock-in mutations to mGluR1α, and resultant mouse models, that disrupt the ability of the receptor to bind $[Ca^{2+}]_o$ while leaving Glu binding intact. Moreover, because many of the key calcium-binding residues defined in our studies are conserved for other family 3 GPCRs, our findings may have relevance for a host of other receptors beyond just mGluR1α (6, 7). Family 3 GPCRs have tremendous potential as therapeutic targets, and therefore the advances described here may facilitate the development of novel family 3 GPCR-targeted drugs for use in the treatment of many different diseases.

4 EFFECTS OF EXTRACELLULAR CA^{2+} ON THE MODULATION OF METABOTROPIC GLUTAMATE RECEPTOR 1 ALPHA (MGLUR1A) BY L-QUIS, (S)-MCPG, CPCCOET AND RO 67-4853

4.1 Introduction

Group I metabotropic glutamate receptors (mGluRs) belong to family C of the superfamily of GPCRs, which activate phospholipase C (PLC) and subsequent IP_3 accumulation followed by Ca^{2+} release from intracellular stores in the ER. These receptors are critical for neuronal plasticity related to long term potentiation (LTP) and long term depression (LTD), in addition to their involvement in chronic neuronal degenerative diseases, such as Parkinson's, Huntington's, and Alzheimer's diseases (81). MGluRs are involved in the activation of PKC, PKB and PKA, and intracellular Ca^{2+} mobilization, thereby inhibiting caspase-coupled apoptosis, and, therefore represent one of as the main protective processes against neuronal injury in stroke, trauma, and Alzheimer's disease. They also slow down the progression of Parkinson's disease. In addition, mGluR1 has also been detected in melanoma and breast cancers, and it was proposed to be a potential therapeutic target for both cancers (4,8,9,107-109). MGluR1 inhibitors have been shown to effectively reduce the proliferation of breast cancer cells. However, the role of glutamatergic modulation in the development of chronic neuronal degenerative diseases remains elusive.

Glutamate receptors are mainly present in central neuronal system, and fall into two categories: ionotropic glutamate receptors (iGluRs) and metabotropic glutamate receptors (mGluRs). iGluRs are a group of ion channels activated by glutamate, which mediate fast excitatory responses. It's very difficult to tune the modulation of this group

of receptors, and blocking these receptors results in severe side effects, such as memory loss and hallucinations. In contrast, mGluRs display relatively slow response rates to changes in extracellular glutamate. Thus, the attention of drug discovery research has increasingly turned to mGluRs as targets to reduce the side effects seen in the central nervous system with iGluRs-based therapeutics, or to decrease the growth of cancer cells. The drugs targeting mGluRs can be classified into orthosteric modulators and allosteric modulators. Orthosteric modulators, including agonists and antagonists, induce and attenuate the activity of the receptor by competitively binding to the L-glutamate binding pocket, respectively, while allosteric modulators bind to sites other than the orthosteric center to affect the activity of the receptor.

L-Quis (L-Quis), the most potent agonist reported to date, with a K_D of around 30 nM (7,110), shares the same binding pocket with L-glutamate. Replacement of T188, D208, Y236 and D318 with Ala, results in loss of the receptor's sensitivity to both L-Glu and L-Quis, while the mutants R78E and R78L exhibit clearly impaired L-Quis binding (16,78). However, the effects of Ca^{2+} upon L-Quis' activation of and binding to mGluR1 are still controversial. Nash and Skirkel et al. claimed that mGluR1α is not a Ca^{2+} sensing receptor, because its initial responsiveness to the agonist is independent of the extracellular Ca^{2+} concentration.

(s)-MCPG is an analog of glutamate, known as a non-selective competitive antagonist that, by occupying the glutamate binding pocket, blocks not only the function of iGluRs, but also those of all the members in the mGluR family (55). Jingami et al. reported that (s)-MCPG could displace tightly bound ^{3}H-quasqulate (111). By wedging into the crevice between the two lobes in the protomer, (s)-MCPG interacts with Y74,

W110, S165, T188, and K409 in lobe one (LB1) and D208, Y236 and D318 in lobe two (LB2). Thus the receptor is stabilized in the resting state, which is referred to as the open/open state (55). (s)-MCPG, also named t-MCPG, partially inhibited the sensitivity of mGluR1α to 5 mM $[Ca^{2+}]_o$ and completely eliminated the response of the receptor to 5 μM $[Glu]_o$ (32). After fusing CFP and YFP to intracellular loops of mGluR1α, 30 μM L-Glu induced increases in the FRET signals were impaired in the presence of 0.5 mM (s)-MCPG (56). In brain slices experiments, (s)-MCPG was shown to reverse DHPG-induced long-term depression (LTD) (112). Thus accumulating evidence supports the antagonism of Glu- or Ca^{2+}-induced activation of mGluR1α by (s)-MCPG.

Ro 67-4853 is positive allosteric modulator of mGluR1, which enhanced the potency of L-Glu by interacting with transmembrane domain of the receptor. Ro 67-4853 has very strong potency upon L-Glu but has no activity to mGluR1 in presence of L-Glu in Ca^{2+} free buffer (38,68). The binding site of Ro 67-4853 along with other positive allosteric modulators (including Ro 01-6128, Ro 67-7476 and CDPPB analogs) were also investigated by Jeff Conn's group, and none of them was capable of replacing [^{3}H]R214127 (68). The mutation V757L abolished the activity of Ro 67-7476, VU-48 and VU-71, but mutations T815M and A818S doesn't affect their potencies (38,68). This suggests that the positive allosteric modulators have different binding pocket as allosteric negative modulators. VU-71 and Ro 67-7476 are proved to be inactive in human, however, VU-48 was interestingly shown activity in human mGluR1 (68). This brought forth a new hope to develop subtype specific drugs which could be applied to clinic trial. The effects of Ro 67-4853 on modulating Ca^{2+} induced response of mGluR1 remains unclear.

Additionally, the Ca^{2+} effect upon another non-competitive drug, CPCCOEt, was also examined. CPCCOEt was known as a negative allosteric modulator that inhibits the activation of mGluR1 by L-glutamate by specifically binding to the third extracellular loop of mGluR1a. In brain slices from mice models with arthritis, 10 μM CPCCOEt effectively inhibited EPSCs recorded using the whole-cell patch technique, indicating that CPCCOEt could relieve arthritis pain (13). When working together with MPEP, the selective mGluR5 antagonist, CPCCOEt, inhibits the long-lasting disinhibition (DLL) induced by low frequency stimulation of the dorsolateral striatum (14). In addition, CPCCOEt was suggested to reduce the somatodendritic dopamine level by inhibiting the intracellular Ca^{2+} release through mGluR1α (36).

MGluR1α has been demonstrated to be a Ca^{2+} sensing receptor. Kubo Y at al. transiently transfected mGluR1α into oocytes, and studies of its activation of Cl- coupled channels showed that mGluR1 senses Ca^{2+} as well as glutamate. Ca^{2+} can activate mGluR1, even when the receptor was saturated with glutamate (32). The Purkinje cells from mGluR1 knockout mice lose sensitivity to Ca^{2+}, while their response to Ca^{2+} was restored after mGluR1 was rescued by knocking in the receptor (95). Furthermore, a Ca^{2+} induced rearrangement of the transmembrane domain was identified using the NFRET technique, which involved fusing CFP and YFP to the intracellular loops of the protomers. Ca^{2+} was found to increase the NFRET signal by bringing the two second intracellular loops closer together in the same dimeric receptor (56). However, Nash and Skirkel at al. claimed mGluR1α is not a Ca^{2+} sensing receptor, because its initial response to the agonist was independent of the extracellular Ca^{2+} concentration (75,76).

Therefore, at this time the role of Ca^{2+} in modulating the actions of drugs on mGluR1 is unclear.

In this article, the effects of Ca^{2+} on the actions of L-Quis (agonist), (s)-MCPG (antagonist), Ro 67-4853 (PAM) and CPCCOEt (NAM) on mGluR1α were investigated. Extracellular Ca^{2+} enhanced an (^{3}H)-L-Quis binding to wild type mGluR1α and D322I, and E325I reduced Ca^{2+} effect upon the agonist. Mutants D318I abolished the L-Quis binding, while D322I and E325I still could bind L-Quis although E325I relatively decreased the binding capability of the receptor to L-Quis. In addition, Ca^{2+} consistently enhanced L-quis-induced intracellular Ca^{2+} release, which further confirms the Ca^{2+} effects on the activation of mGluR1α by its agonists. Obviously, extracellular Ca^{2+} increases the action of the agonist on the receptor by enhancing its binding affinity to our previously reported Ca^{2+} binding site (D318, D322 and E325). Furthermore, the role of Ca^{2+} in the inhibition of the receptor by the antagonists was studied by measuring the action of (s)-MCPG on mGluR1α in the absence or presence of Ca^{2+}. (s)-MCPG not only inhibits glutamate-induced intracellular Ca^{2+} release and IP_1 accumulation mediated by mGluR1α, but it also partially reduces the likelihood of Ca^{2+} activating the receptor. (s)-MCPG efficiently antagonizes both glutamate and Ca^{2+} at low concentrations, but increasing the concentration of glutamate or Ca^{2+} could overcome the inhibition of the receptor. Utilizing Lineweaver-Burke (LB)-plot analysis, we concluded that Ca^{2+} could attenuate the function of (s)-MCPG by competitively replacing this compound's binding to the receptor. In addition, CPCCOEt non-competitively inhibits the activation of mGluR1α by L-glutamate and also attenuates the Ca^{2+} response of the receptor. The documentation that Ca^{2+} modulates the sensitivity of mGluR1α to its agonists, antagon-

ists and allosteric modulators opens a new avenue for developing subtype-specific drugs targeting Group I mGluRs.

4.2 Results

4.2.1 An L-Quis binding pocket predicted by Autodock-Vina.

To understand the molecular basis of mGluR1α activation by L-Quis, both Ca^{2+} and L-Quis were docked into the crystal structure (1EWK, closed-open form) of the receptor. The coordinates of L-glu were removed before docking. The contacts of L-Quis within 6 Å were analyzed using an LPC server. As suggested in Fig. 4-1A, the L-Quis binding pocket corresponds well with the glutamate-binding residues suggested in the crystal structure. Ca^{2+} that resides at our reported Ca^{2+}-binding site containing D318, D322 and E325 (89), appeared to bind to L-Quis. This suggests that L-Quis possibly associates with Ca^{2+} to modulate mGluR1α, mimicking the synergistic function of L-glutamate and Ca^{2+} on this receptor.

4.2.2 Glutamate or (s)-MCPG induced hinge motion by binding to ECD-mGluR1α.

The crystal structure of mGluR1α bound with (s)-MCPG was determined in 2002 (55). By looking at the structure, we see that the (s)-MCPG binding pocket is markedly similar to that for glutamate, involving Y74, R78, W110, S165, S186, T188, D208, D318, R323, K409 (Fig. 4-1B). The glutamate-binding pocket has been further confirmed by our previous work and that of Jingami's group (78). Basically, the binding of agonist to mGluR1α was believed to activate the receptor by closing the two lobes in the both protomers, while antagonist binding would keep the receptor in its resting state. As suggested in table 1, compared to the free form of the receptor, the two lobes in the protomer were relatively rigid upon binding to L-glutamate (agonist) or (s)-MCPG (antagonist). This result indicated the ligand binding induced closure of the two lobes but did not affect intra-lobe conformation. L-Glu closed the two lobes more than 20 degrees, while (s)-MCPG only around 6 degrees.

4.2.3 Mutational effects on the correlated motion in ECD-mGluR1α

Three mutations of Ca^{2+} binding site 1, including D318I, D322I and E325I, were introduced into the model structure of ECD-mGluR1α. All the model structures were loaded with L-Glu and Ca^{2+}, and molecular dynamics simulation was performed. To understand the effects of mutations on correlated motion of the receptor, the assembles of MD simulation were collected for correlation calculation. As shown in Fig. 4-2, comparing to WT, the overall intensities of red and blue color of D318I were increased. As we showed in chapter 3, D318I abolished both the L-Glu and Ca^{2+} sensitivity of mGluR1. The MD calculation also indicates that D318 plays a vital role in mGluR1α, which is consistent with our previous imaging data. In addition, both D322I and E325I

decreased the correlation, suggesting that these two mutants could impair the correlated motion induced by L-Glu and Ca^{2+}. D322I and E325I are known to reduce both the Ca^{2+} and L-Glu responses of the receptor, although the maximal responses of these two mutations were increased. Thus, the correlation calculation of D322I and E325I also clearly supported our imaging data. In particular, the correlation of the region around Ca^{2+} binding site 1 was obviously changed by mutations, D318I, D322I and E325I. D318I has higher intensity in the Ca^{2+} binding site region, but that of D322I and E325I decreased. This brought forth the conclusion that the Ca^{2+} binding site 1 plays a very important role in the correlation of the ECD-mGluR1α.

4.2.4 Ca^{2+} enhances [^{3}H]-L-Quis binding to mGluR1α through binding to Ca^{2+} binding site 1 of the receptor.

Up to now, L-Quis is the strongest orthosteric agonist of mGluR1α with an EC50 of 30 nM. However, the role of Ca^{2+} in enhancing L-Quis binding to mGluR1α is still controversial. In our previous work, Ca^{2+} and glutamate were suggested to modulate mGluR1α synergistically, and a novel Ca^{2+}-binding pocket adjacent to the glutamate binding site was investigated. To determine the impact of Ca^{2+} upon agonist-induced activation of mGluR1α, the binding of the radioactive compound ([^{3}H]-L-Quis) to mGluR1α was tested in the absence or presence of Ca^{2+}. Ca^{2+} significantly enhanced L-Quis binding to the receptor (Fig 4-2B). A mutation in the Ca^{2+}-binding pocket, D318I abolished L-Quis binding, while D322I and E325I retained the binding property of the wild type receptor (Fig 4-2A). D322I and E325I were proven to enhance the maximal responses of the receptor to L-Glu but reduced the EC50, while D322I still had a comparable EC_{50} (89). To investigate the role of the Ca^{2+} binding site in the Ca^{2+} modulation of drugs binding to mGluR1, the Ca^{2+} effects on L-Quis binding to D322I and E325I were also studied. D322I relatively increased the effects of Ca^{2+}, while E325I obviously reduced Ca^{2+} effects on L-Quis binding to the receptor (Fig 4-2). This suggests that Ca^{2+} modulates the drug binding to mGluR1 by interacting with the predicted Ca^{2+}-binding site 1 in hinge region.

Intracellular Ca^{2+} mobilization is believed to be linked to an ECD conformational change induced by L-Quis binding. To further confirm the role of Ca^{2+} in the activation of mGluR1α by L-Quis, a single cell imaging assay was then performed measuring changes in $[Ca^{2+}]_i$. HEK293 cells transiently transfected with mGluR1α were

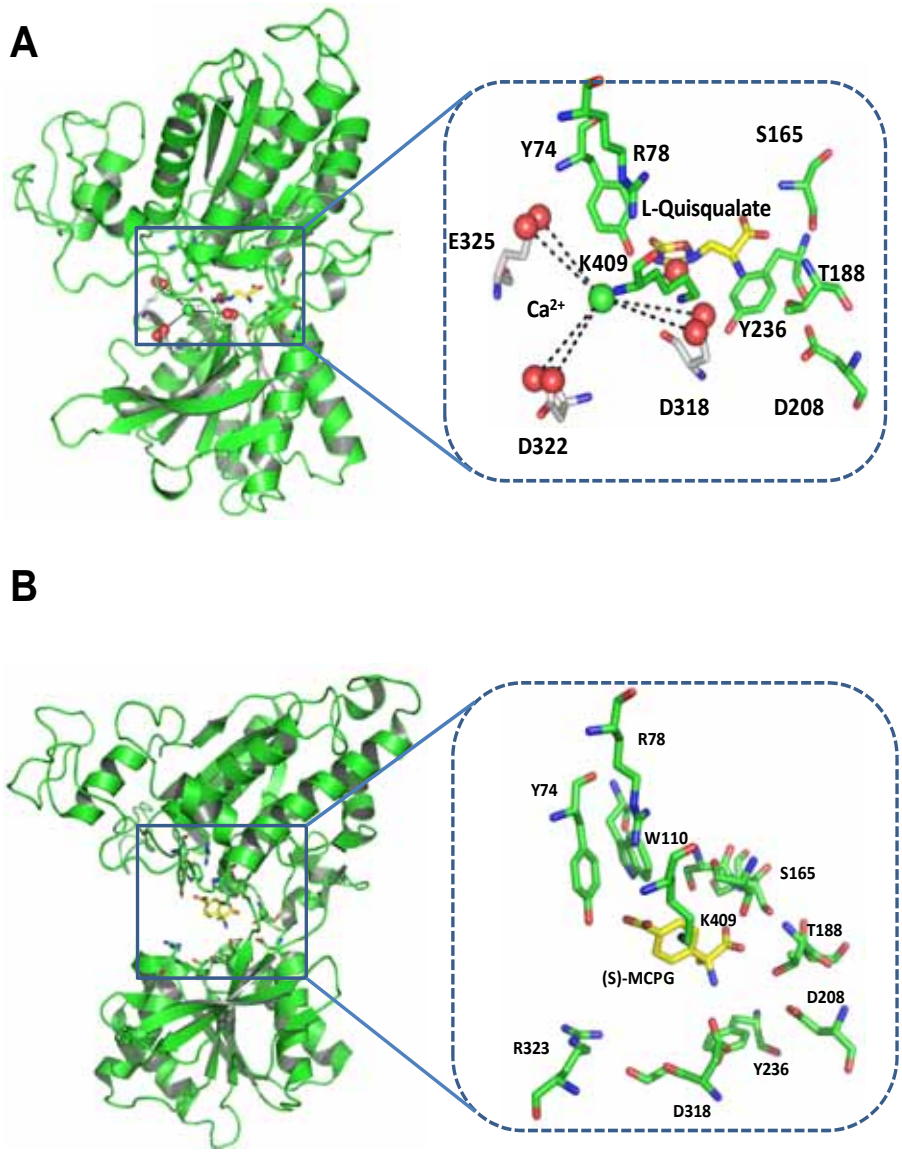

Figure 4-1 Structural models of mGluR1α bound with orthosteric ligands, L-Quis and (s)-MCPG. (A) Docking model of mGluR1α with L-Quis. The residues within 6 Å were highlighted. Similar ~~as~~ to the L-Glu binding pocket, Y74, R78, S165, T188, D208, Y236, D318, and K409 form the L-Quis binding pocket. The oxygen on the ring of L-quis was suggested to bind to Ca^{2+}. (B) Crystal structure of mGluR1α bound with (s)-MCPG. (s)-MCPG wedges into the LBD and maintaining the model structure of the receptor in its resting form.

Table 4-1 Hinge motion analysis using DynDom

PDB codes		Two-domain arrangement	Backbone RMSD (Å)	Hinge Motion		
Free Form	Bound Form			Rotation Angle (deg)	Translation (Å)	Closure (%)
1EWT	1EWK	D1 (38-209; 344-474; 476-476)	0.62	21.0	0.6	97.8
		D2 (210-343; 475-475; 477-510)	0.67			
1EWT	1ISR	D1 (38-209; 344-477)	0.66	22.3	0.7	99.7
		D2 (210-343; 478-510)	0.60			
1EWT	1ISS	D1 (38-208; 343-481; 501-506)	0.56	6.5	0.1	61.6
		D2 (209-232;482-500; 507-510)	0.62			

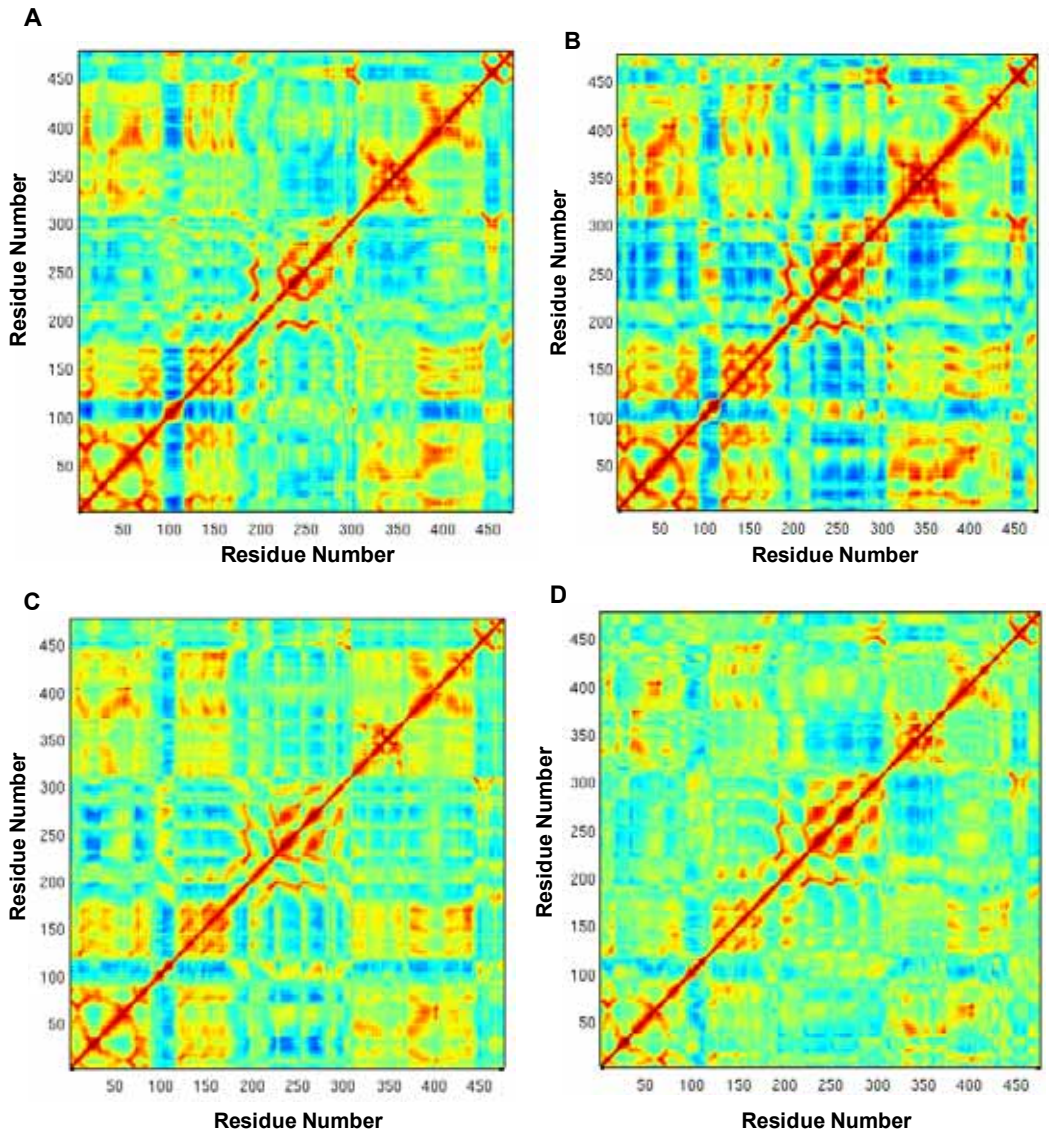

Figure 4-2 The effects of mutations of Ca^{2+} binding site 1 on correlated motion of ECD-mGluR1α. Model structures of mGluR1a and Ca^{2+} binding site 1 mutants were loaded with L-Glu and Ca^{2+}, and molecular dynamics was performed. The intensity of the red color represents the extent of positive correlation, and blue color stands for negative correlation. The correlated motions of the structures were analyzed by correlation map. D318I significantly changed the correlations of the residues within the receptor, while E325I and D322I diminished the correlations. Compared to D322I, E325I has larger effects on the correlation of the receptor. (A) Correlation map of wild type mGluR1. (B) Correlation map of D318I. (C) Correlation map of D322I. (D) Correlation map of E325I.

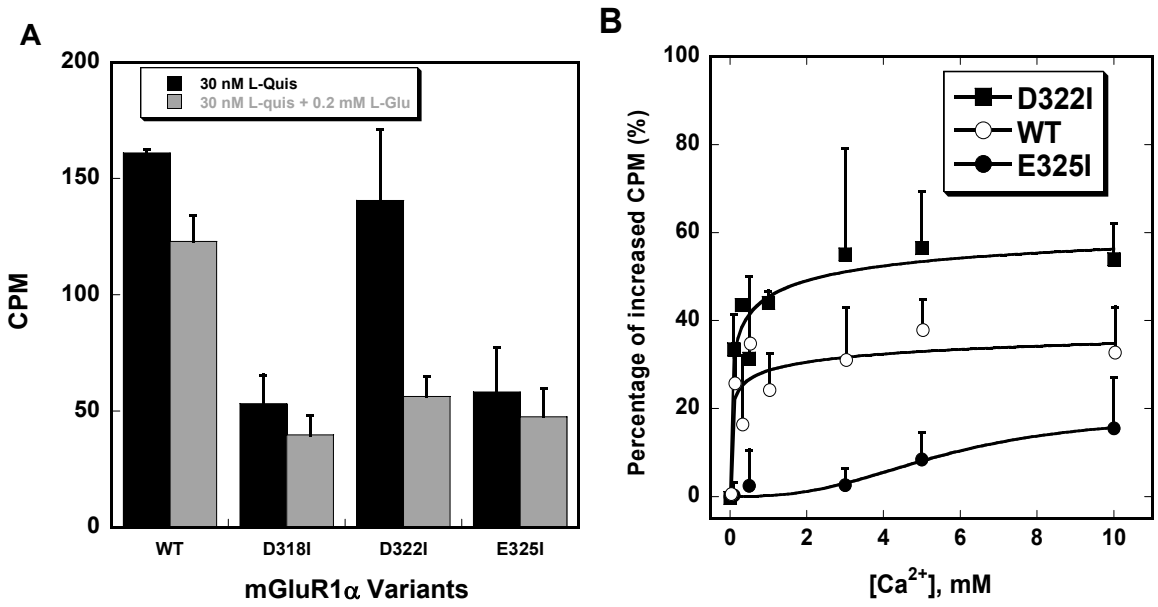

Figure 4-3 [^{3}H]-L-Quis binding to mGluR1α and its variants. (A) [^{3}H]-L-Quis binds to wild type mGluR1α in the absence of Ca^{2+}, but mutations in the Ca^{2+}-binding site decreased L-Quis binding. D318I and E325I eliminate L-Quis binding, while D322I still retains L-Quis binding. (B) Effect of Ca^{2+} on L-Quis binding to wild type mGluR1α, D322I and E325I. Increasing Ca^{2+} enhances L-Quis binding to wild type mGluR1α and D322I, whereas Ca^{2+} effects were abolished in E325I. The binding buffer used is hypotonic buffer with 20 mM HEPES, 100 mM NaCl, 5 mM $MgCl_2$, 5 mM KCl, 0.5 mM EDTA, 1% protease inhibitor and pH 7.0-7.5. (n=3)

Table 4-2 $[Ca^{2+}]_o$ enhances L-Quis induced activation of mGluR1α

Ca^{2+} Concentration	EC50	n_{Hill}	Maximal Response[a]
mM	nM		%
0	14.8	0.4	42 ± 1
1.8	2.4	1.6	70 ± 1

a. The maximal responses are normalized to the maximal response of wild type mGluR1α to Glu.

grown on coverslips and perfused with saline buffer in the perfusion chamber of a fluorescent microscope. The cytosolic free Ca^{2+} was monitored using cells pre-loaded with fura-2. In a nominal Ca^{2+}-free buffer (less than 2 μM), mGluR1α first starts to respond to L-Quis at 3 nM, while the addition of 1.8 mM Ca^{2+} reduces the EC_{50} to around 16%. The maximal response was increased from 42 ± 1 to 70 ± 1 (Fig. 4-3A and Table 4-2). These $[Ca^{2+}]_i$ imaging data further support the idea that Ca^{2+} plays a key role in causing L-Quis to activate the receptor by competitively binding to the L-Glu-binding pocket.

4.2.5 (s)-MCPG inhibits the sensitivity of mGluR1α to extracellular glutamate and Ca^{2+}.

(s)-MCPG is a non-selective competitive antagonist of glutamate for group I mGluRs and iGluRs. (s)-MCPG has been reported to completely inhibit the Cl^- current induced by glutamate, while the current triggered by Ca^{2+} was partially reduced (32). Consistent results were obtained in our experiments utilizing single cell imaging. Fig. 4-5 shows that 1.0 mM (s)-MCPG completely eliminates the sensitivity of mGluR1α to L-Glu, but the receptor still can sense Ca^{2+} even in the presence of 1.5 mM (s)-MCPG (Fig 4-6D). As revealed in the crystal structure (PDBID: 1ISS), (s)-MCPG shares most of the residues of the glutamate-binding pocket (55), which are adjacent to the Ca^{2+}-binding site. As shown in figure 4-5 and 4-6, intracellular Ca^{2+} mobilization (Fig. 4-4A, 4-5A) and IP_1 accumulation (Fig. 4-4C, 4-5C), which are modulated by both glutamate and Ca^{2+} were obviously attenuated in the presence of 0.5 mM (s)-MCPG. In addition, the EC_{50} value for $[Ca^{2+}]_o$ increased by ~1.7 fold (Fig.4-4A, table 4-3). When the receptor was saturated with Ca^{2+} or glutamate, the maximal responses were not affected by 0.5 mM MCPG,

Table 4-3 Addition of 0.5 mM (s)-MCPG decreases the responses of mGluR1α to Ca^{2+} and L-Glu

(s)-MCPG (mM)	5 mM Ca2+			5 uM L-Glu	
	EC50	n_{Hill}	Maximal response[a]	EC50	Maximal response[a]
0	3.5	6.4	85 ± 2	1.7	100 ± 2
0.5	6.0	2.6	67 ± 2	0.8	94 ± 6

a. The maximal responses are normalized to the maximal response of wild type mGluR1α to Glu.

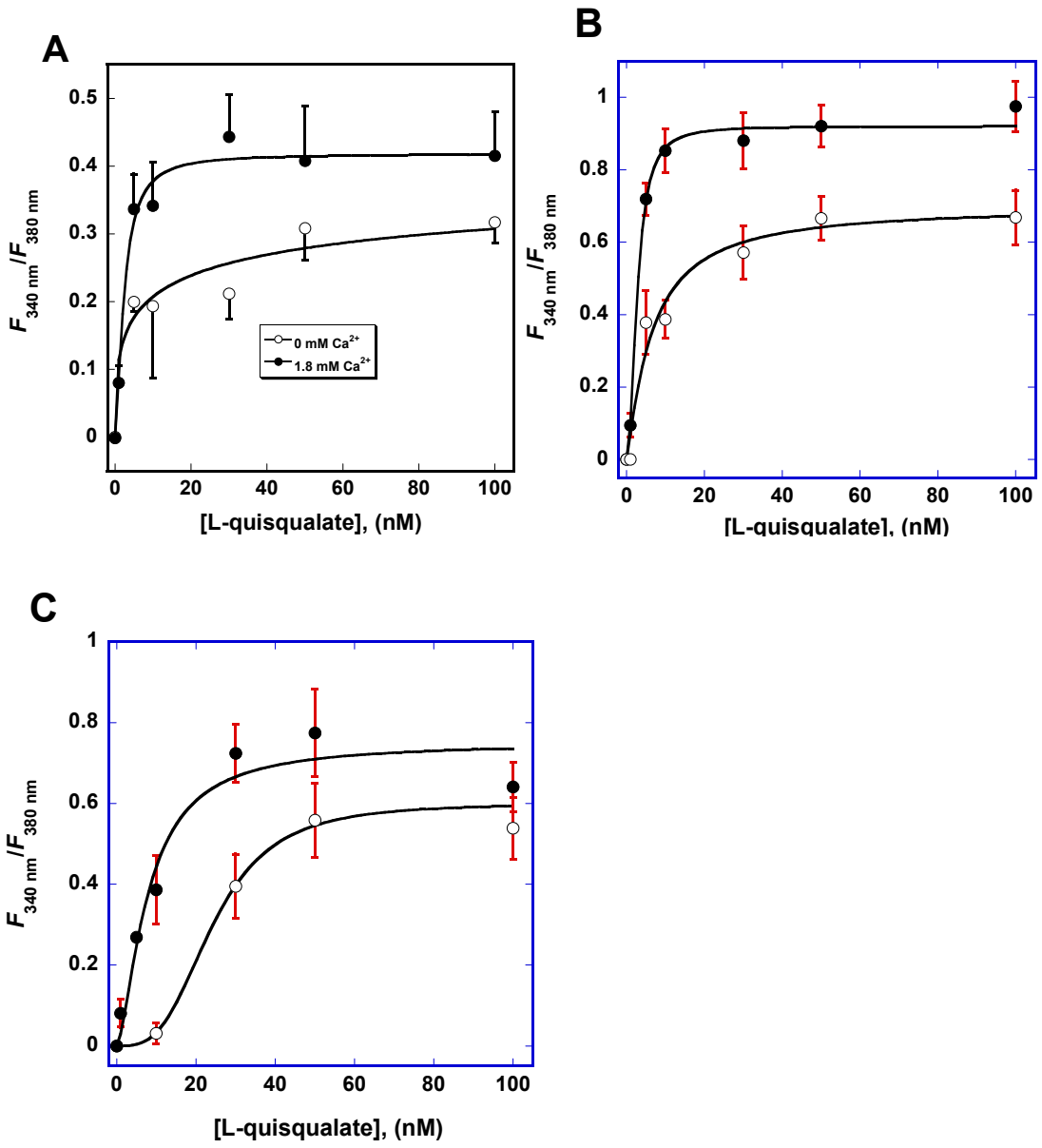

Figure 4-4 Extracellular Ca^{2+} enhances L-Quis activation of mGluR1α variants. (A) Addition of 1.8 mM Ca^{2+} increases the L-Quis-induced intracellular Ca^{2+} release from the ER mediated by activation of mGluR1α. (B) In the presence of 1.8 mM Ca^{2+}, the L-Quis sensitivity of D322I was increased. (C) 1.8 mM Ca^{2+} enhances L-Quis potency upon E325I. All the experiments were performed in the buffer with 10 mM HEPES, 140 mM NaCl, 5 mM KCl, 0.55 mM $MgCl_2$, 1 mM $CaCl_2$ and pH 7.4. (n=3)

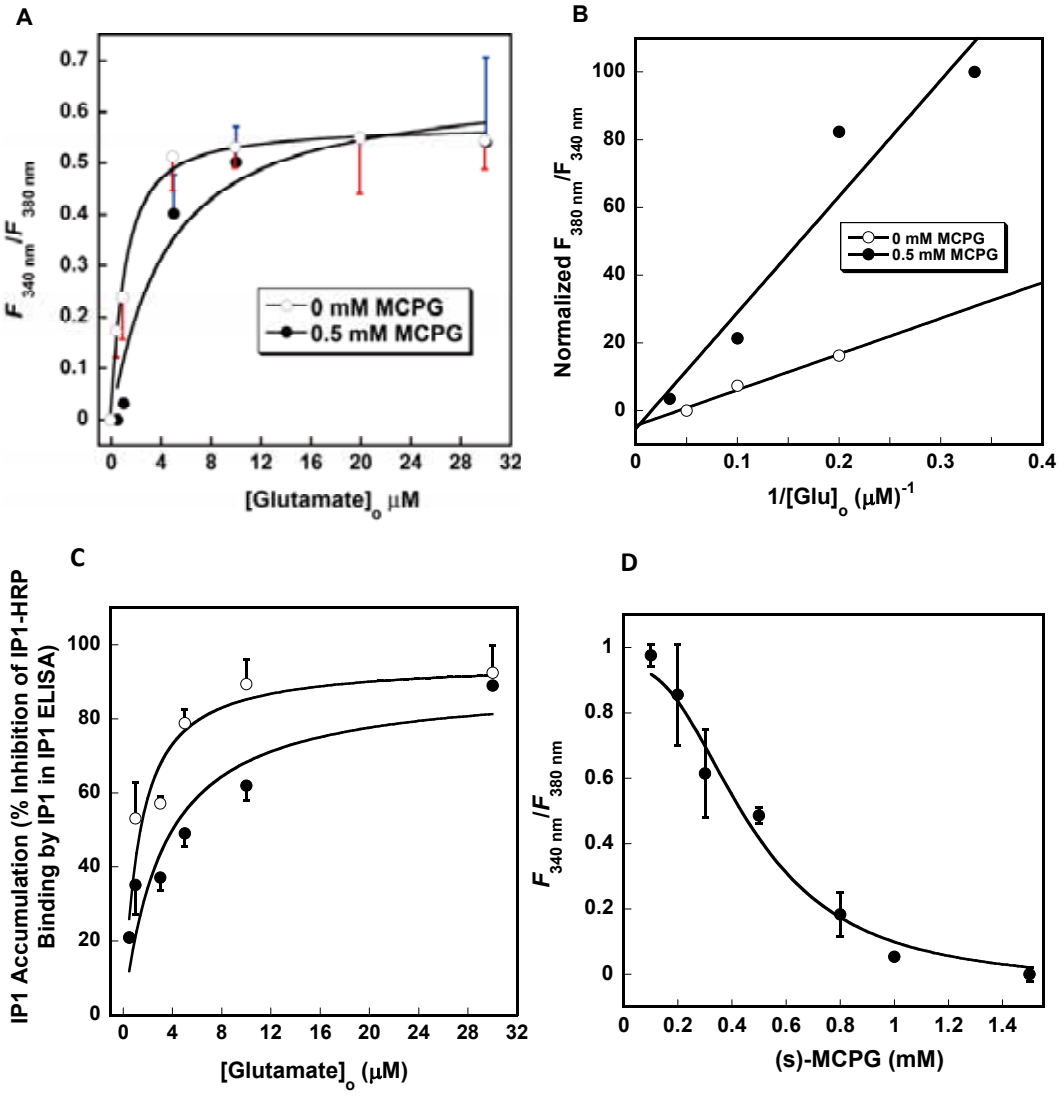

Figure 4-5 (s)-MCPG competitively inhibits the response of wild type mGluR1α to extracellular L-glutamate. (A) 0.5 mM (s)-MCPG competitively inhibits L-glutamate induced intracellular Ca^{2+} mobilization. (B) An L-B plot shows that (s)-MCPG can compete with L-glutamate. (C) An ELISA assay measuring intracellular IP1 accumulation suggests that (s)-MCPG antagonizes mGluR1α by competing with L-glutamate. (D) Increasing the concentration of (s)-MCPG inhibits mGluR1α in the presence of 5 µM L-glutamate, and 1.5 mM (s)-MCPG entirely blocks the activation of the receptor by L-glutamate. All the experiments were performed in the buffer with 10 mM HEPES, 140 mM NaCl, 5 mM KCl, 0.55 mM $MgCl_2$, 1 mM $CaCl_2$ and pH 7.4. (n=3)

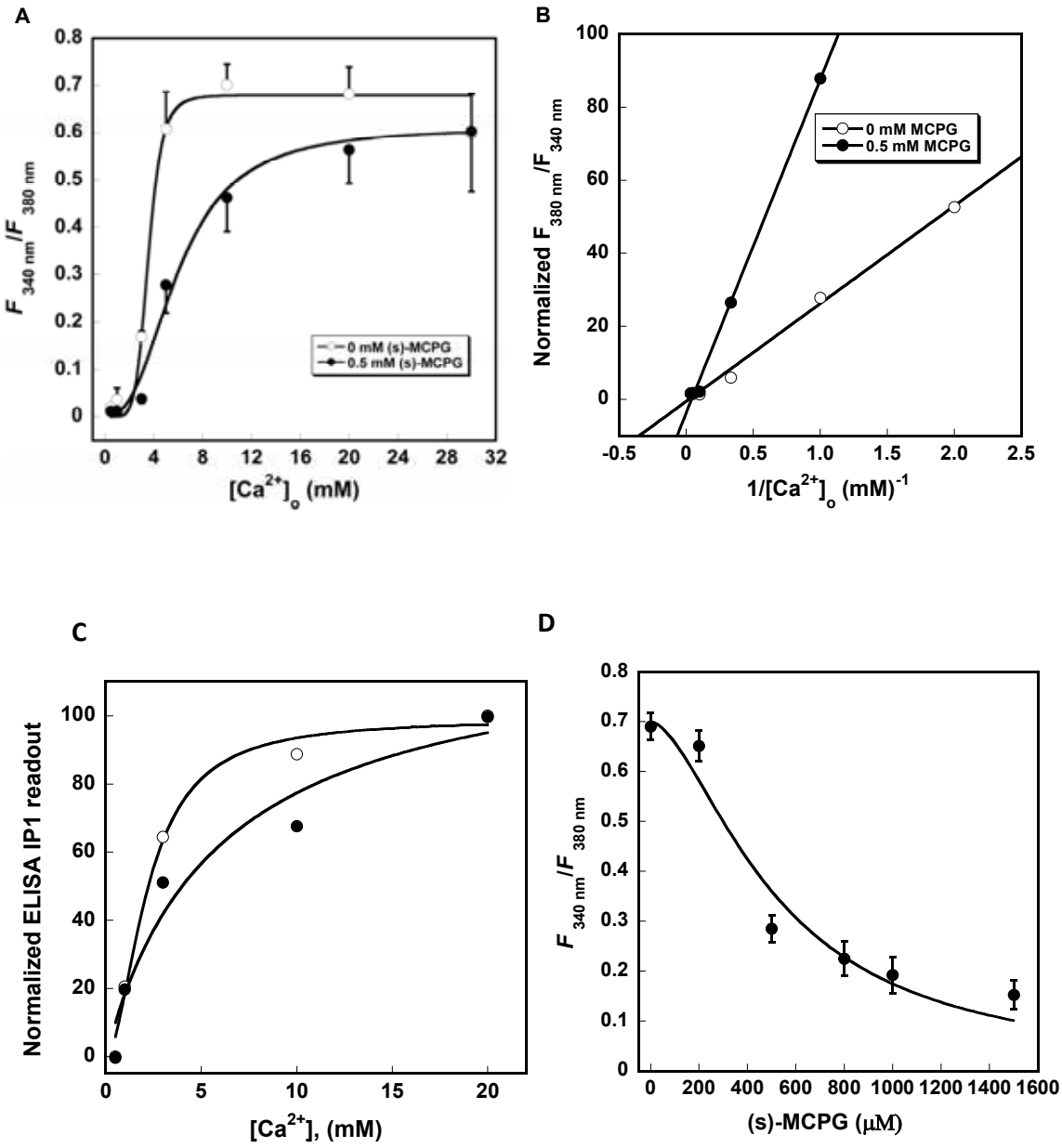

Figure 4-6 (s)-MCPG competitively inhibits the potentiation of mGluR1α potentiated by $[Ca^{2+}]_o$ in L-Glu free buffer. (A) 0.5 mM (s)-MCPG inhibits low $[Ca^{2+}]_o$-induced intracellular Ca^{2+} release, but high $[Ca^{2+}]_o$ restores the response of the receptor. (B) An L-B plot suggests that (s)-MCPG competitively inhibits $[Ca^{2+}]_o$-induced responses of mGluR1α. (C) ELISA results measuring intracellular IP1 accumulation indicate that (s)-MCPG reduces the sensitivity of mGluR1α to low but not to high concentrations of $[Ca^{2+}]_o$. (D) (s)-MCPG attenuates the responsiveness of mGluR1α to 5 mM $[Ca^{2+}]_o$, and 1.5 mM MCPG cannot completely inhibit the capacity of the receptor to sense $[Ca^{2+}]_o$.

which indicates that a high concentration of Ca^{2+} or glutamate could overcome the antagonism of (s)-MCPG. The curves plotted using the L-B equation confirmed that glutamate or Ca^{2+} do compete with (s)-MCPG (Fig. 4-5B, 4-6B). Increasing concentrations of (s)-MCPG entirely eliminated the 5 μM glutamate-induced activation of mGluR1α, while mGluR1 still could sense Ca^{2+} even in presence of 1.5 mM MCPG (Fig.4-5D, Fig. 4-6D). This may suggest that (s)-MCPG antagonizes the capacity of glutamate to activate mGluR1 by competing with glutamate at the binding pocket and interfering with Ca^{2+}-binding to its nearby site. However, it couldn't abolish all Ca^{2+}-binding pockets on this receptor.

4.2.6 Ca^{2+} enhances the potency of Ro 67-4853 to mGluR1α.

Ro 67-4853 is a positive allosteric modulator binding to the extracellular loops of the transmembrane domain of mGluR1α, but its binding pocket is different from several known negative allosteric modulators, such as CPCCOEt and R214127 (23,113). In the absence of L-Glu, Ro 67-4853 was unable to activate mGluR1α (68,69). To successfully obtain functional readout of Ro 67-4853 upon mGluR1α, HEK293 cells transiently expressing mGluR1α were pre-incubated with 0.5 mM Ca^{2+} and 5 nM Ro 67-4853 for more than 10 minutes. In the presence of 0.5 mM Ca^{2+}, Ro 67-4853 is capable of activating mGluR1α, translocating Ca^{2+} from the ER lumen to the cytoplasm. Increasing Ca^{2+} to 1.8 mM increased the maximal response induced by Ro 67-4853 through mGluR1α (Figure 4-7). At the same time, the EC_{50} value was reduced from 21.6 nM to 8.1 nM (Figure 4-7, table 4-6). Interestingly, intracellular Ca^{2+} oscillations were observed while the cells were treated with Ro 67-4853. Similar to the Ca^{2+} sensing receptor, three different patterns of response were discovered. As shown in figure 4-8A, most of the

cells displayed a transient spike. Some cells started oscillating after the first peak, while others had a transient peak and oscillation first appeared a few minutes later. By analyzing the number of cells oscillating out of the responsive cells, 1.8 mM Ca^{2+} significantly increases the number of oscillatory cells comparing to the cells in 0.5 mM Ca^{2+}. The starting point of oscillation was also shifted leftward (figure 4-8B). This suggests that extracellular Ca^{2+} enhances the potency of Ro 67-4853 to mGluR1α.

4.2.7 CPCCOEt noncompetitively inhibits L-glutamate induced responses, but only slightly affects Ca^{2+}-mediated responses of mGluR1α.

Most orthosteric drugs targeting mGluRs are known to lack subtype selectivity, which could lead to severe side effects due to the highly conserved endogenous agonist binding pockets on the other receptors. Because of this, a great deal of effort has been directed at developing drugs targeting sites other than the orthosteric center. CPCCOEt is known as a selective non-competitive antagonist of mGluR1 that binds to residues T815 and A818 in the 7th transmembrane domain (TM) of the receptor (42). CPCCOEt depressed IP_3 accumulation induced by the orthosteric agonists, L-Glu, L-Quis, DHPG, and ACPD, but the ^{3}H-glutamate binding capacity of mGluR1α remained intact (33). As shown in Fig. 4-9A, L-glutamate-triggered intracellular Ca^{2+} release was significantly depressed in the presence of 5 and 40 uM CPCCOEt. In the presence of 40 μM CPCCOEt, the maximal response decreased to only about half of the control level while the EC_{50} value was increased from 1.5 to 6.7 μM (Fig. 4-9A, table 4-5). By plotting using the L-B equation, the inhibition pattern displays as non-competitive behavior (Fig. 4-9B). To determine the effects of CPCCOEt on the activation of mGluR1α by Ca^{2+}, we next examined the Ca^{2+}-induced intracellular Ca^{2+} mobilization observed while gradually in-

creasing the CPCCOEt concentration. Fig. 4-10A reveals that CPCCOEt significantly reduced the Ca^{2+} sensitivity of mGluR1α. In the presence of 5 uM CPCCOEt, the EC_{50} of mGluR1α to Ca^{2+} was increased from 3.0 mM to 16.7 mM, while 40 uM CPCCOEt resulted in an even higher EC_{50} value of 28.7 mM (Fig. 4-10, Table 4-5). The maximal response was also significantly decreased by 40 uM CPCCOEt, although the maximal response with 5 uM CPCCOEt was still comparable. This indicates that 30 mM Ca^{2+} could not completely reverse the antagonism induced by CPCCOEt, so the inhibition pattern of CPCCOEt to Ca^{2+} on mGluR1α is non-competitive (Fig. 4-10, Table 4-5).

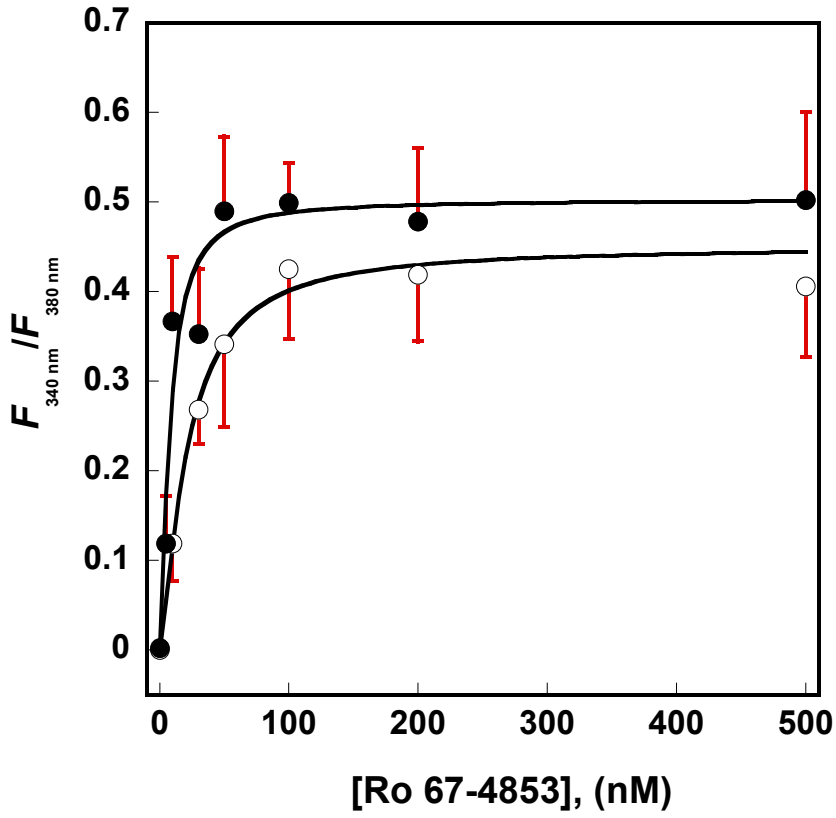

Figure 4-7 Extracellular Ca^{2+} enhances the potency of Ro 67-4853 on mGluR1α. HEK293 cells growing on coverslip were transiently expressed wild type mGluR1α. After dye loading, the cells were pre-incubated in 10 mM HEPES, 140 mM NaCl, 5 mM KCl, 0.55 mM $MgCl_2$, 0.5 mM $CaCl_2$ and 5 nM Ro 67-4853 (pH 7.4) for 10 mins. Then, addition Ca^{2+} and Ro 67-4853 were applied to the cells. Ro 67-4853 displays activity to mGluR1α in presence of 0.5 mM Ca^{2+} (empty circle), while 1.8 mM enhances its potency (solid dots).

Table 4-4 Ca^{2+} effects on Ro 67-4853 modulating mGluR1α

	EC50 (nM)	Maximal response
0.5 mM Ca^{2+}	21.6	74.9 ± 3.7
1.8 mM Ca^{2+}	8.1	79.5 ± 4.0

A

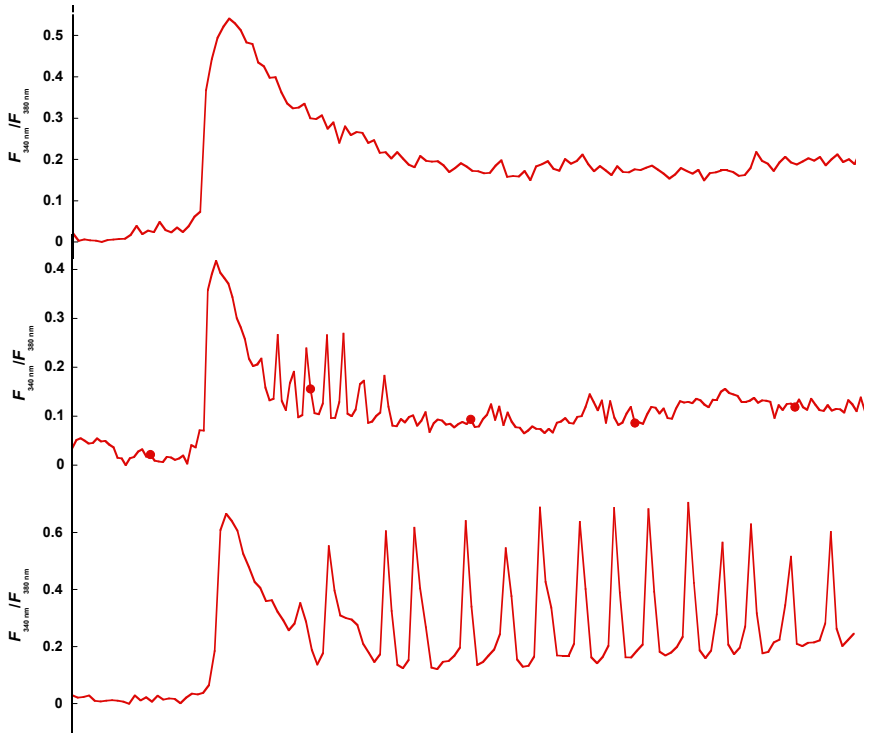
F340 nm /F380 nm
0.5
0.4
0.3
0.2
0.1
0
F340 nm /F380 nm
0.4
0.3
0.2
0.1
0
F340 nm /F380 nm
0.6
0.4
0.2
0

B

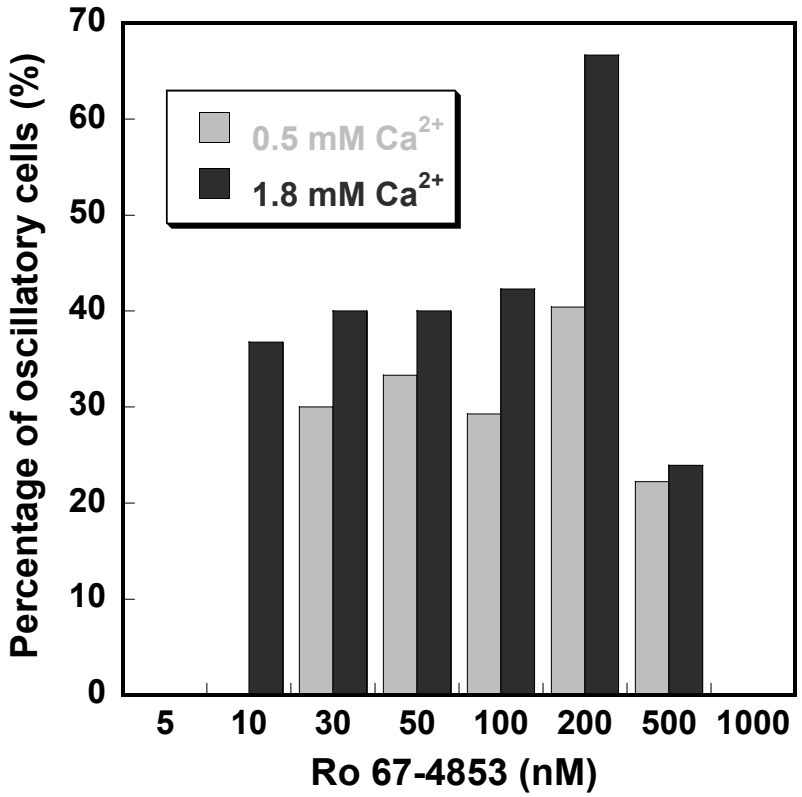
Percentage of oscillatory cells (%)
70
60
50
40
30
20
10
0
0.5 mM Ca2+
1.8 mM Ca2+
5
10
30
50
100
200
500
1000
Ro 67-4853 (nM)

Figure 4-8 Extracellular Ca^{2+} increases oscillatory events induced by Ro 67-4853. (A) Three different oscillation patterns were observed in HEK293 cells transiently expressing mGluR1a. HEK293 cells were perfused with medium containing 0.5 mM Ca^{2+} and 5 nM Ro 67-4853 in 10 mM HEPES, 140 mM NaCl, 5 mM KCl, 0.55 mM $MgCl_2$ for more than 10 mins in saline buffer, and an additional 1.8 mM Ca^{2+} and 100 nM Ro 67-4853 induced transient peak and oscillatory responses. More than half of the responding cells showed a transient peak, while the cells with oscillation fell into two categories: cells with constant oscillation and those starting with oscillations but diminishing later. (B) Ca^{2+} effects on Ro 67-4853 induced oscillation. Oscillation was observed in HEK cells expressing mGluR1a. Ro 67-4853 triggered intracellular Ca^{2+} release with 0.5 mM extracellular Ca^{2+}, and numerous cells display oscillatory behavior. In presence of 1.8 mM extracellular Ca^{2+}, the number of cells showing oscillations increases relative to the total number of responsive cells. At the same time, oscillatory cells appear at lower concentration of Ro 67-4853 when 1.8 mM Ca^{2+} was added.

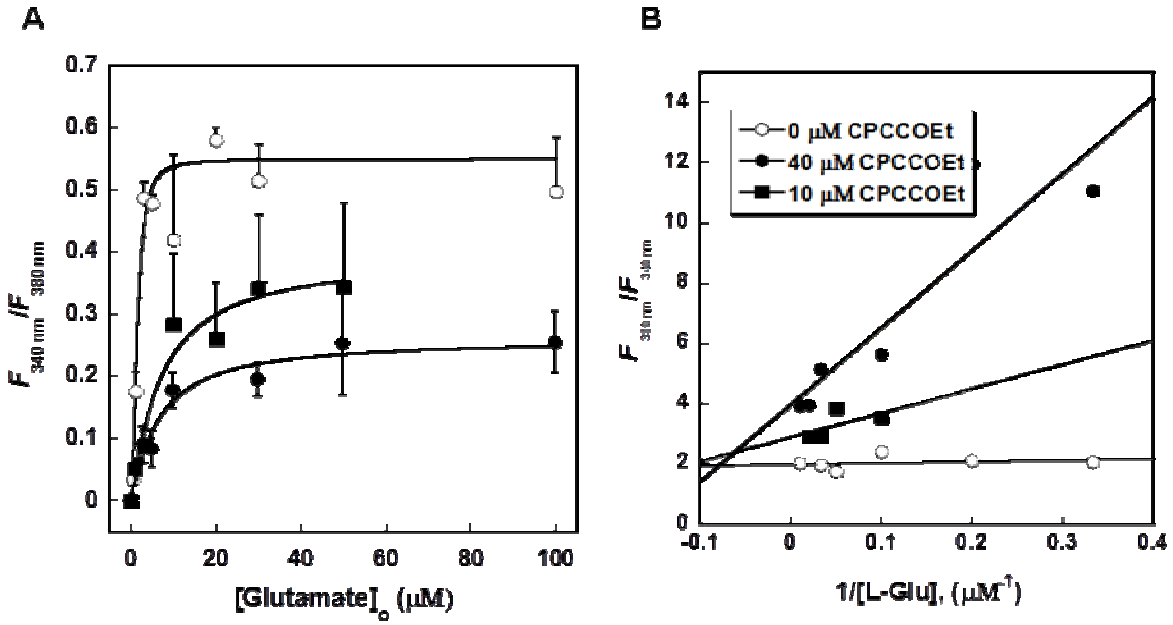

Figure 4-9 CPCCOEt non-competitively reduces L-Glu sensitivity of mGluR1α. (A) In the presence of 5 or 40 μM CPCCOEt, the sensitivity of mGluR1α to extracellular L-Glu was inhibited. The maximal response was reduced to about 50% in the presence of 40 μM CPCCOEt. (B) L-B plot analysis of the inhibition pattern of CPCCOEt displayed as non-competitive. The HEK293 cells transiently expressing wild type mGluR1α were mounted on the coverslip, and Ca^{2+} change indicated by fura-2AM was collected. All the image work was performed in the saline buffer with 10 mM HEPES, 140 mM NaCl, 5 mM KCl, 0.55 mM $MgCl_2$, 1.8 mM $CaCl_2$ and pH 7.4. (n=3)

Table 4-5 CPCCOEt inhibits the L-Glu sensitivity of mGluR1α

CPCCOEt Concentration	EC50	nHill	Maximal Response[a]
μM	mM		%
0	3.0	1.7	90 ± 2
5	16.7	1.0	88 ± 4
40	28.7	1.0	70 ± 2

a. The maximal responses are normalized to the maximal response of wild type mGluR1α to Glu.

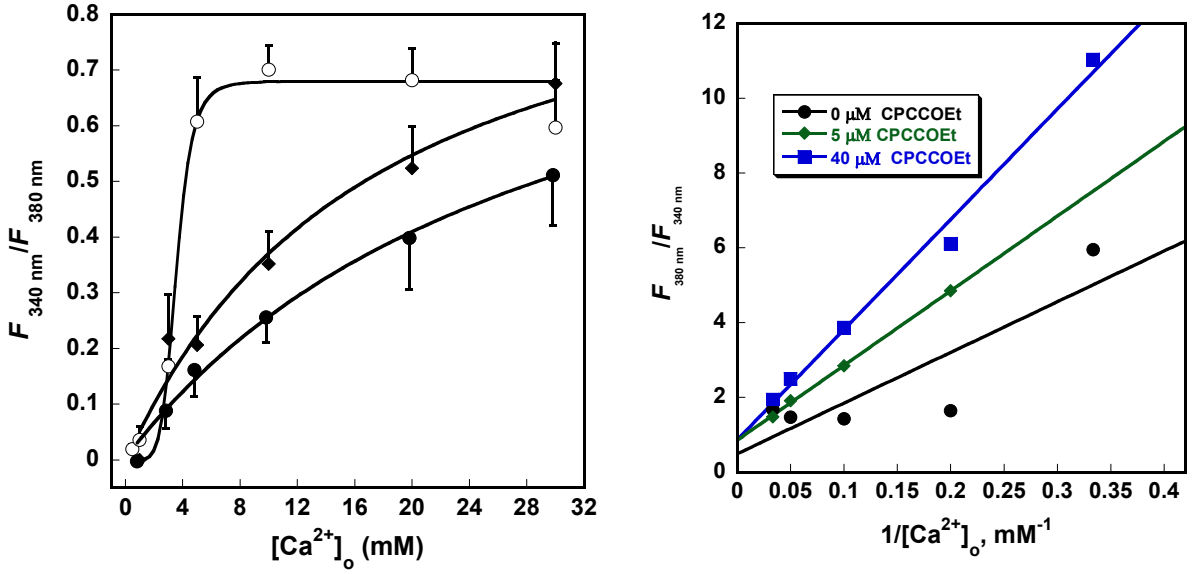

Figure 4-10 Effects of CPCCOEt upon the responses of wild type mGluR1α to Ca^{2+}. (A) The Ca^{2+} sensitivity of wild type mGluR1a was reduced by the addition of 5 or 40 μM CPCCOEt. Cytosolic Ca^{2+} was measured using Fura-2 AM in the absence (solid dots) or presence of 5 μM (solid square) and 40 μM (empty circle) CPCCOEt. In the cells inhibited by CPCCOEt (5 or 40 μM), increasing extracellular Ca^{2+} counteracted the inhibitory effects of CPCCOEt. (B) L-B plot suggests the CPCCOEt non-competitively inhibits the Ca^{2+} response of mGluR1. This work was done in the saline buffer with 10 mM HEPES, 140 mM NaCl, 5 mM KCl, 0.55 mM $MgCl_2$, 1.8 mM $CaCl_2$ and pH 7.4. (n=3)

4.3 Discussion

As described in our previous paper, a novel Ca^{2+}-binding pocket, which resides adjacent to the glutamate binding pocket (Chapter 3), was identified by site-directed mutagenesis and an intracellular Ca^{2+} readout. The mutations D318I and E325I were shown to lose their sensitivity to extracellular Ca^{2+}, while D318I also eliminated the response to glutamate. D322I impaired both the Ca^{2+} and glutamate sensitivity of the receptor. Ca^{2+} was proven to synergistically enhance the capacity of glutamate to modulate mGluR1α (89). However, the effects of Ca^{2+} in modulating the actions of the drugs upon mGluR1α remain controversial. In this chapter, we studied the effects of Ca^{2+} on the modulation of mGluR1α by the agonist L-Quis, the antagonist (s)-MCPG, the positive allosteric modulator Ro 67-4853 and the negative allosteric modulator CPCCOEt. As suggested by the AutoDock model, the L-Quis binding pocket overlapped extensively with the L-glutamate binding pocket in the reported crystal structure. At the same time, L-Quis could serve as a Ca^{2+}-binding ligand that closely mimics the behavior of L-glutamate.

To date, besides allosteric modulators, the orthosteric modulators include agonists and antagonists that are analogs of L-glutamate and share the same binding residues in the hinge region. Upon agonist binding, LB1 (lobe 1) and LB2 (lobe 2) in the extracellular domain move toward each other, and the whole dimeric ECD twists in a clockwise manner. Conversely, the receptors bound to the antagonists are regarded as being in the resting form. MGluR1α bound to (s)-MCPG was visualized by X-ray crystallography, which showed that the (s)-MCPG is wedged into the hinge region, thereby preventing the two lobes from closing and locking the receptor in its inactive form (55).

The function of L-Quis has been well studied. Activation of glutamate receptors triggered by L-Quis is known as Quis-effects. In mGluR1α, L-Quis is believed to function as an orthosteric modulator binding to the glutamate binding site, because the mutants T188A, D208A, Y236A and D318A, which have been determined to be specifically bound to the α-amino group, abolished the sensitivity of the receptor to both L-Quis and L-glutamate (78). MGluR1α is known to sense not only L-glutamate, and L-Quis, but also extracellular Ca^{2+} (32,89). To determine the effects of Ca^{2+} on the agonists, Nash et al. assessed intracellular Ca^{2+} mobilization and IP_3 accumulation in mGluR1α over-expressing CHO cells stimulated by L-Quis in the presence of 1.3 mM Ca^{2+}. Both IP_3 and intracellular Ca^{2+} readouts indicated that the response of the receptor to L-Quis was not altered with regard to the peak amplitude of the response curve, but the plateau was higher when Ca^{2+} was present (75). This suggests extracellular Ca^{2+} did enhance the increase in the cytosolic Ca^{2+} concentration although the transient increase was not affected. Moreover, another group (76) measured L-Quis binding using the purified ECD of mGluR1α, and they also claimed that Ca^{2+} had no effect on L-Quis binding to the receptor (76). Because C -terminal of mGluR1α can form a complex with the C-terminal of the $GABA_B$ receptor ($GABA_BR$), and $GABA_BR$ was suggested to respond to Ca^{2+}, Tabata et al. suspected that the intracellular Ca^{2+} response mediated by mGluR1α was the consequence of the $GABA_BR$ responding to extracellular Ca^{2+} (114). To clarify the ambiguity of the Ca^{2+}-sensing properties of mGluR1α, we performed (^3H)-L-Quis binding assays to confirm the role of the Ca^{2+}-binding site described in our previous paper. Our binding data support the contention that Ca^{2+} enhances L-Quis binding to mGluR1α. Increasing the extracellular Ca^{2+} concentration enhanced L-Quis binding to HEK293 cells

over-expressing mGluR1α, while E325I abolished this effect of Ca^{2+} (Fig 4-3). Moreover, we can see the obvious difference in L-quisqulate binding in the presence of a very low Ca^{2+} concentration. This caused us to suggest that concentrations of 4 mM Ca^{2+} and below might not be high enough to observe the difference owing to the strong binding affinity of L-Quis and the low sensitivity of Ca^{2+} imaging and the IP1 readout. Referring to our previous work, with lower than 3 mM Ca^{2+}, it is difficult for us to observe the effects of Ca^{2+} on the function of the receptor. However, Nash et al. never provided the surface expression level in their study, so the receptor expression level in the cells they chose for analysis could be questioned. In our binding data, low Ca^{2+} (0.1 mM) caused a significant increase in L-Quis binding. Additionally, for efficient binding with L-quis, the cysteine-rich domain or transmembrane domain is indispensable, but Selkirk's group only purified the ECD-mGluR1α for L-Quis binding.

Another glutamate analog, (s)-MCPG, also called t-MCPG, is known as a competitive antagonist of mGluR1α, which completely inhibits L-glutamate-potentiated Ca^{2+}-activated Cl- currents in *Xenopus Laevis* oocytes transiently expressing mGluR1 (32). By respectively tagging the FRET pair YFP/CFP to the two intracellular loops 2 (i2) of the dimeric mGluR1α, Muto et al. observed that the re-arrangement of the transmembrane domain induced by glutamate was reversed by (s)-MCPG (56). MGluR1 bound to (s)-MCPG was proposed to be in the resting state. This was determined by X-ray crystallography (PDBID: 1ISS), suggesting that (s)-MCPG wedges in the hinge region of the clam shell-like structure by occupying most of the residues involved in glutamate binding (55). In the meantime, Ca^{2+}-induced responses mediated by mGluR1α were found to be partially antagonized by (s)-MCPG, but the mechanism of (s)-MCPG on the bind-

ing of Ca^{2+} is not clear (32). We first tested the Ca^{2+} responses by gradually increasing the (s)-MCPG concentration. These experiments suggested that (s)-MCPG did impair the Ca^{2+} sensitivity of mGluR1α, although it couldn't completely reverse it (Fig. 4-6D). With increases in the Ca^{2+} concentration, the inhibition of (s)-MCPG was reversed by Ca^{2+}, as well as by L-glutamate (Fig. 4-6A-C). Thus, we can postulate that Ca^{2+} may share the residues involved in L-glutamate and (s)-MCPG binding, or (s)-MCPG at least disturbed the binding of Ca^{2+} to the extracellular domain of mGluR1α.

In the past decade, allosteric modulators drew more and more research interests due to their subtype specificities, and numerous positive and negative allosteric modulators have been developed. Mainly, the allosteric modulators target to the transmembrane domain of mGluR1, but the binding sites of positive and negative modulators are distinct (68). The allosteric modulators effectively modulate the receptor activity by L-Glu and other agonists. However, little is known about the effects of the endogenous mineral ion, Ca^{2+}, on these modulators. In this study, the Ca^{2+} effects on Ro 67-4853 (PAM) and CPCCOEt (NAM) were identified. Ca^{2+} in physiological level (1.8 mM) enhanced the potency of Ro 67-4853 in modulating mGluR1α, while increasing Ca^{2+} diminished the inhibitory effects of CPCCOEt (Figures 4-7, 4-8, 4-9 and 4-10, Table 4-4 and 4-5). This further proves that Ca^{2+} is capable of modulating mGluR1α. Because both Ro 67-4853 and CPCCOEt were proved to interact with the transmembrane domain of the receptor, these data suggest that the activation signal of mGluR1α is transferred to downstream signaling pathways through the transmembrane domain. Thus Ca^{2+} has the potential to even more widely modulate the profile of drugs acting on mGluR1α, including agonists, antagonists or allosteric modulators.

In conclusion, we investigated the effects of Ca^{2+} on agonist, antagonist, and allosteric modulators of mGluR1α, and found that Ca^{2+} enhances the functions of agonists and positive allosteric modulators, but attenuates the action of antagonists and negative allosteric modulators. Given the severe side effects of the drugs currently available for diseases of the nervous system, our findings could potentially provide new options for the drug industry. In the present studies, we further confirmed our reported Ca^{2+}-binding site adjacent to the ligand, glutamate. This will be very exciting information for the development of new orthosteric drugs for mGluR1α.

5 THE FUNCTION OF CALCIUM ON MGLUR1 FOLDING IN THE ER

5.1 Introduction

Metabotropic glutamate receptor 1 (mGluR1), a member of family C GPCR, senses extracellular ligands by virtue of its expression on the membrane of the post-synapstic neurons. Poor expression of mGluR1 attenuates the capacity of these neurons to respond to the extracellular environment, thus reducing their functional capabilities. The possibilities underlying a low expression level could be a low overall expression, poor forward trafficking from the ER, or poor recycling to the plasma membrane flowing internalization of the receptors. One of the reasons for poor forward trafficking is anchor proteins. For example, Homer 1b was reported to retain mGluR5 in the ER by interacting with the C-terminal of the receptor, while a point mutation that disturbed this interaction released the receptor to the membrane (115). Another reason could be misfolding of the receptor in the ER, so that the receptor is degraded pathway rather than trafficking to the membrane. Chaperone proteins and the ionic environment are believed to determine the fate of receptors during their biosynthesis. Kelly et al. stated that a chaperone facilitates protein folding in the presence of high Ca^{2+} in the ER (116). The proteostasis of the mutant glucocerebrosidase (GC) was enhanced when the ER Ca^{2+} level was increased by reducing Ca^{2+} efflux and increasing Ca^{2+} influx. There is also ~~a~~ evidence showing that depletion of Ca^{2+} in the ER using thapsigargin reduced VSVG (Vesicular stomatitis virus G protein) folding, but its trafficking to the membrane was only slightly impaired (117). Since mGluR1 itself contains several Ca^{2+}-binding sites and the ER has a very high Ca^{2+} concentration in the millimolar range, we hypothesized that Ca^{2+} ions could also contribute to protein folding.

In the experiments described in this chapter, we investigated a novel Ca^{2+}-binding site in the ECD of mGluR1α, which resides right at the L-Glu binding pocket. This Ca^{2+}-binding pocket was confirmed using a single cell imaging assay and site-directed mutagenesis. Mutations of the novel Ca^{2+}-binding site attenuated the Ca^{2+} sensitivity of the receptor, although several of them also eliminated L-glutamate responses, reflecting the extensive overlap of the calcium and glu-binding sites. Reducing ER Ca^{2+} using thapsigargin (TG) inhibited wild type mGluR1α trafficking to the cell surface. TG is known as a non-competitive inhibitor of sarco/endoplasmic reticulum Ca^{2+} ATPase (SERCA)(118), which irreversibly inhibits Ca^{2+} refill of SR/ER. A thermal stability assay using purified ECD-mGluR1α suggests that Ca^{2+} is important to the protein stability. This may indicate that Ca^{2+} is a key factor in the process of mGluR1α folding in the ER, potentially, at least in part, by binding to the calcium-binding site identified in our studies described in chapter 3.

5.2 Results

5.2.1 Determine surface expression of WT-mGluR1α and its mutants

The surface expression levels of wild type mGluR1α or its mutants are likely to be very important for the response of cells to the agonists. To detect the number of membrane receptors, mCherry was engineered to the C-terminal of the receptor, which could enable assessment of the overall expression of the mGluR1, while a green, secondary antibody to stain the surface expressing receptors on HEK293 cells were seeded onto the coverslips. The ratio of the fluorescence of FITC over mCherry indicates the proportion of the receptor expressing on the cell membrane. As suggested in

Fig. 5-1, wild type mGluR1α, S165A, T188A, and N335I were comparably expressed, when D208I, Y236F and E325I expression levels were decreased to ~ 50% of wild type.

5.2.2 Effects of mutations of Ca^{2+}-binding site 2 to extracellular Ca^{2+}

As suggested by the MUG algorithm and the alignment with Ca^{+} binding site 1 of the Calcium sensing receptor (46), S165, T188, D208, Y236, and D318 could form another Ca^{2+}-binding site. Combined with Ca^{2+}-binding site 1, including D318, D322 and E325, these two Ca^{2+}-binding sites reside at the hinge region side by side, sharing a common residue D318. To determine if these residues are critical for mGluR1α to sense extracellular Ca^{2+}, the proposed residues in the Ca^{2+}-binding site were replaced by apolar residues using site-directed mutagenesis. As shown in Figure 5-2, all mutants reduced the response of mGluR1α to extracellular Ca^{2+}, either the maximal responses or the EC_{50}. Herein, the maximal intensities of the transient peak on T188A and D208I were decreased to only half of wild type mGluR1. The EC_{50} values of T188A, Y236F, and D208I were slightly increased, while S165A increased by 2-fold over that of the wild type (Table 3-4). As previously described, D318I eliminated the capacity of both L-Glu and Ca^{2+} to activate mGluR1α.

Thapsigargin reduces the membrane expression of mGluR1α. To determine the role of Ca^{2+} in the ER in mGluR1α folding and trafficking, thapsigargin (TG), which blocks the pumping of calcium into the ER, was applied to the cells to reduce the Ca^{2+} concentration in the ER lumen. After mGluR1α was well expressed on the membrane of HEK293 cells, an additional 300 nM TG was added to the cell culture medium for over 24 hours. The receptors expressed on the cell surface were stained using antiFlag primary antibody and 488 Alexa-tagged secondary antibody. The overall level of mGluR1α

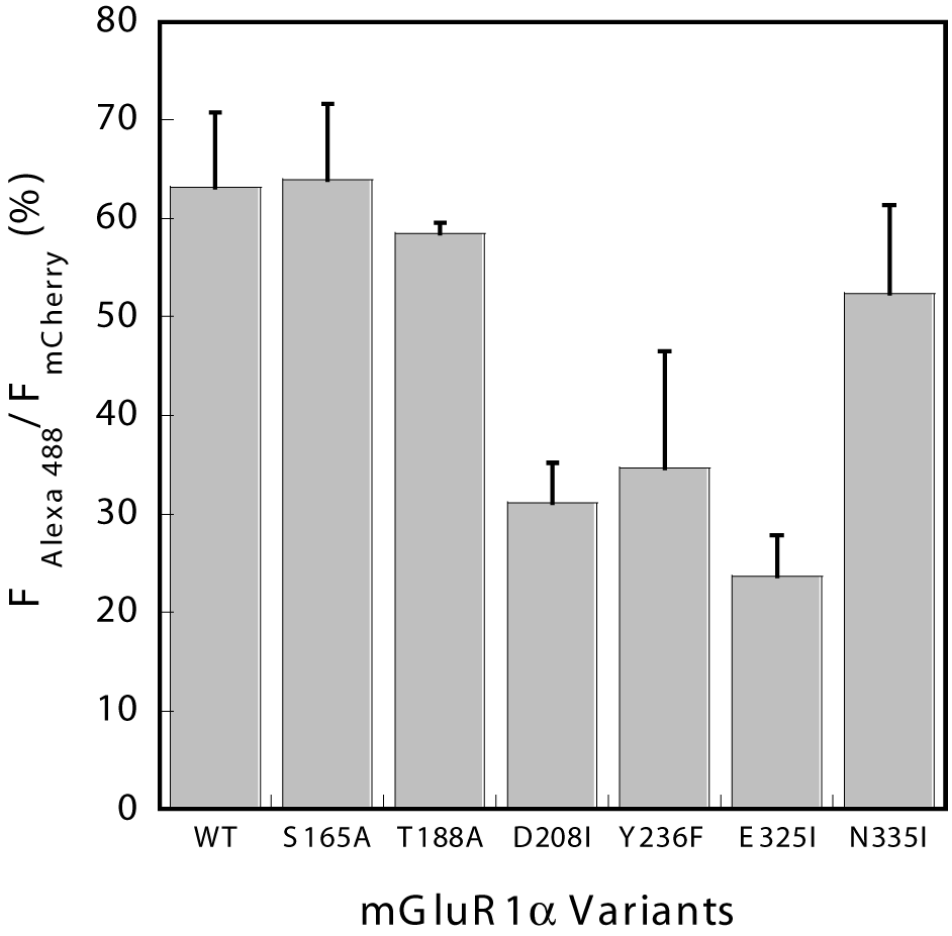

Figure 5-1 Surface expression of mutants in Ca^{2+}-binding site 2 determined by FACS. Surface expression of mGluR1α and its variants are determined by the ratio of surface receptors and overall expression of mGluR1α in HEK293 cells. Overall expression of mGluR1 was measured by the tagged mCherry while surface receptors were stained by Flag tag which can be labeled by secondary antibody conjugated with green fluorescence. The ratio of readout of green fluorescence and red fluorescence suggests the proportion of surface expression of the receptors. The mutations on the predicted Ca^{2+} binding site obviously reduced surface expression (D208I, Y236F and E325I).

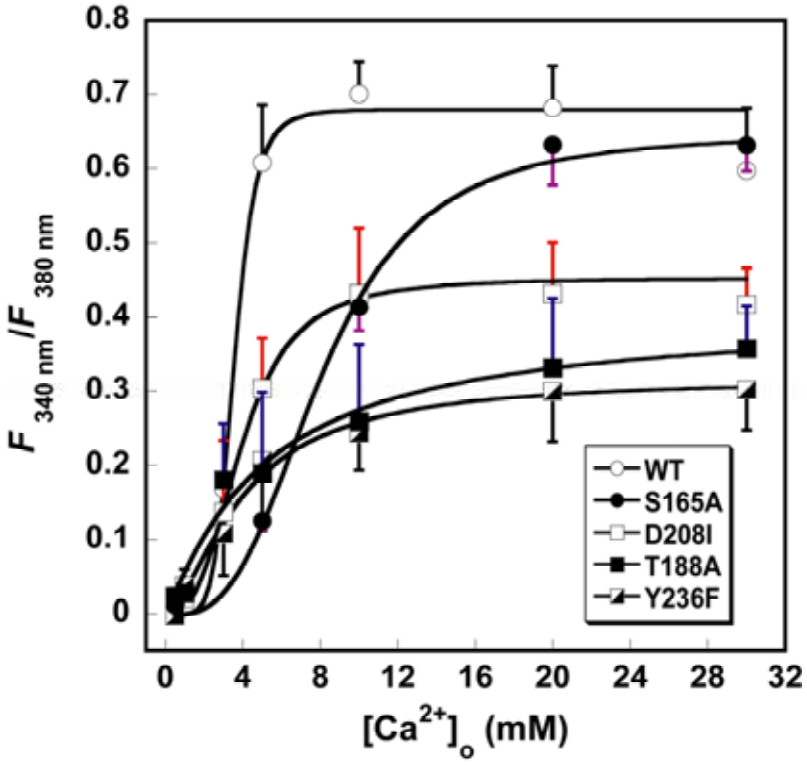

EC50
WT: 3.6 mM (3.0 mM)
S165A: 8.1 mM (8.1 mM)
T188A: 5.0 mM (3.4 mM)
D208I: 4.0 mM (4.6 mM)
Y236F: 4.0 mM (3.3 mM)

Figure 5-2 Mutations on the predicted Ca^{2+}-binding site 2 reduced intracellular Ca^{2+} mobilization triggered by extracellular Ca^{2+}. Ca^{2+} response of wild type mGluR1a and its mutants on Ca^{2+} binding site 4 were measured by pre-loaded Fura-2AM. Despite of the attenuation of surface expression, S165A, T188A, D208I and Y236F reduced Ca^{2+} response by decreasing maximal response and increasing EC50 value.

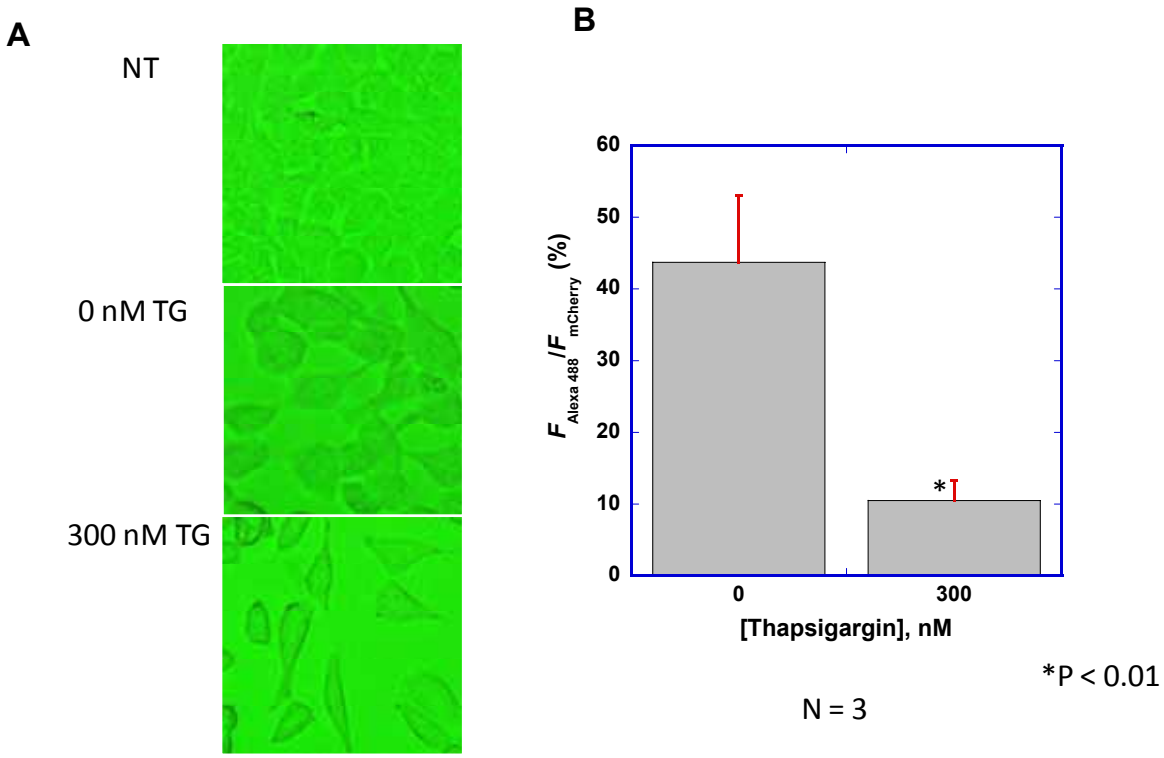

Figure 5-3 Treatment of 300 nM thapsigagin reduces the surface expression of wild type mGluR1α. (A) Transfection of wild type mGluR1α impaired cell proliferation but didn't influence cell morphology. (B) The surface expression of mGluR1α was reduced with 300 nM Thapsigargin for 24 hours.

expression was revealed by mCherry tagged to its C-terminal. As shown in Fig. 5-3, 300 nM TG effectively attenuated the surface expression of mGluR1α on HEK293 cells. The percentage of overall surface expression of mGluR1α in the TG-treated cells was reduced to 22% of the non-treated group. However, when looking at cell proliferation, cell numbers were dramatically decreased when 300 nM TG was included in the medium.

5.3 Discussion

Using our computational algorithm, we previously reported three Ca^{2+}-binding sites on ECD-mGluR1α. Of special interest is when Ca^{2+}-binding to the Ca^{2+}-binding site residing at the hinge region synergistically co-activate mGluR1α along with its endogenous agonist, L-Glu (89). Mutations in this Ca^{2+}-binding pocket eliminate or reduce the Ca^{2+} sensitivity of the receptor. A radioactive binding assay using [^{3}H]-L-Quis further confirmed that mGluR1α is a Ca^{2+}-sensing receptor. In the presence of Ca^{2+}, [^{3}H]-L-Quis binding was significantly enhanced (Fig. 4-3). By applying our newest prediction algorithm, which includes more subtle filters and a rotation library, a novel Ca^{2+}-binding site was discovered. The Ca^{2+}-binding site consists of S165, D208, Y236, and D318, which completely overlaps the L-Glu binding pocket. The L-Glu binding pocket was revealed by X-ray crystallography. It contained Y74, S165, S186, T188, D208, Y236, G293, D318, R323, and K409 (47). As shown in the electron density map of crystal structure, the amino group of L-Glu and the aromatic ring of Y236 form a π-cation interaction. Amino group of L-Glu could be regarded as a cation ion. This suggests that a Ca^{2+} ion could replace the location which occupied by amino group in crystal structure if L-Glu is removed. The ER serves as a Ca^{2+} store with high concentrations of Ca^{2+}, but if it's not clear that ER contains substantial concentrations of L-Glu. Thus, we hypothesize

that Ca^{2+}-binding to this novel Ca^{2+}-binding site might contribute to mGluR1α folding in the ER.

Protein folding is well regulated or assisted in the ER or other organelles by the ionic concentration, enzymes, and chaperones (119-121). These chaperones include heat shock proteins in the (HSPs) family, such as HSP40, HSP70, HSP90 and HSP100, along with some small HSPs and co-chaperones. In some cases, the protein folding assisted by HSPs is ATP-driven and coupled with metals (122). As reported by Kelly, in the presence of EGTA or EDTA, the interaction between calnexin and L444P GC was markedly impaired (116). Therefore, the author concluded that calnexin, interacting with GC, was dependent on the ER Ca^{2+}. However, at this time there is no direct evidence to conclude that the protein folding in the ER or other subcompartments in the cells is Ca^{2+} independent. TG was known as an irreversible inhibitor of SERCA pump. By inhibiting SERCA pump, the ER Ca^{2+} could be released out to cytosol. Considering low Ca^{2+} may lead to cell death or low proliferation, the endurance and dosage of TG need be well screened. In our study, 300 nM TG was applied to the cells for around 24 hours, and both cell surface expression and proliferation were reduced, but no cell death was observed.

As suggested by the MUGSR algorithm and structural analysis, S165, T188, Y236, and D318 form a novel Ca^{2+}-binding site. This site completely overlaps the L-Glu binding site. By looking at the electronic map of the crystal structure associated with L-Glu (PDBID: 1EWK), it can be seen that the amine group, which carries a positive charge, forms a cation-π interaction with the aromatic ring of Y236. In the absence of L-Glu, the positively charged Ca^{2+} might occupy the site instead of the amine group of L-

Glu. Considering the possibility of a low L-Glu concentration in the ER lumen, the high level of Ca^{2+} may contribute to mGluR1α folding by interacting with this Ca^{2+}-binding pocket. In an in vitro folding study, the proteins are usually less than 60 amino acids, because the folding of large proteins is far more complicated than small proteins. Determining the Ca^{2+} effect on the folding process of ECD-mGluR1α by using a re-folding assay is not feasible. The purified ECD has more than 520 amino acids with very slow folding kinetics, and it is too huge to handle in a refolding system. As we know, opposite to the folding process is unfolding. Increasing the temperature of the system denatures the proteins, so the thermostability of the proteins could be presented by the melting temperature. The Ca^{2+} effects on purified protein were determined by circular dichroism (CD).

6 DEVELOPING an ER CALCIUM SENSOR USING MCHERRY

6.1 Introduction

Ca^{2+}, which is involved in almost all of the cellular processes, plays important roles in embryogenesis, bone formation, growth, and proliferation of cells. Outside of the cells, Ca^{2+} works as a first messenger. Inside the cells, there are different concentrations of Ca^{2+} in different compartments where calcium serves as a Ca^{2+} store, second messenger, or co-factor. A change in theCa^{2+} concentration(s) in these sites can disturb signaling pathways in the cells, thereby causing diseases.

In order to dynamically monitor the change in the concentration of Ca^{2+} in different organelles in real time, our lab designed Ca^{2+} biosensors based on mCherry. MCherry was developed from DsRed by random PCR screening (123). More than ten mutations were made to the protein to disturb the hydrophobic interface, thereby reducing the aggregation of the protein (Figure 6-1). MCherry has the highest photostability, fastest maturation, and excellent pH resistance among the mFruits family (124). Therefore, mCherry is a good candidate for sensor development. By adding special signal peptides, the sensor can be anchored to the target organelles. To date, several Ca^{2+} indicators have been developed, including small organic dyes and genetically encoded fluorescent proteins. However, the small organic dyes cannot be specifically targeted to the cellular compartments, and the small dynamic range of genetically encoded sensors, to date, limit their application. In addition to these limitations, current genetically encoded sensors utilize the FRET technique by fusing the fluorescent protein with a Ca^{2+}-binding protein, calmodulin (CaM). Overexpression of CaM can disturb the signaling pathways in cells. Our previous EGFP based sensor Ca-G1 can successfully detect the change of

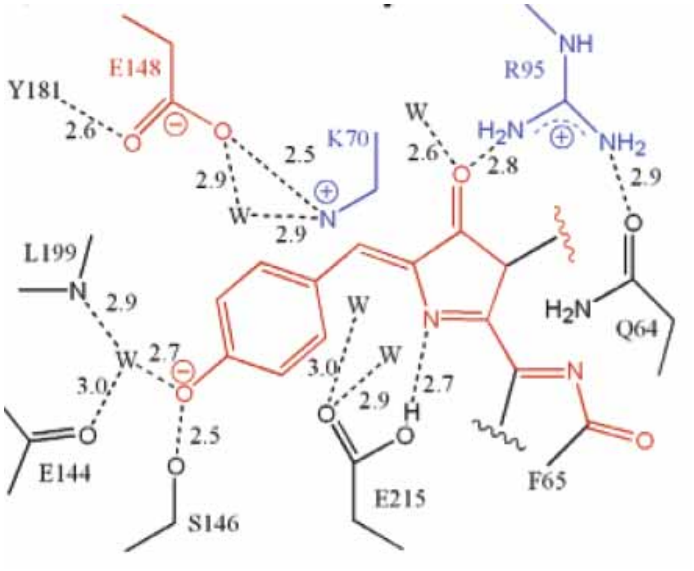

Figure 6-1 The Chromophore environment of mCherry (124). The crystal structure (PDBID: 2H5Q) indicates the mature chromophore is interacting with some residues on the barrel. R95, S146, and E215 directly form H-bonds with the chormophore while, E144 and L199 interact with chromophore through a water molecule.

Ca^{2+} concentration in vitro, but it is a pH sensitive sensor which can only be applied in the endoplasmic reticulum.

Our lab uses two strategies to develop Ca^{2+} sensor. Jin Zou et al. grafted a Ca^{2+}-binding loop III of calmodulin into EGFP with two additional mutations (M153T and V163A), and the sensor successfully senses changes in ER Ca^{2+}. In addition to the grafting approach, our lab also uses site-directed mutagenesis to construct a Ca^{2+}-binding pocket at the chromophore-sensitive location of EGFP. Using this technique, our lab developed the EGFP-based sensor, CatchER, which experiences a Ca^{2+}-induced fluorescence change upon binding Ca^{2+} thereby facilitating quantitative measurement both in vitro and in vivo (125). In this study, we used the same design strategy as that used with CatchER to create a Ca^{2+}-binding site at the chromophore-sensitive loci of mCherry. Two sensor candidates (MC-D1 and MC-D2) respond to Ca^{2+} in vitro, but the dynamic ranges were relatively low when expressing the sensors in the ER by adding CRsig and KDEL signal peptides to the protein.

6.2 Results

6.2.1 Mutation effects on mCherry

To investigate which residues on mCherry could be mutated without affecting its fluorescent properties, more than ten mutations were generated to disturb the local charge balance. As shown in Figure 6-2 and Table 6-1, mutations made to residues on the β-sheets of the protein, including H17N, H17Q, H17D, S21E, K50N, R36D, T41E, K121L, K123L, R125L, R216E, and R220L, which retained fluorescence, while mutants on the loops located at the lid of the barrel eliminated the fluorescence.

Table 6-1 Mutation effects on the fluorescence of mCherry

With fluorescence	Lose fluorescence
H17N	K74D
S21E	Y82E, S86D
R36D	
H17Q, S21E	
S21E, K50N	
R36D, T41E	
S21E, K50N, K123L, R125L	
S21E, K50N, K121L, K123L, R125L	
R36D, T41E, R216E, R220L	

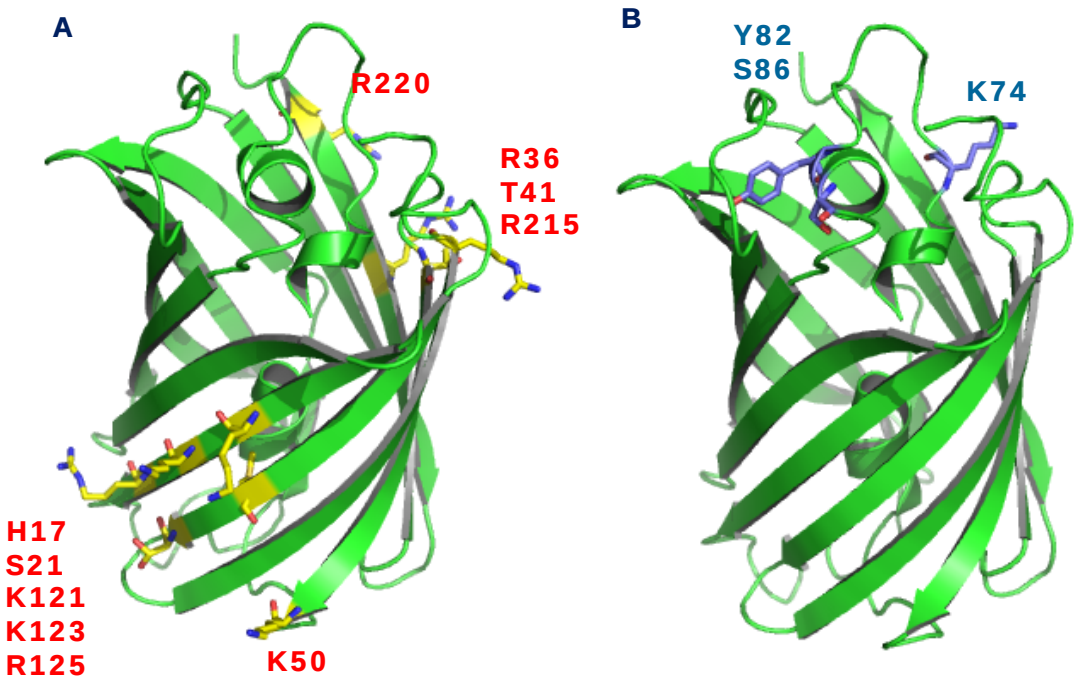

Figure 6-2 Mutation effects on mCherry. (A) MCherry remains fluorescent when the red residues were replaced by apolar or charged residues. (B) The substitution of the highlighted residues by negative charged residues results in fluorescence loss.

Bacterium grew well in the LB medium, and expressed and purified proteins showed the expected sizes. Excitation maximum at 587 nm and emission maximum at 610 nm were detected to determine their optical properties.

6.2.2 Designing a Ca^{2+}-binding pocket on mCherry

In our previous study, the variants of CD2 with designed Ca^{2+}-binding pockets sense Ca^{2+} very well by performing Tb^{3+} binding and Ca^{2+} competition assay. Later on, our lab successfully constructed CatchER using EGFP. The rationale for designing this sensor was the creation of a Ca^{2+}-binding pocket at the locations with residues interacting with chromophore. The creation of the binding site was done by mimicking the pocket of a CD2 variant named 7E15. As shown in figure 6-2., a short loop comprising from W143 to S146 displays high solvent accessibility, and in the crystal structure, S146 and E215 directly contact the chromophore, while E144 links to it through a water molecule. In addition to these residues, L199 and E215, residing at the adjacent β-sheet, also have interaction with the chromophore. We created two mCherry variants with a Ca^{2+}-binding site at this sensitive location. The sensor candidates were named MCD1 (A145E, N196D, K198D, R216E, E218) and MCD2 (E144, K198D, D200, Y214E, R216E). As shown in Figure 6-3, both candidates retain fluorescence.

6.2.3 Determining the Ca^{2+} sensing properties of MC-D1 and MC-D2 in vitro

Both sensor candidates were expressed in *E. coli* (BL21-DE3) and purified using a nickel-Histag column. To determine the pH preference of the proteins, an emission scan was performed in a profile of pH buffers excited at 587 nm. Figure 6-3 and table 6-2 reveal that MC-D2 has a pK_a of 5.5, and at a range of pH 7.0 to pH 8.0, the fluorescence of the sensors is not affected. The pH independence of fluorescence in this range

suggests the sensors are not sensitive to pH under physiological conditions, and are applicable to the organelles with physiological pH, for example ER has pH at 7.2 ± 0.2 (74,126). Next, we measured the Ca^{2+} responses of MC-D2 at pH 7.0. MC-D2 shows a dose-dependent response to Ca^{2+} and was saturated with the addition of 6 mM Ca^{2+}. MC-D2 has a K_D value around 200 μM and a dynamic range around 17%.

6.2.4 Determining the Ca^{2+} sensing properties of MC-D1 and MC-D2 in vivo

To determine if MC-D1 and MC-D2 were sensitive to Ca^{2+}, WT-mCherry, MC-D1, and MC-D2 were subcloned into pcDNA 3.1($^{+}$). The mCherry variants were expressed in the cytoplasm of HeLa and BHK cells. Both MC-D1 and MC-D2 have no response to extracellular Ca^{2+}, TG, or ionomycin, even though they expressed well in these cells. Since the K_D values of MC-D1 and MC-D2 are close to the submillimolar level, the dynamic change of cytoplasmic Ca^{2+} could be too small. Next, the signal peptides, calreticulin signal sequence and KDEL, were added to WT-mCherry, MC-D1, and MC-D2. As shown in figure 6-5 and 6-6, MC-D1 can sense increasing concentrations of extracellular Ca^{2+} in the presence of intracellular buffer. MC-D1 in HeLa cells is less sensitive to Ca^{2+} then in BHK cells.

Table 6-2 Fluorescent properties of MC-D1 and MC-D2

	Excitation (nm)	Emission (nm)	pKa
MC-D1	590	608	ND
MC-D2	586	606	5.5

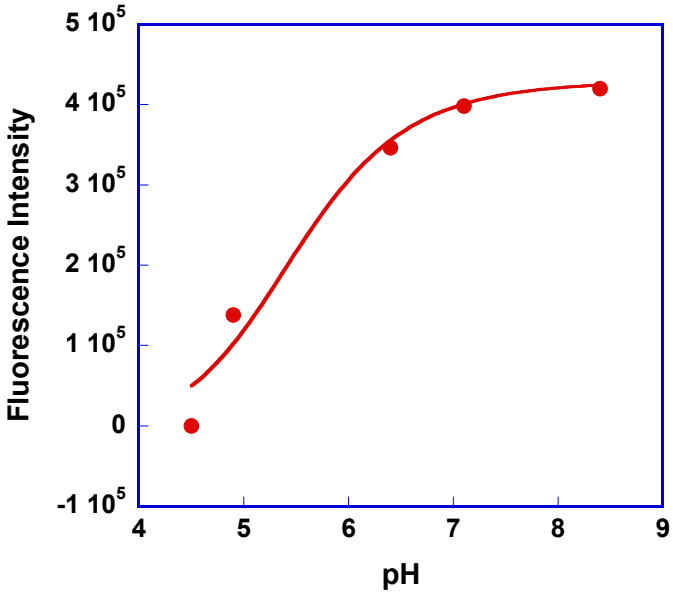

Figure 6-3 pH profile of MC-D2. The pH effects observed with 2 μM purified MC-D2 were measured using various buffer systems with different pH values

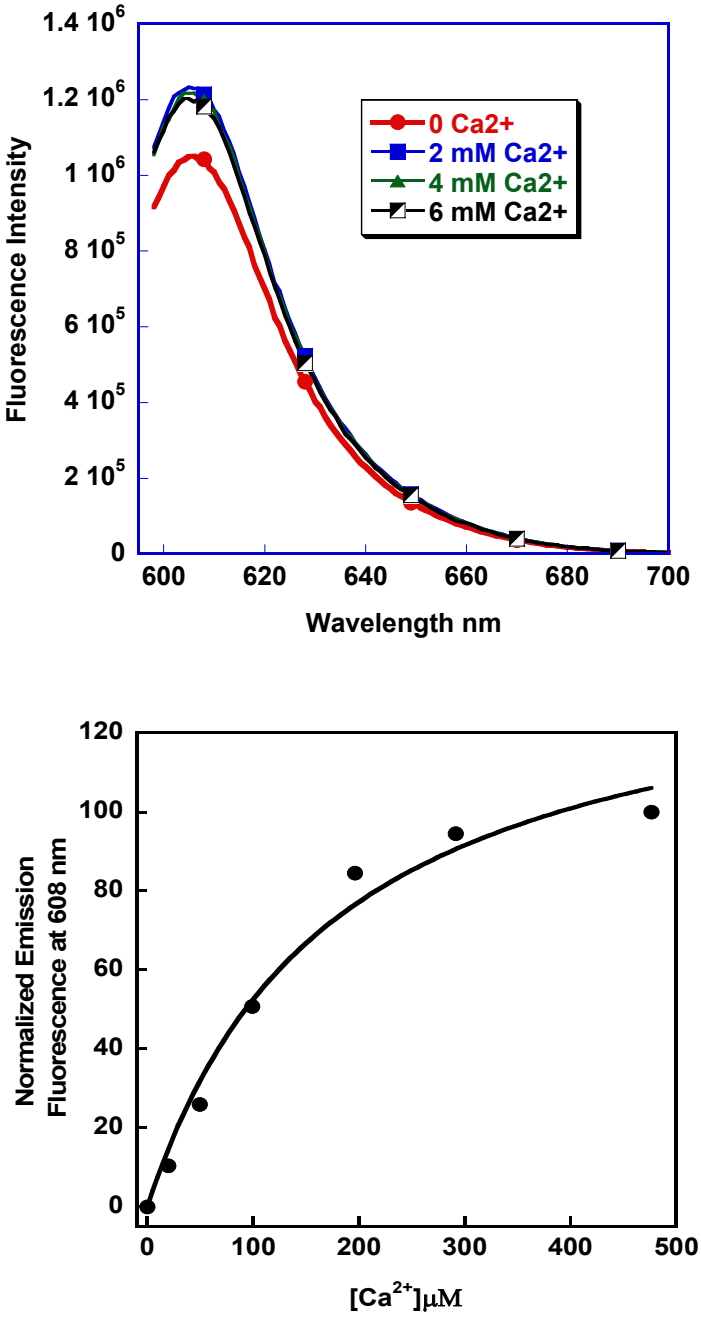

Figure 6-4 Ca^{2+} response of MC-D2. (A) The additional of Ca^{2+} increases the fluorescence of MC-D2. (B) Fluorescence of MC-D2 at 608 nm was measured in 10 mM HEPES, 50 nM NaCl. The pH value was fluctuated in the range of 7.04 to 7.11

6.3 Discussion

Ca^{2+} indicators were tremendously needed to quantitatively and dynamically monitor the Ca^{2+} change in a variety of subcellular compartments. Small organic dyes, such as fura-2 AM, Mag-fura-2, and the fluo family can be loaded into the specific organelles to some extent. However, these foreign organic compounds either have no specificity for the organelles in the cells due to their diffusion, or they are easily pumped out by living cells, thereby impairing the resolution of the Ca^{2+} concentration measurement. Fluorescent protein-based Ca^{2+} sensors were also engineered by fusing a FRET pair to the Ca^{2+}-binding protein, CaM, namely GCaMP. CaM is a substantial signaling protein in living cells, and overexpressing a sensor utilizing this protein will disturb related signaling pathways. As described in previous chapters, monitoring ER Ca^{2+} is important in understanding the functions of mGluR1α. We utilized fura-2 AM as a Ca^{2+} indicator to measure Ca^{2+} release from the ER. Although fura-2 AM can be efficiently loaded into the cytosol, its specificity for various organelles inside the cell remains unknown. After half an hour, fura-2 AM was pumped out of the cells. This lack of targeting ability leads to low sensitivity and resolution while detecting the Ca^{2+} change for long periods of time. As mentioned previously, genetically encoded fluorescent proteins were used in metal sensor development. In our previous work, we successfully engineered two sets of Ca^{2+} sensors which have been applied to ER/SR Ca^{2+} measurement. CatchER has been applied to monitor SR lumen Ca^{2+} in muscle fibers (125).

First, we tested some residues away from the sensitive region of the molecule, as we also tried to form a local Ca^{2+}-binding site. MCherry was developed from DsRed, and a few residues were suggested to be tolerant to mutations. As described by Camp-

bell et al, in the process of constructing monomeric RFP from DsRed, about 33 mutations (R2A, K5E, N6D, T21S, H41T, N42Q, V44A, V71A, K83L, C117E, F124L, I125R, V127T, L150M, R153E, V156A, H162K, K163M, A164R, L174D, V175A, F177V, S179T, I180T, Y192A, Y194A, V195T, S197I, T217A, H222S, L223T, F224G, and L225A) were made, and most of them were located at the wall of the β-barrel (127). In our study, we also mutated S21, T41, and R125, with all the substitutions maintaining fluorescence. Furthermore, our other mutations, R36D, K50N, K121L, K123L, R125L, R215E, and R220E also sustained fluorescence. However, the mutations on the lid of the beta barrel, including K74D, Y82D, and S86D, eliminated the fluorescence (Figure 6-2, Table 6-1). These findings suggest that most of the residues on the β-sheets are tolerant of mutations, while the residues on the lid are chromophore-sensitive. In particular, K74 is adjacent to the chromophore in the primary sequence, and it might be important for the maturation of the chromophore.

Next, Palmer A. et al. modified the interacting interface of CaM and M13, and the new sensor was claimed to overcome the effects of CaM (128,129). However, this sensor still has some limitations that hinder its ability to quantitatively monitor the fast kinetics of Ca^{2+} in the SR of muscle cells (130). CatchER overcomes this shortcoming. By targeting the ER/SR of the cells, it could dynamically and quantitatively reflect the Ca^{2+} change due to its fast Ca^{2+} off-rate (125). As mentioned, EGFP is sensitive to pH in the physiological environment, and does not mature well at 37^{o}C. As for the mCherry-based sensors, they are stable at pH value ranging from 6.5 to 8.0, and fold well *in situ*. Although the dynamic range of the mCherry sensors needs to be improved, this scaffold protein shows more promise than EGFP.

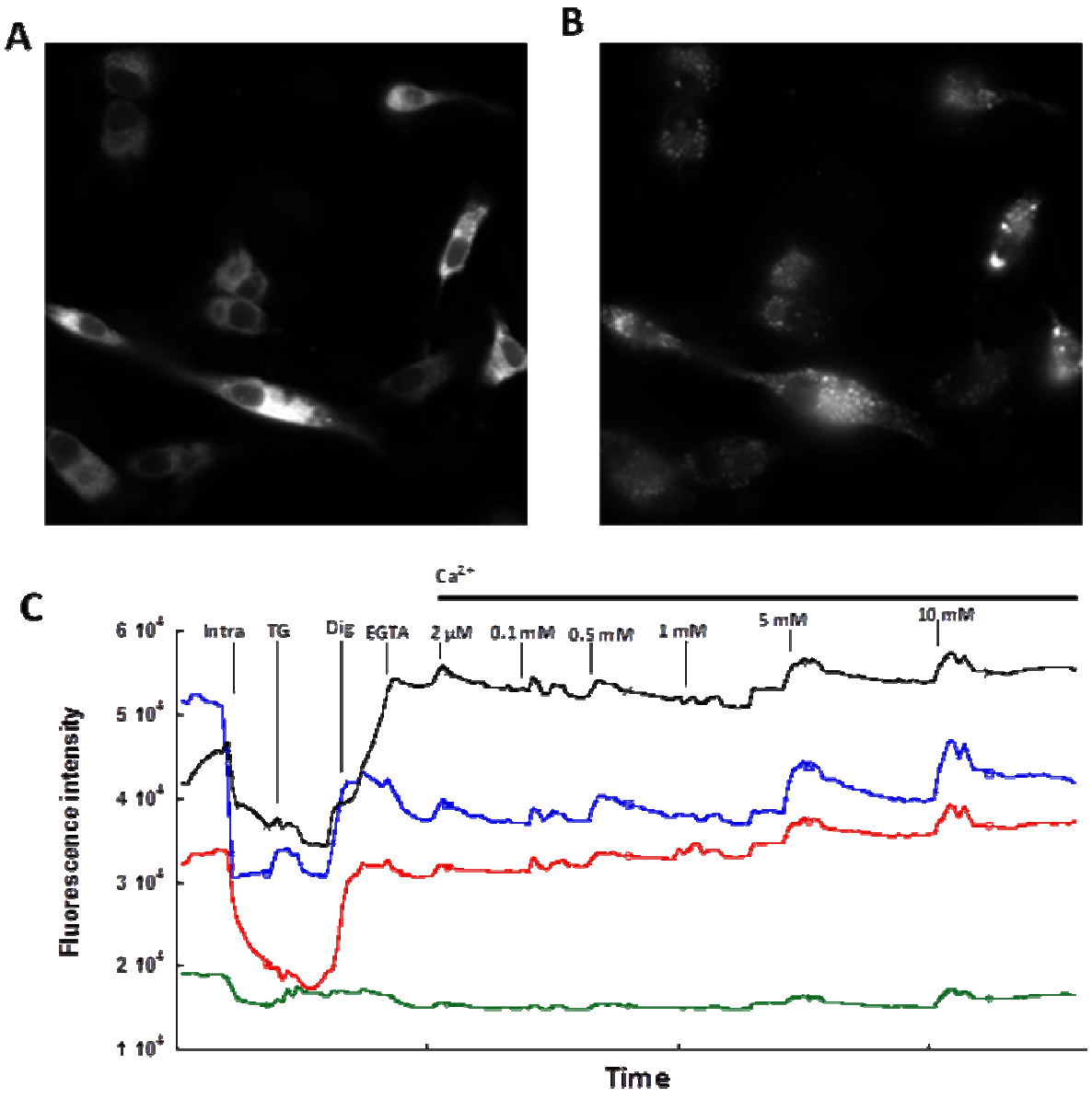

Figure 6-5 Ca^{2+} response of MC-D1 expressing in BHK cells. (A) BHK cells expressing MC-D1. (B) Treatment of intracellular buffer. After permeating the cell membranes, the cells containing the intracellular buffer were loaded into chamber. The fluorescence was congregated due to the intracellular buffer. (C) Fluorescence change upon extracellular environment change. TG depleted ER Ca^{2+} reduces fluorescence of MC-D1, while increasing Ca^{2+} enhances MC-D1 fluorescent intensity.

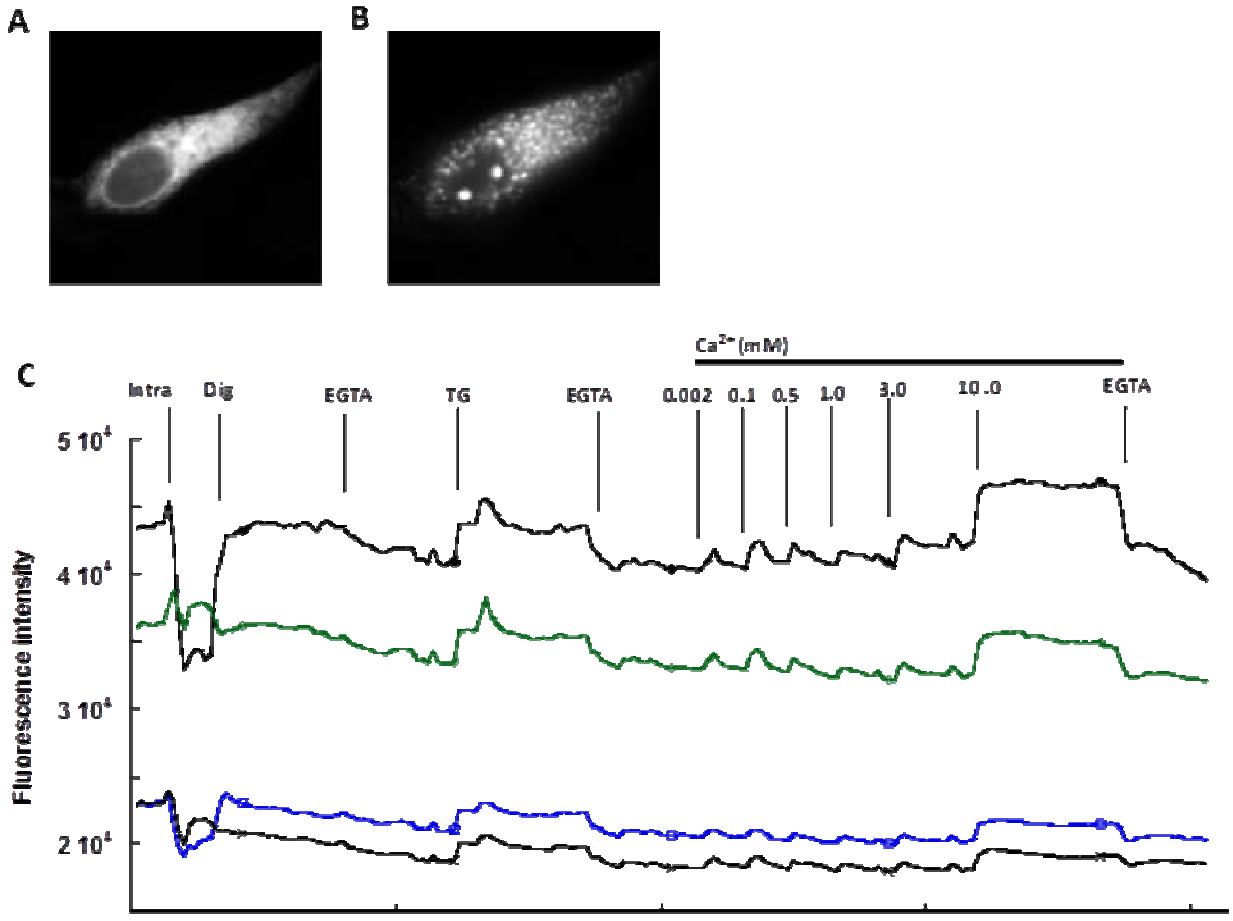

Figure 6-6 Ca^{2+} response of MC-D1-expressing in HeLa cells. (A) MC-D1 expressed well in HeLa cells. (B) In the presence of intracellular buffer, cells decreased in size, and the distribution of MC-D1 in cells was clustered. (C) MC-D1 in HeLa cells slightly responds to Ca^{2+}.

7 SIGNIFICANCE OF THIS WORK

In this dissertation, we first illustrated Ca^{2+}-binding sites not previously identified on ECD-mGluR1α, clarifying the controversial question of whether mGluR1α is a Ca^{2+} sensing receptor. Based on our understanding of Ca^{2+}-binding sites, we demonstrated the synergism of Ca^{2+} and L-Glu on mGluR1α. For the first time, we also illustrated how two endogenous signaling molecules co-activate mGluR1α in the central nervous system. Second, the effect of Ca^{2+} on three categories of drugs was investigated. Evidence for the effectiveness of Ca^{2+} in modulating the actions of some antagonists of mGluR1 will open a new avenue for targeting mGluR1α by drug development. Third, the function of Ca^{2+} in the process of mGluR1 trafficking provides the possibility of regulating membrane expression of the receptor by adjusting the ER Ca^{2+}. This could be an alternative way to rescue the function of neurons with deficient cell surface expression of mGluR1α.

7.1 The impact of determination of Ca^{2+}-binding sites.

Ca^{2+} was known to be an activator of mGluR1α, but it is invisible in the crystal structure that was determined of the extracellular domain of the receptor. The fast off-rate of Ca^{2+} in the setting of its low binding affinity presumably makes the protein unable to retain the ions at the time of crystal formation. However, the geometry of Ca^{2+}-binding sites is mostly generated in the absence of Ca^{2+} ion. Using a computational algorithm based on the geometry of known Ca^{2+}-binding sites, we successfully predicted four putative Ca^{2+}-binding pockets on ECD-mGluR1α. Site-directed mutagenesis and intracellular Ca^{2+} imaging of $[Ca^{2+}]_i$ further confirmed the functions of the predicted Ca^{2+}-binding

sites. The discovery of Ca^{2+}-binding sites on the one hand clarified the controversy regarding whether mGluR1 is a Ca^{2+}-sensing receptor. At the same time, the roles of the Ca^{2+}-binding sites were identified and the mechanism of the regulation of the receptor by Ca^{2+} was also demonstrated. On the other hand, new drugs could be designed to target Ca^{2+}-binding sites that could offer new opportunities for drug development. Due to the severe side effects of orthosteric modulators, the interest of drug discovery targeting mGluRs has turned away from the L-Glu-binding pocket, which could lead to the development of high subtype-selective drugs. However, the allosteric drugs also have another problem. Their targeted locations are not conserved in different species; thus, the drugs developed in animal models usually failed to be applicable to humans. As we described, the Ca^{2+}-binding site adjacent to L-Glu-binding pocket was only conserved in Group I mGluRs, which could play a central role in the Ca^{2+}-sensing properties of mGluR1 and mGluR5. Drugs targeting Ca^{2+}-binding sites could display subtype specificity, while the L-Glu-binding pocket is highly conserved in most of species, which will facilitates drug development.

7.2 The importance of discovery on Ca^{2+} effects on the developed drugs.

In this dissertation, Ca^{2+} was demonstrated to be a co-factor for four different classes of drugs targeting mGluR1a. Ca^{2+} and L-Glu synergistically activate mGluR1a, while Ca^{2+} enhances L-Quis activity by increasing its binding to ECD-mGluR1a. In addition, Ca^{2+} also enhances the sensitivity of the receptor to a positive allosteric modulator binding to the transmembrane domain. Intracellular Ca^{2+} oscillations and the maximal response of mGluR1a to Ro 87-4853 were clearly enhanced by extracellular Ca^{2+}. Meanwhile, the inhibitory effects of both (s)-MCPG and CPCCOEt were attenuated by

Ca^{2+}. In rats, the physiological level of Ca^{2+} ranges from 1.5 to 3.0 mM (131). As shown in Kubo's work, upon exposure to extracellular Ca^{2+} fluctuations in the range of 0 to 1.5 mM Ca^{2+}, mGluR1 was activated (32). Our results indicate that 1.8 mM Ca^{2+} is sufficient to modulate the activities of the drugs on the receptors. Understanding the role of Ca^{2+} on these drugs will allow us to tune drug potency by the local Ca^{2+} level. Moreover, taking drugs with Ca^{2+} will be a way to reduce side effects or enhance drug effects.

7.3 The role of Ca^{2+} in the process of protein folding and trafficking.

Dysfunction of proteins causes many diseases. Normally, the loss of function of proteins is due to mutation-related misfolding, which prevents proteins from trafficking to their appropriate cellular destinations. For receptors to be expressed on the cell surface, for example mGluR1α, there must be a sufficient expression level and a normally folded protein. In our study, mutations on Ca^{2+} binding sites (Y236F, D208I and E325I) reduced surface expression of mGluR1α. Depletion of ER Ca^{2+} by TG significantly decreased receptor trafficking to cell surface. The accumulating evidence supports the conclusion that Ca^{2+} plays a vital role in modulating mGluR1α either by affecting its folding in ER or trafficking to the cell surface. Elucidating the Ca^{2+} dependency of protein folding and trafficking will help us to control protein function by tuning its surface expression using Ca^{2+}. This will open a new strategy for drug development.

7.4 The significance of development of genetically encoded biosensor

Monitoring Ca^{2+} or other metals in specific organelles is still a challenge. The organic dyes are unable to target to the expected location and can be extruded by living cells. Our engineered sensor used red fluorescence protein as a host, which has good pH tolerance and brightness. Especially, by adding different tags or signal peptides, the

sensor could be targeted the locations we interested in, even in living animals. By utilizing this sensor, it allowed us to track the Ca^{2+} change in a disease model, which will help us to discover the role of Ca^{2+} in the disease process so that some appropriate drugs could be designed. Furthermore, by modifying the Ca^{2+} binding pocket, the K_D of the sensor can be tuned. Even more, the sensor could be developed into a sensor of other metal, like Zn^{2+}, Mg^{2+}, and so forth. All in all, this work will open a brand new field for metal related study.

REFERENCES

1. Berridge, M. J., Bootman, M. D., and Lipp, P. (1998) *Nature* **395**, 645-648
2. Dvorak, M. M., and Riccardi, D. (2004) *Cell calcium* **35**, 249-255
3. Niki, I., Yokokura, H., Sudo, T., Kato, M., and Hidaka, H. (1996) *Journal of biochemistry* **120**, 685-698
4. Roderick, H. L., and Cook, S. J. (2008) *Nature reviews. Cancer* **8**, 361-375
5. Pearce, S. H. (1998) *Journal of the Royal College of Physicians of London* **32**, 10-14
6. Sharan, K., Siddiqui, J. A., Swarnkar, G., and Chattopadhyay, N. (2008) *The Indian journal of medical research* **127**, 274-286
7. Chen, Y., Zhou, Y., Lin, X., Wong, H. C., Xu, Q., Jiang, J., Wang, S., Lurtz, M. M., Louis, C. F., Veenstra, R. D., and Yang, J. J. (2011) *The Biochemical journal* **435**, 711-722
8. Dodd, R., Peracchia, C., Stolady, D., and Torok, K. (2008) *The Journal of biological chemistry* **283**, 26911-26920
9. Fruen, B. R., Black, D. J., Bloomquist, R. A., Bardy, J. M., Johnson, J. D., Louis, C. F., and Balog, E. M. (2003) *Biochemistry* **42**, 2740-2747
10. Rodney, G. G., Krol, J., Williams, B., Beckingham, K., and Hamilton, S. L. (2001) *Biochemistry* **40**, 12430-12435
11. Zhang, S. L., Yu, Y., Roos, J., Kozak, J. A., Deerinck, T. J., Ellisman, M. H., Stauderman, K. A., and Cahalan, M. D. (2005) *Nature* **437**, 902-905

12. Kim, S. A., Tai, C. Y., Mok, L. P., Mosser, E. A., and Schuman, E. M. (2011) *Proceedings of the National Academy of Sciences of the United States of America* **108**, 9857-9862

13. Nagar, B., Overduin, M., Ikura, M., and Rini, J. M. (1996) *Nature* **380**, 360-364

14. Tamura, K., Shan, W. S., Hendrickson, W. A., Colman, D. R., and Shapiro, L. (1998) *Neuron* **20**, 1153-1163

15. Huang, C., and Miller, R. T. (2007) *Current opinion in nephrology and hypertension* **16**, 437-443

16. Levant, J. A., Walsh, J. H., and Isenberg, J. I. (1973) *The New England journal of medicine* **289**, 555-558

17. Floyd, R., and Wray, S. (2007) *Cell calcium* **42**, 467-476

18. Jiang, J., Zhou, Y., Zou, J., Chen, Y., Patel, P., Yang, J. J., and Balog, E. M. (2010) *The Biochemical journal* **432**, 89-99

19. Fruen, B. R., Balog, E. M., Schafer, J., Nitu, F. R., Thomas, D. D., and Cornea, R. L. (2005) *Biochemistry* **44**, 278-284

20. Burr, G. S., Mitchell, C. K., Keflemariam, Y. J., Heidelberger, R., and O'Brien, J. (2005) *Biochemical and biophysical research communications* **335**, 1191-1198

21. Torok, K., Stauffer, K., and Evans, W. H. (1997) *The Biochemical journal* **326 (Pt 2)**, 479-483

22. Dorr, P., Westby, M., Dobbs, S., Griffin, P., Irvine, B., Macartney, M., Mori, J., Rickett, G., Smith-Burchnell, C., Napier, C., Webster, R., Armour, D., Price, D., Stammen, B., Wood, A., and Perros, M. (2005) *Antimicrobial agents and chemotherapy* **49**, 4721-4732

23. Lavreysen, H., Janssen, C., Bischoff, F., Langlois, X., Leysen, J. E., and Lesage, A. S. (2003) *Molecular pharmacology* **63**, 1082-1093

24. Huang, Y., Zhou, Y., Wong, H. C., Chen, Y., Chen, Y., Wang, S., Castiblanco, A., Liu, A., and Yang, J. J. (2009) *The FEBS journal* **276**, 5589-5597

25. Wang, Y., Deng, X., Mancarella, S., Hendron, E., Eguchi, S., Soboloff, J., Tang, X. D., and Gill, D. L. (2010) *Science* **330**, 105-109

26. Takeichi, M. (1990) *Annual review of biochemistry* **59**, 237-252

27. Nature Reviews Drug Discovery, G. Q. P. (2004) *Nature reviews. Drug discovery* **3**, 575, 577-626

28. Wettschureck, N., and Offermanns, S. (2005) *Physiological reviews* **85**, 1159-1204

29. Palczewski, K. (2006) *Annual review of biochemistry* **75**, 743-767

30. Palczewski, K., Kumasaka, T., Hori, T., Behnke, C. A., Motoshima, H., Fox, B. A., Le Trong, I., Teller, D. C., Okada, T., Stenkamp, R. E., Yamamoto, M., and Miyano, M. (2000) *Science* **289**, 739-745

31. Lindsley, C. W., Wisnoski, D. D., Leister, W. H., O'Brien J, A., Lemaire, W., Williams, D. L., Jr., Burno, M., Sur, C., Kinney, G. G., Pettibone, D. J., Tiller, P. R., Smith, S., Duggan, M. E., Hartman, G. D., Conn, P. J., and Huff, J. R. (2004) *Journal of medicinal chemistry* **47**, 5825-5828

32. Kubo, Y., Miyashita, T., and Murata, Y. (1998) *Science* **279**, 1722-1725

33. Rodriguez, A. L., Nong, Y., Sekaran, N. K., Alagille, D., Tamagnan, G. D., and Conn, P. J. (2005) *Molecular pharmacology* **68**, 1793-1802

34. Chun, L., Zhang, W. H., and Liu, J. F. *Acta Pharmacol Sin* **33**, 312-323

35. Chapple, J. P., and Cheetham, M. E. (2003) *The Journal of biological chemistry* **278**, 19087-19094

36. Conn, P. J., Christopoulos, A., and Lindsley, C. W. (2009) *Nature reviews. Drug discovery* **8**, 41-54

37. Binet, V., Brajon, C., Le Corre, L., Acher, F., Pin, J. P., and Prezeau, L. (2004) *The Journal of biological chemistry* **279**, 29085-29091

38. Knoflach, F., Mutel, V., Jolidon, S., Kew, J. N., Malherbe, P., Vieira, E., Wichmann, J., and Kemp, J. A. (2001) *Proceedings of the National Academy of Sciences of the United States of America* **98**, 13402-13407

39. Nemeth, E. F., Steffey, M. E., Hammerland, L. G., Hung, B. C., Van Wagenen, B. C., DelMar, E. G., and Balandrin, M. F. (1998) *Proceedings of the National Academy of Sciences of the United States of America* **95**, 4040-4045

40. Urwyler, S. *Pharmacol Rev* **63**, 59-126

41. Urwyler, S., Mosbacher, J., Lingenhoehl, K., Heid, J., Hofstetter, K., Froestl, W., Bettler, B., and Kaupmann, K. (2001) *Molecular pharmacology* **60**, 963-971

42. Harrington, P. E., and Fotsch, C. (2007) *Current medicinal chemistry* **14**, 3027-3034

43. Conigrave, A. D., Quinn, S. J., and Brown, E. M. (2000) *Proc Natl Acad Sci U S A* **97**, 4814-4819

44. Silve, C., Petrel, C., Leroy, C., Bruel, H., Mallet, E., Rognan, D., and Ruat, M. (2005) *The Journal of biological chemistry* **280**, 37917-37923

45. Huang, Y., Zhou, Y., Castiblanco, A., Yang, W., Brown, E. M., and Yang, J. J. (2009) *Biochemistry* **48**, 388-398

46. Huang, Y., Zhou, Y., Yang, W., Butters, R., Lee, H. W., Li, S., Castiblanco, A., Brown, E. M., and Yang, J. J. (2007) *The Journal of biological chemistry* **282**, 19000-19010

47. Kunishima, N., Shimada, Y., Tsuji, Y., Sato, T., Yamamoto, M., Kumasaka, T., Nakanishi, S., Jingami, H., and Morikawa, K. (2000) *Nature* **407**, 971-977

48. Conigrave, A. D., and Hampson, D. R. *Pharmacol Ther* **127**, 252-260

49. Flower, D. R. (1999) *Biochimica et biophysica acta* **1422**, 207-234

50. Kano, M., and Kato, M. (1987) *Nature* **325**, 276-279

51. Houamed, K. M., Kuijper, J. L., Gilbert, T. L., Haldeman, B. A., O'Hara, P. J., Mulvihill, E. R., Almers, W., and Hagen, F. S. (1991) *Science* **252**, 1318-1321

52. Masu, M., Tanabe, Y., Tsuchida, K., Shigemoto, R., and Nakanishi, S. (1991) *Nature* **349**, 760-765

53. Ray, K., and Hauschild, B. C. (2000) *The Journal of biological chemistry* **275**, 34245-34251

54. O'Hara, P. J., Sheppard, P. O., Thogersen, H., Venezia, D., Haldeman, B. A., McGrane, V., Houamed, K. M., Thomsen, C., Gilbert, T. L., and Mulvihill, E. R. (1993) *Neuron* **11**, 41-52

55. Tsuchiya, D., Kunishima, N., Kamiya, N., Jingami, H., and Morikawa, K. (2002) *Proceedings of the National Academy of Sciences of the United States of America* **99**, 2660-2665

56. Tateyama, M., Abe, H., Nakata, H., Saito, O., and Kubo, Y. (2004) *Nat Struct Mol Biol* **11**, 637-642

57. Brody, S. A., Conquet, F., and Geyer, M. A. (2003) *Eur J Neurosci* **18**, 3361-3366

58. Dolen, G., Osterweil, E., Rao, B. S., Smith, G. B., Auerbach, B. D., Chattarji, S., and Bear, M. F. (2007) *Neuron* **56**, 955-962

59. Marino, M. J., Williams, D. L., Jr., O'Brien, J. A., Valenti, O., McDonald, T. P., Clements, M. K., Wang, R., DiLella, A. G., Hess, J. F., Kinney, G. G., and Conn, P. J. (2003) *Proc Natl Acad Sci U S A* **100**, 13668-13673

60. Patil, S. T., Zhang, L., Martenyi, F., Lowe, S. L., Jackson, K. A., Andreev, B. V., Avedisova, A. S., Bardenstein, L. M., Gurovich, I. Y., Morozova, M. A., Mosolov, S. N., Neznanov, N. G., Reznik, A. M., Smulevich, A. B., Tochilov, V. A., Johnson, B. G., Monn, J. A., and Schoepp, D. D. (2007) *Nat Med* **13**, 1102-1107

61. Drake, M. T., Shenoy, S. K., and Lefkowitz, R. J. (2006) *Circ Res* **99**, 570-582

62. Pelkey, K. A., Lavezzari, G., Racca, C., Roche, K. W., and McBain, C. J. (2005) *Neuron* **46**, 89-102

63. Fourgeaud, L., Mato, S., Bouchet, D., Hemar, A., Worley, P. F., and Manzoni, O. J. (2004) *J Neurosci* **24**, 6939-6945

64. Francesconi, A., Kumari, R., and Zukin, R. S. (2009) *J Neurosci* **29**, 3590-3602

65. Lee, J. H., Lee, J., Choi, K. Y., Hepp, R., Lee, J. Y., Lim, M. K., Chatani-Hinze, M., Roche, P. A., Kim, D. G., Ahn, Y. S., Kim, C. H., and Roche, K. W. (2008) *Proc Natl Acad Sci U S A* **105**, 12575-12580

66. El Far, O., Bofill-Cardona, E., Airas, J. M., O'Connor, V., Boehm, S., Freissmuth, M., Nanoff, C., and Betz, H. (2001) *The Journal of biological chemistry* **276**, 30662-30669

67. Nakajima, Y., Yamamoto, T., Nakayama, T., and Nakanishi, S. (1999) *The Journal of biological chemistry* **274**, 27573-27577

68. Hemstapat, K., de Paulis, T., Chen, Y., Brady, A. E., Grover, V. K., Alagille, D., Tamagnan, G. D., and Conn, P. J. (2006) *Molecular pharmacology* **70**, 616-626

69. Sheffler, D. J., and Conn, P. J. (2008) *Neuropharmacology* **55**, 419-427

70. Francesconi, A., and Duvoisin, R. M. (2004) *J Neurosci Res* **75**, 472-479

71. Kawabata, S., Kohara, A., Tsutsumi, R., Itahana, H., Hayashibe, S., Yamaguchi, T., and Okada, M. (1998) *The Journal of biological chemistry* **273**, 17381-17385

72. Wu, M. M., Llopis, J., Adams, S. R., McCaffery, J. M., Teter, K., Kulomaa, M. S., Machen, T. E., Moore, H. P., and Tsien, R. Y. (2000) *Methods in enzymology* **327**, 546-564

73. Galvez, T., Urwyler, S., Prezeau, L., Mosbacher, J., Joly, C., Malitschek, B., Heid, J., Brabet, I., Froestl, W., Bettler, B., Kaupmann, K., and Pin, J. P. (2000) *Molecular pharmacology* **57**, 419-426

74. Zou, J., Hofer, A. M., Lurtz, M. M., Gadda, G., Ellis, A. L., Chen, N., Huang, Y., Holder, A., Ye, Y., Louis, C. F., Welshhans, K., Rehder, V., and Yang, J. J. (2007) *Biochemistry* **46**, 12275-12288

75. Nash, M. S., Saunders, R., Young, K. W., Challiss, R. A., and Nahorski, S. R. (2001) *The Journal of biological chemistry* **276**, 19286-19293

76. Selkirk, J. V., Price, G. W., Nahorski, S. R., and Challiss, R. A. (2001) *Neuropharmacology* **40**, 645-656

77. Fillaut, J. L., Andries, J., Perruchon, J., Desvergne, J. P., Toupet, L., Fadel, L., Zouchoune, B., and Saillard, J. Y. (2007) *Inorganic chemistry* **46**, 5922-5932

78. Sato, T., Shimada, Y., Nagasawa, N., Nakanishi, S., and Jingami, H. (2003) *The Journal of biological chemistry* **278**, 4314-4321

79. Vassilev, P. M., Mitchel, J., Vassilev, M., Kanazirska, M., and Brown, E. M. (1997) *Biophysical journal* **72**, 2103-2116

80. Hardingham, N. R., Bannister, N. J., Read, J. C., Fox, K. D., Hardingham, G. E., and Jack, J. J. (2006) *J Neurosci* **26**, 6337-6345

81. Whang, P. G., O'Hara, B. J., Ratliff, J., Sharan, A., Brown, Z., and Vaccaro, A. R. (2008) *Orthopedics* **31**

82. Wellendorph, P., and Brauner-Osborne, H. (2009) *Br J Pharmacol* **156**, 869-884

83. Deng, H., Chen, G., Yang, W., and Yang, J. J. (2006) *Proteins* **64**, 34-42

84. Falke, J. J., Drake, S. K., Hazard, A. L., and Peersen, O. B. (1994) *Quarterly reviews of biophysics* **27**, 219-290

85. Glusker, J. P. (1991) *Advances in protein chemistry* **42**, 1-76

86. Honig, B., and Nicholls, A. (1995) *Science* **268**, 1144-1149

87. Nicholls, A., Sharp, K. A., and Honig, B. (1991) *Proteins* **11**, 281-296

88. Whitmore, L., and Wallace, B. A. (2008) *Biopolymers* **89**, 392-400

89. Jiang, Y., Huang, Y., Wong, H. C., Zhou, Y., Wang, X., Yang, J., Hall, R. A., Brown, E. M., and Yang, J. J. *The Journal of biological chemistry* **285**, 33463-33474

90. Kaupmann, K., Huggel, K., Heid, J., Flor, P. J., Bischoff, S., Mickel, S. J., McMaster, G., Angst, C., Bittiger, H., Froestl, W., and Bettler, B. (1997) *Nature* **386**, 239-246

91. Nakanishi, S. (1994) *Neuron* **13**, 1031-1037

92. Conn, P. J., and Pin, J. P. (1997) *Annu Rev Pharmacol Toxicol* **37**, 205-237

93. Kniazeff, J., Bessis, A. S., Maurel, D., Ansanay, H., Prezeau, L., and Pin, J. P. (2004) *Nat Struct Mol Biol* **11**, 706-713

94. Kubokawa, K., Miyashita, T., Nagasawa, H., and Kubo, Y. (1996) *FEBS Lett* **392**, 71-76

95. Tabata, T., Aiba, A., and Kano, M. (2002) *Mol Cell Neurosci* **20**, 56-68

96. Tabata, T., and Kano, M. (2004) *Mol Neurobiol* **29**, 261-270

97. Muto, T., Tsuchiya, D., Morikawa, K., and Jingami, H. (2007) *Proceedings of the National Academy of Sciences of the United States of America* **104**, 3759-3764

98. Abe, H., Tateyama, M., and Kubo, Y. (2003) *FEBS Lett* **545**, 233-238

99. Kirberger, M., Wang, X., Deng, H., Yang, W., Chen, G., and Yang, J. J. (2008) *J Biol Inorg Chem* **13**, 1169-1181

100. Yang, W., Wilkins, A. L., Ye, Y., Liu, Z. R., Li, S. Y., Urbauer, J. L., Hellinga, H. W., Kearney, A., van der Merwe, P. A., and Yang, J. J. (2005) *Journal of the American Chemical Society* **127**, 2085-2093

101. Wang, X., Kirberger, M., Qiu, F., Chen, G., and Yang, J. J. (2009) *Proteins* **75**, 787-798

102. Wang, X., Zhao, K., Kirberger, M., Wong, H., Chen, G., and Yang, J. J. (2010) *Protein science : a publication of the Protein Society* **19**, 1180-1190

103. Sali, A., and Blundell, T. L. (1993) *J Mol Biol* **234**, 779-815

104. Ye, Y., Shealy, S., Lee, H. W., Torshin, I., Harrison, R., and Yang, J. J. (2003) *Protein engineering* **16**, 429-434

105. Ye, Y., Lee, H. W., Yang, W., Shealy, S., and Yang, J. J. (2005) *Journal of the American Chemical Society* **127**, 3743-3750

106. Zhou, Y., Tzeng, W. P., Yang, W., Ye, Y., Lee, H. W., Frey, T. K., and Yang, J. (2007) *Journal of virology* **81**, 7517-7528

107. Balog, E. M., Norton, L. E., Bloomquist, R. A., Cornea, R. L., Black, D. J., Louis, C. F., Thomas, D. D., and Fruen, B. R. (2003) *The Journal of biological chemistry* **278**, 15615-15621

108. Rodney, G. G., Moore, C. P., Williams, B. Y., Zhang, J. Z., Krol, J., Pedersen, S. E., and Hamilton, S. L. (2001) *The Journal of biological chemistry* **276**, 2069-2074

109. Niki, Y., and Kishimoto, T. (1996) *Clinical microbiology and infection : the official publication of the European Society of Clinical Microbiology and Infectious Diseases* **1 Suppl 1**, S11-S13

110. Yuan, K., Jing, G., Chen, J., Liu, H., Zhang, K., Li, Y., Wu, H., McDonald, J. M., and Chen, Y. (2011) *The Journal of biological chemistry* **286**, 24776-24784

111. Pan, D., Yan, Q., Chen, Y., McDonald, J. M., and Song, Y. (2011) *Proteins* **79**, 2543-2556

112. Piccinin, S., Thuault, S. J., Doherty, A. J., Brown, J. T., Randall, A. D., Davies, C. H., Bortolotto, Z. A., and Collingridge, G. L. (2008) *Neuropharmacology* **55**, 459-463

113. Litschig, S., Gasparini, F., Rueegg, D., Stoehr, N., Flor, P. J., Vranesic, I., Prezeau, L., Pin, J. P., Thomsen, C., and Kuhn, R. (1999) *Molecular pharmacology* **55**, 453-461

114. Tabata, T., Araishi, K., Hashimoto, K., Hashimotodani, Y., van der Putten, H., Bettler, B., and Kano, M. (2004) *Proceedings of the National Academy of Sciences of the United States of America* **101**, 16952-16957

115. Roche, K. W., Tu, J. C., Petralia, R. S., Xiao, B., Wenthold, R. J., and Worley, P. F. (1999) *The Journal of biological chemistry* **274**, 25953-25957

116. Ong, D. S., Mu, T. W., Palmer, A. E., and Kelly, J. W. (2010) *Nature chemical biology* **6**, 424-432

117. Preston, A. M., Gurisik, E., Bartley, C., Laybutt, D. R., and Biden, T. J. (2009) *Diabetologia* **52**, 2369-2373

118. Rogers, T. B., Inesi, G., Wade, R., and Lederer, W. J. (1995) *Biosci Rep* **15**, 341-349

119. Bukau, B., Weissman, J., and Horwich, A. (2006) *Cell* **125**, 443-451

120. Deuerling, E., and Bukau, B. (2004) *Critical reviews in biochemistry and molecular biology* **39**, 261-277

121. Tang, Y. C., Chang, H. C., Chakraborty, K., Hartl, F. U., and Hayer-Hartl, M. (2008) *The EMBO journal* **27**, 1458-1468

122. Bukau, B., and Horwich, A. L. (1998) *Cell* **92**, 351-366

123. Shaner, N. C., Campbell, R. E., Steinbach, P. A., Giepmans, B. N., Palmer, A. E., and Tsien, R. Y. (2004) *Nat Biotechnol* **22**, 1567-1572

124. Shu, X., Shaner, N. C., Yarbrough, C. A., Tsien, R. Y., and Remington, S. J. (2006) *Biochemistry* **45**, 9639-9647

125. Tang, S., Wong, H. C., Wang, Z. M., Huang, Y., Zou, J., Zhuo, Y., Pennati, A., Gadda, G., Delbono, O., and Yang, J. J. (2011) *Proceedings of the National Academy of Sciences of the United States of America* **108**, 16265-16270

126. Wu, M. M., Llopis, J., Adams, S., McCaffery, J. M., Kulomaa, M. S., Machen, T. E., Moore, H. P., and Tsien, R. Y. (2000) *Chemistry & biology* **7**, 197-209

127. Campbell, R. E., Tour, O., Palmer, A. E., Steinbach, P. A., Baird, G. S., Zacharias, D. A., and Tsien, R. Y. (2002) *Proceedings of the National Academy of Sciences of the United States of America* **99**, 7877-7882

128. Palmer, A. E., Giacomello, M., Kortemme, T., Hires, S. A., Lev-Ram, V., Baker, D., and Tsien, R. Y. (2006) *Chemistry & biology* **13**, 521-530

129. Palmer, A. E., Jin, C., Reed, J. C., and Tsien, R. Y. (2004) *Proceedings of the National Academy of Sciences of the United States of America* **101**, 17404-17409

130. Jimenez-Moreno, R., Wang, Z. M., Messi, M. L., and Delbono, O. (2010) *Pflugers Arch* **459**, 725-735

131. Jones, H. C., and Keep, R. F. (1988) *J Physiol* **402**, 579-593

APPENDIX

Optimizing EGFP-based Ca^{2+} sensor by circular permutation

1. Introduction

Ca^{2+} is very important in biological and physiological process, and functions as first and second messaeger in signaling transduction. Ca^{2+} is also involved in pathological processes in organisms. Therefore, it is significant to develop the sensors or techniques to observe or monitor the change of Ca^{2+} in cells. Our lab has successfully developed a Ca^{2+} sensor based on EGFP using grafting strategy, but it is pH sensitive and has small dynamic change. Protein can be introduced in new ends by opening a certain site other than initial ends after joining the old termini with peptide linker. The properties of re-organized protein were changed in most cases. Through screening the new circular permutated variants, the re-constructed protein could retain Ca^{2+} sensing property as well as fluorescence. In this research, we joined two initial termini of EGFP172C2 by SG linker which was encoded by restriction endonulease, Spe I. The circular DNA of EGFP172C2 was randomly cleaved by DNase I. Relineared DNA was repaired by T4 ligase and T4 PNK, and the random re-organized EGFP172C2 fragment library was inserted into pRsetB vector with pre-engineered triple stop codon. The new permutated variants of EGFP172C2 were screened using UV light.

2. Methods:

2.1 Primer design and PCR

Spe I recognized sequence, which encodes SG, was introduced into two primers of EGFP172C2. Spe I recognized sequence was protected by extra three bases. Fragments with Spe I recognition sites were obtained by running PCR.

2.2 Construct recombinant plasmid with pGEM-4Z

PGEM-4Z was digested by Sma I following the protocol in SmaI kit. The blunt PCR fragments then were inserted into pGEM-4Z, and the ratio of inserted fragments over vector in the reaction was set to 1:1, 2:1 or 10:1. After the ligation products were

transformed into DH5a, the plate was sorted by Blue-White Screening by mixing X-gal and ITPG in bacteria solution. pGEM-4Z contain LAZ gene which will give out blue color induced by ITPG with the performance of X-gal. White colonies then were picked, sequenced and then duplicated by Maxiprep.

2.3 Constructing circular EGFP172C2-Spe I

Recombinant plasmid was digested by Spe I, and the linear fragments were purified by gel extraction. 5 µg digested DNA was circularized at a conc. of 2.5 ng/ µl with 90 weiss units T4 DNA ligase 16^{o}C overnight. According to the concentration of DNA, dilute to final concentration of 2.5ng/µl, 10µl T4 DNA ligase.

2.4 Ethanol Precipitation

Transfer DNA to a container which can contain 4 times of DNA solution. 1/10 volume of Sodium Acetate to equalize ion concentrations. At least 2 volumes (3 volumes) of -20 ^{o}C 100% ethanol, let stand in -80 ^{o}C at least one hour. Centrifuge in 4 ^{o}C with 15 mins at highest speed. Remove all supernatant. 200 µl (or more, 600 µl) 70% ethanol for washing DNA; centrifuge for 5mins in 4 ^{o}C at highest speed. Remove supernatant, evaporate remaining ethanol in room temperature. Resuspend DNA in desired volume of water or TE buffer. Circular DNA was collected by gel extraction.

2.5 Relinearization of circularized DNA with DNase I

Digest DNA at a conc. 5milliunits/ µg DNase I in 50mM Tris.HCl, pH7.5, 1mM MnCl2, DNA 5 µg/ml at room temperature for 15mins. This reaction is stopped by 10 µl 0.5M EDTA, and desalted by QIA quick columns into EB or collected by gel extraction (10mM Tris.HCl, pH8.5). 10X reaction buffer can be stored in -80 ^{o}C.

2.6 Repair by T4 DNA polymerase

T4 DNA polymerase: 1unit/ µg DNA

T4 ligase : 2 Weiss units/ µg DNA

dNTPs Final Conc. : 150 µM (use KOD dNTPs mixture)

In T4 ligase buffer at room temperature for 1hour, and collect repaired DNA by Gel Extraction

2.7 Preparation of pRsetB-V

The vector was digested by EcoR V, dephosphorylated and collected by gel electrophoresis.

2.8 Ligation and Transformation

Random circularly permutated EGFP172C2 DNA fragments were connected to pRsetB-V. The recombinant library then was introduced into expression strain—BL21DE3.

2.9 Library Screening

The colonies can be screened through their fluorescence by treating with UV light.

3. Results

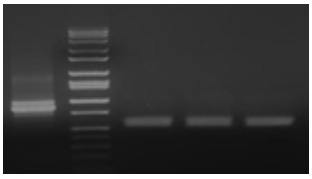

Figure 1 Circularized EGFP172C2-Spe I

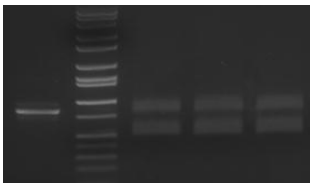

Figure 2 Random relinearized EGFP172C2

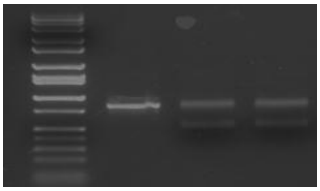

Figure 3 Repair of DNase I treated EGFP172C2

As shown in figure 1, the circularized fragments moved faster than linear PCR products. In figure 2, the DNase I digested DNA band shows wide and diffusive due to loss of nucleotide of some DNA fragments. After repair, the gaps and nicks were fulfilled by dNTPs, DNA bands look thinner.